A FRAMEWORK FOR DAMAGE INDEX CALCULATION IN LIGHT WOOD-FRAME BUILDINGS

by

MD Sultanur Ashikin

B.Sc., Bangladesh University of Engineering and Technology, 2022

THESIS SUBMITTED IN PARTIAL FULFILLMENT OF
THE REQUIREMENTS FOR THE DEGREE OF
MASTER OF APPLIED SCIENCE
IN
ENGINEERING

UNIVERSITY OF NORTHERN BRITISH COLUMBIA

April 2025

Abstract

Seismic events present significant challenges to the structural performance of buildings, with light wood-frame structures being particularly susceptible due to their unique material variability, reliance on non-structural components, and diverse construction practices. Existing seismic damage models, such as the Park and Ang Damage Index (DI), have demonstrated utility for steel and concrete structures but remain underdeveloped and unvalidated for light wood-frame buildings. This research addresses these gaps by proposing a global-level calibration framework for the β parameter in the Park and Ang DI model, tailored specifically for light wood-frame structures. Unlike traditional component level calibration, the global approach emphasizes system-level behavior, capturing the cumulative effects of deformation and energy dissipation across the entire structure.

The study integrates experimental data from benchmark tests conducted independent of this study scope, the NEESWood project, to validate the accuracy of the calculated DI values against observed damage patterns. By correlating DI values with actual damage, the research establishes a comprehensive and validated methodology for assessing seismic damage in light wood-frame buildings.

Furthermore, the proposed framework provides valuable insights into the progression of damage under varying seismic intensities, offering thresholds that link DI values with observed structural and non-structural damage. These findings significantly advance the practical application of the Damage Index framework for light wood-frame structures, contributing to performance-based seismic design and risk assessment efforts.

Table of Content

ABSTRACT ..... **II**

TABLE OF CONTENT ..... **III**

LIST OF TABLES ..... **VII**

LIST OF FIGURES ..... **IX**

1 INTRODUCTION **1**

1.1 BACKGROUND 1

1.2 PROBLEM STATEMENT 4

1.3 RESEARCH OBJECTIVES 6

1.4 THESIS STRUCTURE 7

2 LITERATURE REVIEW **9**

2.1 OVERVIEW OF SEISMIC DAMAGE ASSESSMENT IN LIGHT WOOD-FRAME BUILDINGS 9

2.1.1 Seismic Damage Assessment Practices *9*

2.2 EVOLUTION OF DAMAGE INDICES IN STRUCTURAL HEALTH MONITORING 10

2.3 ENERGY AND DEFORMATION BASED DAMAGE MODEL: PARK AND ANG DAMAGE INDEX 12

2.3.1 Park and Ang Damage Index Model *13*

2.3.2 Mathematical Expression of the Park and Ang Damage Index *14*

2.3.3 Ultimate Displacement Parameter *15*

2.3.4 Equivalent Yield Force Parameter *16*

2.3.5 Component Level Parameter Values Derived from Experimental Shear Wall Test *17*

2.3.6 Beta β Parameter *19*

2.3.7 Finite Element Modeling of Light Wood Frame Building *20*

2.3.8 Global Level Modeling of Light Wood Frame Building *21*

2.3.8.1 MSTEW Model Parameters and Their Effectiveness in Timber3D 22
2.3.8.2 Out-of-plane Stiffness of Light Wood Frame Buildings 26
2.3.9 Mass Distribution in Numerical Modeling *27*
2.4 INCREMENTAL DYNAMIC ANALYSIS 28
2.4.1 FEMA Guidelines for Conducting IDA *29*
3 SHAKING TABLE TESTS USED FOR DAMAGE OBSERVATION AND MODEL VALIDATION 32
3.1 BACKGROUND OF THE PROJECT 32
3.2 TEST BUILDING ARCHITECTURE 33
3.3 SHAKE TABLE SETUP 36
3.4 TEST PHASES 37
3.5 GROUND MOTIONS 39
3.5.1 Ground Motion Selection *39*
3.5.2 Ground Motion Scaling *40*
3.6 INSTRUMENTATION OF SHAKE TABLE TEST 43
3.7 OBSERVED DAMAGE IN PHASE 5 TESTING 43
4 NUMERICAL MODEL DEVELOPMENT 49
4.1 OVERVIEW OF TIMBER 3D AND NONLINEAR MODELING 49
4.2 MODELING APPROACH 50
4.2.1 Structural Representation *50*
4.2.2 Master-Slave Nodal System *50*
4.2.3 Diaphragm and Shear Wall Modeling *50*
4.2.4 Dynamic Analysis *51*
4.2.5 Validation *51*
4.2.6 Spring Parameters *51*
4.2.6.1 In-Plane Shear Spring Parameters 51
4.2.6.2 Parallel Spring Theory 56
4.2.6.3 Out-of-Plane Bending Spring Parameters 61
4.2.6.4 Nodal Restraints 63

4.2.6.5 Diaphragm Beam 63
4.2.6.6 Mass Distribution 66
4.2.6.7 Timber 3D Modeling 66
4.2.7 Damping Ratios in Phase 5 ..... *68*
4.3 MODEL VALIDATION 68
4.3.1 Modal Analysis *68*
4.3.2 Structural Response *70*
4.3.2.1 Displacement Response 70
4.3.2.2 Force Time History 74
4.3.2.3 Global Hysteresis 76
4.3.2.4 Energy Dissipation 77
4.3.2.5 Roof Displacement Profile 79
5 DAMAGE INDEX MODEL CALIBRATION 83
5.1 INCREMENTAL DYNAMIC ANALYSIS (IDA) OF THE NEESWOOD BUILDING 85
5.2 IDA CURVE 88
5.2.1 Scattered Plot Observed Trends: *88*
5.2.2 Median Curve *90*
5.3 PUSHOVER ANALYSIS OF NEESWOOD TWO STORY NUMERICAL MODEL 92
5.4 GLOBAL BETA CALIBRATION CALCULATION FOR THE BENCHMARK TWO-STORY LIGHT WOOD FRAME BUILDING 93
5.4.1 Scaled Response Spectrum Northridge Earthquake *94*
5.4.2 Global Response *95*
5.4.3 Beta Value Sample Calculation *97*
6 DAMAGE INDEX CALCULATION AND DAMAGE CORRELATION 100
6.1 DAMAGE INDEX CALCULATION FOR PHASE 5, TEST 8: NUMERICAL ANALYSIS OF BENCHMARK RESPONSE 101
6.1.1 Sample DI Calculation for Wall 1Y First Floor *103*
6.1.2 Global Damage Index Calculation *104*

6.2 DAMAGE CORRELATION 106

6.3 CORRELATING DAMAGE ACROSS A RANGE OF INTENSITY LEVELS 108

7 CONCLUSION 117

7.1 FUTURE WORK 118

8 REFERENCES 121

List of Tables

Table 1 Summary of test phases and building configurations 38

Table 2 Ground Motion Information for NEESWood Benchmark Tests 41

Table 3 Summary of Observed Damage in Phase 5 48

Table 4 First story in plane shear spring parameters in x direction 54

Table 5 Second story in plane shear spring parameters in x direction..... 54

Table 6 First story in plane shear spring parameters in y direction 55

Table 7 Second story in plane shear spring parameters in y direction..... 55

Table 8 Case Study: E27 Wall and Combined Parameters..... 58

Table 9 Combined MSTEW backbone parameters for in-plane shear springs..... 60

Table 10 Out-of-plane stiffness of the shear walls 62

Table 11 Equivalent diaphragm beam element properties..... 65

Table 12. Damping ratio of Phase 5 structure used in the numerical model 68

Table 13 Comparison of modal periods between the benchmark test model and numerical model 70

Table 14. Summary of Validation Results – Phase 05 Test 08..... 82

Table 15. Key information on 11 significant earthquakes used in the IDA analysis, including their year of occurrence, magnitude, location, and notable features. 87

Table 17. Wall-wise DI values and corresponding energy dissipation..... 102

Table 16. Table presenting the calculated Damage Index (DI) for each wall on the first and second floors of the NEESWood two-story light wood frame numerical model. The Northridge earthquake, scaled by a factor of 1.2, was utilized for the dynamic analysis of the Timber 3D model. The DI values are tabulated for the corresponding walls using calibrated Beta values. 103

Table 18. Component-wise Damage Index (DI) calculation for the NEESWood two-story light wood frame structure utilizing numerical response of Northridge earthquake ground motion with scale factor 1.20 105

Table 19. Peak Ground Acceleration (PGA) in X and Y directions from NEESWood benchmark tests used in numerical analysis and obtained Global DI from numerical response..... 110

Table 20. Comparison of Global DI values obtained from numerical response and experimental benchmark test response, demonstrating the validity of the beta calibration and the reliability of the developed framework..... 114

List of Figures

Figure 1. (a) $Dult$ and $Fyield$ as a function of nail spacing (b) β as a function of nail spacing and damage limit state. (Van De Lindt, 2005)(c) schematic representation of edge and inside nail spacing of a typical shear wall (d) schematic of the test set-up for shear wall testing (Van De Lindt, 2005) 18

Figure 2. Backbone curves of MSTEW model (Pan et al., 2018) 23

Figure 3 Elevation view of the NEESWood two-story residential project building (Christovasilis et al., n.d., 2009) 34

Figure 4 Floor plan layour of the NEESWood project building (Christovasilis et al., n.d., 2009) 35

Figure 5 Isometric view of the project building..... 35

Figure 6 (a) Extension frame of shake tables connected by steel link structure, and (b) Foundation of Test Building under Construction building (Christovasilis et al., n.d., 2009)..... 36

Figure 7 South-east external view of the benchmark structure after the installation of the exterior stucco finish (Christovasilis et al., n.d., 2009)..... 42

Figure 8 Cracking and Spalling of Stucco at the Bottom of Garage Wall (Christovasilis et al., n.d., 2009) 44

Figure 9 Cracking and Spalling of Stucco at the Corner of Garage Wall Opening (Christovasilis et al., n.d., 2009) 45

Figure 10 Cracking and separation of sill plate through entire length of garage narrow wall piers (Christovasilis et al., n.d., 2009) 45

Figure 11 Cracking of stud above hold-down anchor (Christovasilis et al., n.d., 2009) 46

Figure 12 Separation of Gypsum Wallboard from Ceiling (Christovasilis et al., n.d., 2009) 46

Figure 13 Horizontal Cracking of Gypsum Wallboard (Christovasilis et al., n.d., 2009) 47
Figure 14 Cracking and Buckling of Gypsum Wallboard at Door Opening (Christovasilis et al., n.d., 2009). Table below summarises the damage observed and shown above: 47
Figure 15 Shear wall plan for the NEESWood two story light wood frame building (a) First Floor (b) Second Floor 52
Figure 16 Equivalent in-plane shear spring system 57
Figure 17 MSTEW hysteresis backbone curve used in this study for numerical model development (a) E27 wall - Phase 03 (b) Gypsum wall board (Pan et al., 2018) (c) Stucco (Pan et al., 2018). 59
Figure 18 MSTEW back bone curve for combined action of Phase 3 shear wall, GWB and Stucco 59
Figure 19 Wall line plan of the NEESWood two story building 63
Figure 20 Diaphragm equivalent beam (a) first floor level (b) second floor level 65
Figure 21 Timber 3D numerical model of NEESWood two-story light wood frame building 67
Figure 22 Comparison of mode shapes obtained from the shake table test (benchmark test) and the Timber 3D numerical model for the NEESWood two-story light wood-frame building. 69
Figure 23 Comparison of nodal displacement time history between the benchmark structure shake table test response and numerical model response for Phase 05 Test 08 – Shear wall E16 in Y direction in 1st floor roof 72
Figure 24 Comparison of nodal displacement time history between the benchmark structure shake table test response and numerical model response for Phase 05 Test 08 – Shear wall E1 in X direction in 1st floor roof 72

Figure 25 Comparison of nodal displacement time history between the benchmark structure shake table test response and numerical model response for Phase 05 Test 08 – Shear wall E28 in Y direction in 2nd floor roof 73
Figure 26 Comparison of nodal displacement time history between the benchmark structure shake table test response and numerical model response for Phase 05 Test 08 – Shear wall E17 in X direction in 2nd floor roof. 73
Figure 27 Base shear force time history comparison between the benchmark test (Phase 05 - Test 08) and the numerical response in X direction (longitudinal direction) 75
Figure 28 Base shear force time history comparison between the benchmark test (Phase 05 - Test 08) and the numerical response in Y direction (transverse direction) 75
Figure 29 Base shear force versus central roof displacement hysteresis loops for Phase 05 – Test 08. Panels (a) and (c) correspond to the benchmark shake table test results in the X (longitudinal) and Y (transverse) directions, respectively. Panels (b) and (d) represent the corresponding numerical model predictions for the X and Y directions. 76
Figure 30 Comparison of global hysteretic energy dissipation of the benchmark test structure and the numerical model in X (longitudinal) direction 78
Figure 31 Comparison of global hysteretic energy dissipation of the benchmark test structure and the numerical model in Y (transverse) direction 79
Figure 32 Numerical model time history analysis deformed shape (15th sec) at scale 100 for Phase 05 Test 08 80
Figure 33 Comparison of maximum roof displacement profile between the benchmark test structure and the numerical model in X direction for Phase 05 Test 08 81

Figure 34 Comparison of maximum roof displacement profile between the benchmark test structure and the numerical model in Y direction for Phase 05 Test 08. The table below summarizes the validation briefly. 81

Figure 35. Flowchart illustrating the systematic process for Damage Index (DI) model calibration, including the development and validation of a numerical model, determination of global parameters via pushover analysis, collapse intensity identification through Incremental Dynamic Analysis (IDA), and global beta calibration based on global hysteresis responses. 84

Figure 36. IDA scattered data points for the NEESWood two story light wood frame building Timber 3D model. 11 wide range of ground motion data and 174 corresponding dynamic analysis result is utilized for this plot.s 89

Figure 37. Median incremental dynamic analysis (IDA) curve illustrating the relationship between drift ratio (%) and spectral acceleration (g). The curve represents the median response of the NEESWood two story light wood frame building model based on scattered IDA points from multiple ground motion records. The collapse point is identified at a drift ratio of 6.5% and spectral acceleration of 1.65g, indicating the intensity level at which the structure reaches its collapse limit state. 90

Figure 38. This figure presents the pushover analysis curve, illustrating the relationship between the base shear force and the roof displacement. The force values are expressed in kN, while the displacement is in mm. The curve provides insights into the nonlinear behavior and lateral load resistance of the structure under increasing displacement. 93

Figure 39. Response spectrum illustrating the variation of spectral acceleration Sa with respect to the period (T) for a single-degree-of-freedom (SDOF) system with 5% damping. The ground motion was scaled to match the collapse intensity level of 1.65g at a period 0.30 seconds. 95

Figure 40. Hysteresis Curve of the System. This figure illustrates the hysteresis response of the global system, showing the relationship between force (kN) and average roof displacement (mm). The curve represents the cyclic behavior of the structure under repeated loading and unloading, capturing its energy dissipation and stiffness degradation over successive cycles. 96
Figure 41. Cumulative Energy Dissipation Over Time. This figure displays the cumulative energy dissipation of the system as a function of time (s). The plot highlights the energy absorbed by the structure during cyclic loading, with energy values calculated in kilojoules (kJ). 97
Figure 42. Layout of the wall lines for the NEESWood two story light wood frame building .. 100
Figure 43. Observed damages for the NEESWood benchmark test after Phase 05 Test 08..... 107
Figure 44. Level of damage observed during different test phases of the NEESWood benchmark test and corresponding global DI value for each of the tests based on numerical dynamic analysis response..... 111
Figure 45. Flowchart outlining the step-by-step framework for seismic damage assessment of light wood-frame buildings using Damage Index (DI). 115

1 Introduction

1.1 Background

The study of seismic performance and damage in structures has been a critical focus in structural engineering for decades. With the increasing need to ensure safety and minimize damage during earthquakes, damage indices have emerged as an essential tool for assessing the vulnerability and performance of various structural systems. Among the early models, the Park and Ang Damage Index (DI) introduced in 1985 has been a landmark contribution to this field, providing a framework for quantifying seismic damage through a combination of deformation and energy-dissipation measures (Y. Park & Ang, 1985; Y.-J. Park et al., 1987). This DI model has been extensively used for steel and reinforced concrete structures, where its parameters are well-calibrated based on established material and structural behavior under seismic loading.

While the Park and Ang DI proved effective for many structural types, its application to light wood-frame buildings introduced unique challenges. Light wood-frame structures are widely used in North America for their cost-effectiveness and favorable thermal properties. However, their inherent material variability, construction diversity, and reliance on non-structural components like stucco and sheathing make them particularly vulnerable under seismic loading. The original DI parameters, especially the calibration factor β, were not tailored to account for the unique cyclic behavior and failure modes of light wood-frame buildings. Consequently, early applications of the DI to such structures often resulted in inconsistencies and inaccuracies, highlighting the need for further development. Despite the widespread use of Damage Indices (DIs) for various structural systems, no rigid framework or standardized guideline has been established for calculating the DI specifically for light wood-frame buildings. The lack of a straightforward and rigorous approach

has created challenges in ensuring consistency and reliability when evaluating seismic performance for these structures using Damage Index. This study aims to address this gap by providing a systematic, step-by-step methodology for calibrating and applying the Damage Index framework to light wood-frame buildings.

Over the years, efforts have been made to adapt and refine the seismic health and risk assessment tools for light wood-frame structures. A significant milestone in this endeavor was the initiation of large-scale experimental studies, such as the NEESWood benchmark test project. This project aimed to address the seismic vulnerabilities of light wood-frame buildings and provide data (independent of this study and only publicly available data is utilized for validation and correlation in this study) to enhance seismic risk assessment tools like Damage Index.

The NEESWood project, conducted at the University at Buffalo, investigated the seismic performance of two-story wood-frame residential buildings. Using real-world seismic data, such as ground motions from the Northridge Earthquake, researchers examined the progression of damage across structural and non-structural components under varying intensities. The findings underscored the role of construction details, such as nail spacing and wall configurations, in influencing damage patterns and structural stability (Christovasilis et al., n.d.; van de Lindt, 2009). This experimental campaign not only expanded the understanding of seismic damage in wood-frame buildings but also provides damage details and response data that can be utilized in validation and calibration of different damage index models. Specifically, the β parameter in the Park and Ang DI, which accounts for material and connection behavior under cyclic loading, was found to vary significantly in light wood-frame structures due to factors like nail spacing, sheathing type, and retrofitting strategies. Incremental Dynamic Analysis (IDA) validated by this NEESWood benchmark test structure has been utilized for beta calibration purpose in this study.

To further advance the understanding of seismic performance and refine the application of the Damage Index (DI) framework for light wood-frame buildings, this study undertook a detailed and systematic approach leveraging data from the NEESWood benchmark project. As discussed earlier, Incremental Dynamic Analysis (IDA) was employed as the primary tool for calibrating the beta parameter in the Park and Ang DI equation, which reflects the hysteretic behavior of structural components. This calibration formed the backbone of the study, ensuring the Damage Index accurately represented the unique cyclic behavior and failure mechanisms of light wood-frame structures.

The core methodology involved several critical steps. First, a nonlinear structural model of the NEESWood two-story light wood-frame benchmark structure was developed using the Timber3D MATLAB package. This package enabled precise modeling of the building's nonlinear dynamic response, accounting for the specific material properties, connection details, and structural configurations. Ground motion data, including records from the Northridge Earthquake, were applied to simulate the seismic behavior under varying intensities.

The beta parameter calibration was conducted through a range of ground motion intensities using IDA. This analysis helped establish a global beta values tailored to the NEESWood two story light wood-frame benchmark structure, ensuring that the DI framework reflected the unique material and connection behavior of the light wood-frame building. Once the beta calibration was complete, the model was rigorously validated against observed responses from the NEESWood benchmark tests. This validation ensured that the numerical model reliably predicted the seismic performance and damage patterns observed during the actual tests, providing confidence in the calibrated beta values.

Following validation, the calibrated beta values were used to calculate the Damage Index for each structural component under various seismic scenarios. The calculated DI values were then compared to observed damage from the benchmark tests to evaluate their reliability and accuracy. This comparison demonstrated how well the calibrated beta values captured the progression of damage across different intensities and structural configurations.

The study also extended the analysis beyond a single intensity level, conducting DI calculations for a series of progressively increasing ground motion intensities. This allowed for an exploration of how damage evolved with seismic intensity, providing insights into the relationship between the Damage Index and the severity of observed damage. By observing trends in DI values and corresponding structural responses, the study captured critical transitions, such as the onset of significant cracking or near-collapse behavior, highlighting the robustness of the calibrated Damage Index framework.

Overall, this comprehensive study represents a significant contribution to the field by providing a systematic methodology for calibrating and validating the Damage Index framework for light wood-frame buildings. The results not only offer a reliable tool for performance-based seismic assessment but also pave the way for future studies to refine damage quantification methods and improve structural design practices.

1.2 Problem Statement

The assessment of seismic damage in structures has relied heavily on the development of frameworks like the Park and Ang Damage Index (DI), which quantify damage by combining deformation and energy-dissipation parameters. While these frameworks have been extensively calibrated and validated for steel and reinforced concrete structures, their application to light

wood-frame buildings remains inadequate. Light wood-frame structures are characterized by significant variability in materials, construction practices, and reliance on non-structural components such as sheathing and finishes, making them particularly complex to assess using existing damage index frameworks. This inherent variability and the diverse ways in which light wood-frame buildings respond to seismic events have highlighted the need for a tailored damage index framework.

Unlike steel and concrete structures, light wood-frame buildings exhibit unique failure modes, such as nail slip, sheathing degradation, and interaction between structural and non-structural elements. These behaviors are influenced by factors such as wall configurations, nail spacing, and construction quality, creating a level of uncertainty that is yet to be addressed by rigorous Damage Index based damage correlation. Furthermore, existing frameworks often rely on global assumptions that fail to capture the nuanced behavior of individual components, which is essential for understanding the overall seismic performance of light wood-frame structures.

To date, there has been no systematic effort to develop or calibrate a comprehensive damage index framework specifically tailored to light wood-frame buildings. Such a framework requires detailed observations and modeling of individual building behaviors to account for the variability inherent in these structures.

This lack of a tailored and reliable damage index framework limits the ability to assess and predict the seismic performance of light wood-frame buildings accurately. Addressing this gap is essential for ensuring the safety and resilience of these widely used structures, particularly in regions prone to seismic activity.

1.3 Research Objectives

This research is focused on addressing critical limitations in the calibration of the β parameter within the Park and Ang Damage Index (DI) as it applies to light wood-frame buildings. Unlike steel or reinforced concrete structures, light wood-frame buildings exhibit unique variability and complexity due to their construction methodologies and material properties. The β parameter, which captures cyclic loading behavior and calibrates the DI equation to correlate anticipated damage in real scale, has not yet been calibrated at a global level for these structures. This lack of calibration hinders the model's accuracy and utility in assessing seismic damage for light wood-frame buildings. To bridge this gap, this study aims to demonstrate a framework for global-level β calibration, moving beyond the impracticality of wall-by-wall calibration approaches and addressing the need for a more holistic understanding of the seismic behavior of entire structures. By integrating results with experimental result from large-scale studies such as NEESWood (Christovasilis et al., 2007; Van de Lindt, 2009), the research will validate β values and calculated DI values to see if they align well with observed damage patterns or not.

The objectives of this study can be summarized as follows:

1. **Demonstrating a Global-Level Calibration of the β Parameter for Light Wood Frame Structure:** Demonstrate a global-level calibration of the β parameter in the Park and Ang Damage Index (DI) framework tailored for light wood-frame buildings, addressing their unique seismic behavior and structural characteristics.
2. **Establishing a Comprehensive and Validated Framework for Damage Index Calculation:** Develop a step-by-step, comprehensive guideline for calculating the Damage Index (DI) for light wood-frame buildings. This framework is validated by correlating the

calculated DI values to the actual damage observed during benchmark experimental tests, ensuring the methodology is both accurate and reliable for practical seismic damage assessment.

1.4 Thesis Structure

This thesis is organized into seven chapters, each addressing a critical component of the study:

- Chapter 1: Introduction

This chapter provides the background, problem statement, and objectives of the study, outlining the motivation and significance of developing a validated Damage Index (DI) framework tailored for light wood-frame buildings.

- Chapter 2: Literature Review

A comprehensive review of existing seismic damage assessment practices, the evolution of damage indices, and the Park and Ang Damage Index model. The chapter also discusses parameters critical for DI calculation, such as ultimate displacement, equivalent yield force, and beta calibration, and explores global-level modeling methodologies.

- Chapter 3: Shaking Table Tests for Validation

This chapter introduces the benchmark NEESWood two-story test building, detailing its architecture, test setup, shaking table instrumentation, and damage observations from Phase 5 testing, which serve as validation data for the proposed framework.

- Chapter 4: Numerical Model Development

Focused on the development and validation of the Timber 3D numerical model, this chapter explains the modeling approach, including structural representation, master-slave systems, diaphragm modeling, and dynamic analysis, followed by detailed validation using modal and response spectrum analyses.

- Chapter 5: Damage Index Model Calibration

This chapter introduces the global beta calibration process, starting from Incremental Dynamic Analysis (IDA) to identify collapse intensities, pushover analysis, and dynamic analysis of the benchmark model. A sample beta value calculation is also presented, highlighting the importance of global-level calibration.

- Chapter 6: Damage Index Calculation and Correlation

This chapter demonstrates the application of the calibrated DI framework, including component-level and global-level damage index calculations. The calculated values are validated against observed damage from the NEESWood tests, and trends across varying seismic intensity levels are analyzed to assess the reliability of the methodology.

- Chapter 7: Conclusion

The thesis concludes by summarizing the study's contributions, emphasizing the validated framework for DI calculation, and providing recommendations for future research on light wood-frame buildings.

2 Literature Review

2.1 Overview of Seismic Damage Assessment in Light Wood-Frame Buildings

Seismic damage assessment is a fundamental aspect of earthquake engineering, aimed at quantifying damage levels to predict building performance and mitigate risks during earthquakes. While general frameworks for damage assessment are well-established for steel and concrete structures, their application to light wood-frame buildings presents unique challenges due to the distinctive behavior of these structures under seismic loads. Light wood-frame buildings, widely used for residential purposes in North America, require specific adaptations to existing methodologies to account for their variability in material properties, reliance on non-structural components, and diverse construction practices (Van de Lindt et al., 2010).

2.1.1 Seismic Damage Assessment Practices

For steel and reinforced concrete structures, damage assessment frameworks have traditionally relied on methodologies that integrate deformation-based indices, such as inter-story drift, with energy-dissipation measures. Tools like the Park and Ang Damage Index (DI) (Park & Ang, 1985) have been extensively used for these structures due to their clear cyclic response behavior, ductile failure modes, and well-established calibration parameters. These approaches utilize a combination of experimental data, numerical modeling, and Incremental Dynamic Analysis (IDA) to quantify structural damage levels under varying seismic intensities. While these methods have been successful for steel and concrete buildings, their direct application to light wood-frame buildings is often problematic. Light wood-frame structures exhibit highly redundant load paths and rely significantly on interactions between structural and non-structural components, such as sheathing, nails, and stucco. This results in unique damage progression mechanisms, including

localized failures, material cracking, and degradation of non-structural components, which are not adequately captured by traditional frameworks.

For light wood-frame structures, damage assessment frameworks need to address their distinct characteristics, including material variability and highly distributed load-sharing mechanisms. Several key methodologies for seismic performance evaluation have emerged, including:

a) **Experimental Testing**: Large-scale experimental studies, such as those conducted under the NEESWood project, have been critical in identifying the damage progression mechanisms of light wood-frame buildings. These studies utilize shake tables to replicate earthquake scenarios and capture detailed failure modes, such as the separation of sheathing from framing and loss of nail connections (van de Lindt, 2008).

b) **Numerical Modeling**: Advanced numerical modeling tools, such as Timber3D, are tailored for simulating the nonlinear response of light wood-frame structures. These models incorporate component-level behaviors, including hysteretic behavior of shear walls and energy dissipation mechanisms, and are validated using experimental data to ensure reliability (Christovasilis et al., 2007).

c) **Hybrid Approaches**: Hybrid approaches combining numerical simulations with empirical and experimental data provide a robust framework for damage assessment. For instance, the calibrated beta parameter in the Park and Ang DI has been adapted using global structural response metrics from numerical model, ensuring the framework aligns with observed damage patterns specific to light wood-frame buildings.

2.2 Evolution of Damage Indices in Structural Health Monitoring

The concept and development of damage indices have advanced significantly over the years to meet the growing demand for precise tools to evaluate seismic damage and assess the health of

structures. A damage index is a quantitative measure that combines parameters such as deformation and energy dissipation to represent the extent of damage sustained by a structure under seismic loads. Early approaches relied on simple deformation-based metrics, offering a rudimentary understanding of structural performance during earthquakes. However, as research expanded, it became evident that these basic metrics were insufficient to capture the complex, nonlinear behavior of structures during seismic events. This led to the evolution of more advanced damage index models, incorporating cyclic loading effects, cumulative energy dissipation, and other parameters critical to accurately reflecting the progressive nature of seismic damage. These refined models have become essential tools in performance-based seismic design and structural health assessment.

One of the earliest breakthroughs was the Park and Ang Damage Index (DI), introduced in 1985. This model combined deformation parameters with energy dissipation metrics, offering a more comprehensive framework for evaluating seismic damage in steel and reinforced concrete structures (Park & Ang, 1985). Its ability to integrate multiple damage mechanisms into a single numerical value marked a significant step forward in structural health monitoring, setting the foundation for subsequent models.

As understanding of seismic behavior deepened, researchers began exploring more specialized approaches. Displacement-based damage indices emerged as an extension of basic deformation models, relying on measurable displacement thresholds to estimate damage levels (Iranmanesh & Ansari, 2014). While these indices provided a straightforward and practical method for damage assessment, they often failed to account for energy dissipation—a critical factor in materials like reinforced concrete and wood that exhibit significant cyclic degradation.

Recognizing this limitation, energy-based damage indices were introduced to capture the cumulative effects of seismic energy input. These models emphasized the role of energy absorption and dissipation in determining structural health, making them particularly valuable for structures subject to repeated loading (Xu et al., 2012). However, their application required precise calibration to account for the distinct hysteretic behaviors of different materials and structural systems.

Building on these advancements, researchers sought to integrate localized and global perspectives of structural damage. This effort led to the development of the Global Damage Index (GDI), which combined displacement and energy metrics into a holistic assessment framework (Pan et al., 2020a). The GDI bridged the gap between local damage states—such as those observed in specific structural elements—and the overall performance of complex systems. While effective for high-rise buildings and reinforced concrete frames, its adaptation for light wood-frame structures remains a challenge due to their unique reliance on non-structural components and connections.

Over time, these developments have shaped the field of structural health monitoring, providing a range of tools tailored to different materials and structural systems. Yet, the application of these indices to light wood-frame buildings is still evolving, requiring further research to address their unique seismic response characteristics.

2.3 Energy and Deformation Based Damage Model: Park and Ang Damage Index

Damage indices have become reliable tools in seismic damage assessment, providing numerical measures to evaluate structural performance during earthquakes. The Park and Ang Damage Index (1985), combining deformation parameters and energy dissipation, is widely used for reinforced concrete and steel structures due to its ability to capture seismic behavior comprehensively (Park

& Ang, 1985). Displacement-based models, focusing solely on deformation thresholds, are effective for straightforward assessments but lack precision for cyclic loading effects (Iranmanesh & Ansari, 2014). Energy-based indices address this limitation by incorporating cumulative energy absorption, offering enhanced applicability for materials with hysteretic behaviors (Xu et al., 2012). These indices have been widely integrated into tools like fragility curves and Incremental Dynamic Analysis (IDA), further solidifying their role in both research and practical seismic risk assessment (Vamvatsikos & Cornell, 2002).

2.3.1 Park and Ang Damage Index Model

The Park and Ang Damage Index (1985) is a landmark contribution to the field of earthquake engineering, reflecting a paradigm shift in how seismic damage is quantified and assessed. Before its establishment, seismic damage assessment primarily relied on simple deformation-based measures or observational damage scales, such as the Modified Mercalli Intensity (MMI) scale, which, while useful, lacked the precision and quantifiability required for advanced structural analysis and design. These methods could not adequately capture the complex, cumulative effects of seismic loading on structures, particularly under repeated and cyclic stresses.

The Park and Ang Damage Index introduced a systematic framework that combined two critical parameters: deformation and energy dissipation. By integrating maximum deformation (displacement) and cumulative hysteretic energy, the model addressed the shortcomings of earlier methods that focused solely on peak displacements. This dual-component approach provided a more comprehensive measure of structural damage by accounting for both the immediate and cumulative effects of seismic forces. It enabled engineers and researchers to evaluate structural performance beyond simple elastic or plastic thresholds, paving the way for more accurate predictions of collapse and failure.

The innovation of the Park and Ang Damage Index lies in its ability to move beyond traditional elastic and plastic thresholds, providing a nuanced understanding of structural behavior under seismic forces. It formed the basis for modern seismic design practices by enabling damage quantification in terms of engineering demand parameters (EDPs) such as drift and energy dissipation, paving the way for tools like fragility curves and Incremental Dynamic Analysis (IDA) (Vamvatsikos & Cornell, 2002). Furthermore, its applicability to various structural systems—including reinforced concrete, steel, and more recently, light wood-frame buildings—demonstrates its versatility and enduring relevance in addressing the unique challenges posed by diverse structural types and seismic conditions (Park & Ang, 1985; Xu et al., 2012).

2.3.2 Mathematical Expression of the Park and Ang Damage Index

The Park and Ang Damage Index (DI) is formulated as a dimensionless parameter that quantifies the cumulative damage sustained by a structure under seismic loading. The key motivation behind developing a dimensionless equation is to ensure that the damage measure remains independent of absolute scale, making it applicable across different structural systems, loading conditions, and material properties.

Unlike traditional displacement-based indices, which rely solely on peak response parameters, the Park and Ang Damage Index integrates both maximum deformation and hysteretic energy dissipation, capturing the cumulative effects of cyclic loading.

The general dimensionless form of the Park and Ang Damage Index is expressed as:

$$DI = \frac{D_{max}}{D_u} + \beta \cdot \frac{E_i}{F_y \cdot D_u} \qquad (1)$$

where:

DI = Park and Ang Damage Index

D_{max} = Maximum displacement

D_u = Ultimate displacement capacity

β = Empirical calibration parameter

E_i = Cumulative hysteretic energy dissipation

F_y = Equivalent yield force

This equation presents two fundamental damage components:

Deformation-based component: The first term, $\frac{D_{max}}{D_u}$ represents the ratio of peak displacement to ultimate displacement, providing a direct measure of how close the structure is to its failure limit.

Energy-based component: The second term, $\beta \cdot \frac{E_i}{F_y \cdot D_u}$, accounts for the effect of cyclic energy dissipation, reflecting the cumulative inelastic deformations sustained by the structure over the duration of seismic loading.

2.3.3 Ultimate Displacement Parameter

The Ultimate Displacement Parameter (D_{ult}) is a critical factor in the Damage Index (DI) equation, representing the maximum allowable displacement a structure or component can sustain before failure. For shear walls, this parameter is typically determined through experimental monotonic or cyclic testing, as discussed extensively in the literature (e.g., (Van De Lindt, 2005)). Such tests involve applying increasing lateral loads to isolated wall specimens with different nail spacings. These experiments have provided standardized values for shear walls commonly used in light wood-frame buildings, facilitating damage index calibration at the component level.

However, when performing global beta calibration for an entire structure, the definition and determination of D_{ult} must shift to reflect the collective behavior of the building under seismic loads. For full-story or full-structure models, the Ultimate Displacement Parameter represents the roof displacement at the anticipated collapse state of the building. This collapse level is

characterized by the point at which no base shear force is observed, as captured in the global pushover curve of the numerical model. Unlike component-level tests, the global D_{ult} is derived from pushover analysis of the entire building model and must account for the dynamic interactions between structural and non-structural elements, as well as the unique properties of the specific building under consideration. The distinction between component-level D_{ult} and global D_{ult} is crucial. While experimental values from shear wall tests can guide initial estimates, the ultimate displacement for global beta calibration must be determined for the specific building being analyzed.

2.3.4 Equivalent Yield Force Parameter

The Equivalent Yield Force Parameter (F_y) quantifies the force at which a structure or component transitions from elastic to inelastic behavior. Similar to D_{ult}, F_y has been extensively studied for shear walls through experimental testing.

For global beta calibration, F_y must represent the equivalent yield force of the entire building rather than individual components. This parameter is derived from the global pushover curve, capturing the force at which the entire structure transitions from elastic to inelastic behavior. Unlike the experimentally determined F_y for shear walls, the global F_y accounts for the cumulative contributions of all structural and non-structural components, as well as their interactions during seismic loading. The pushover analysis of the numerical model provides a comprehensive framework for determining this parameter, ensuring that it reflects the unique properties and configuration of the specific building under analysis.

2.3.5 Component Level Parameter Values Derived from Experimental Shear Wall Test

To date, many studies (Van De Lindt, 2004) have been done to evaluated these two key parameters and through that, it is well-established that experimental monotonic testing is essential for accurately determining them. However, to perform monotonic shear wall tests for each building to calculate the Damage Index (DI) is neither time-efficient nor practical. Nevertheless, wood-frame buildings are constructed according to standard guidelines that standardize construction procedures for wood shear walls; for example, the use of 2x4 studs is common in stick-frame wood construction. Yet, a significant variable in wood shear walls is nail spacing, which directly influences the strength properties of the wall. Consequently, research has focused on this variable when determining the two key parameters for wood shear walls.

$$F_{yield} = -0.16s + 38.5 \quad (2)$$

$$D_{ult} = 0.28s + 121 \quad (3)$$

In a study conducted by Van De Lindt in 2005 on wood frame shear walls, static displacement tests were performed on various shear wall specimens with different nail spacing configurations (76 mm, 102 mm, and 152 mm). Figure 1(c) shows typical schematic of a wood shear wall where the edge nails (highlighted in red) are spaced closely together, while the nails on the inside (highlighted in blue) are spaced farther apart. Figure 1(d) presents the schematic of the test setup used by Van De Lindt for conducting experiments, which provided the parameters for the DI equation. The findings of this study (Van De Lindt, 2005) led to the proposal of relationships between nail spacing and the corresponding equivalent yield force and ultimate displacement. These proposed relationships as shown in the equation (2) and (3), are graphically presented in Figure 1(a), illustrating the correlation between nail spacing and D_{ult} as well as F_{yield} for wood shear walls. Here, s is the nail spacing in mm and D_{ult} & F_{yield} are in mm and KN respectively.

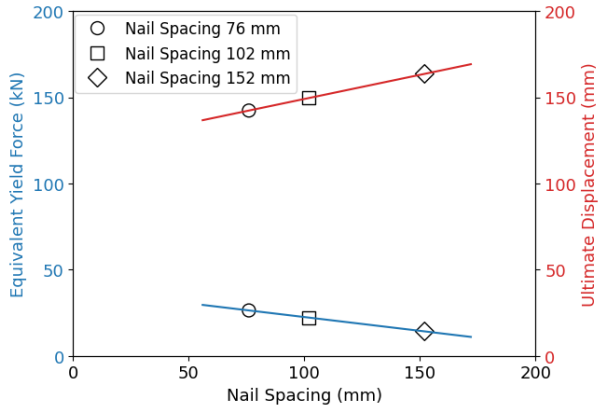

(a)

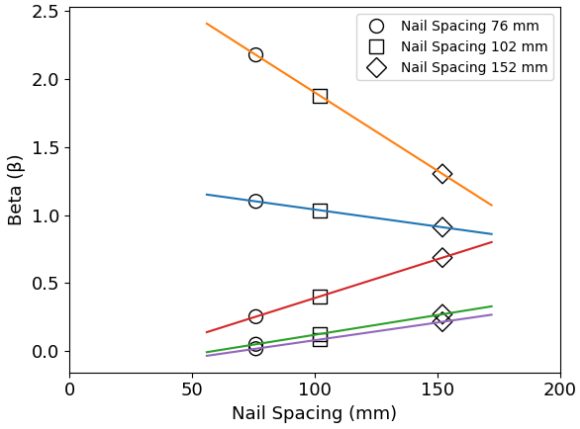

(b)

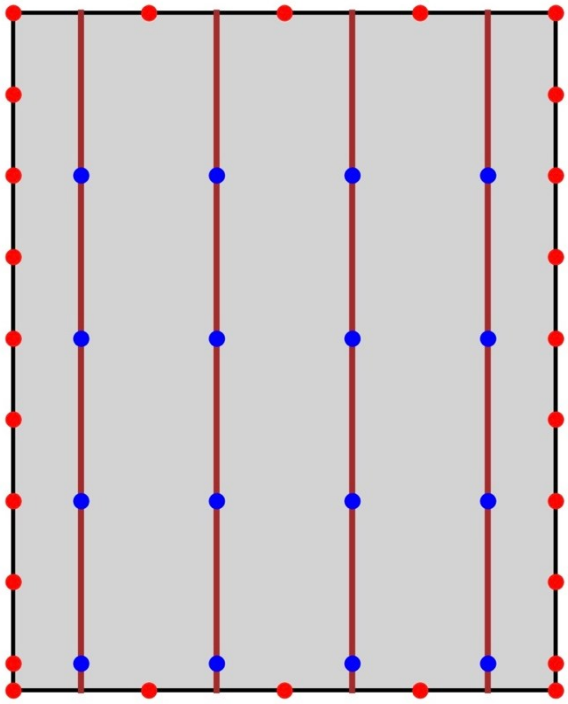

(c)

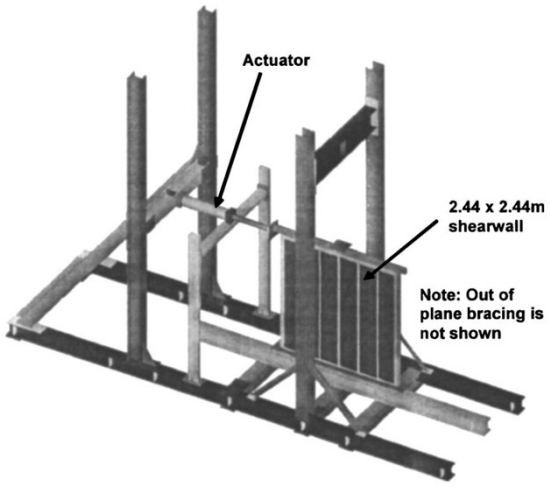

(d)

Figure 1. (a) D_{ult} and F_{yield} as a function of nail spacing (b) β as a function of nail spacing and damage limit state. (Van De Lindt, 2005)(c) schematic representation of edge and inside nail spacing of a typical shear wall (d) schematic of the test set-up for shear wall testing (Van De Lindt, 2005)

Another study (Pei et al., 2013) conducted on 9 different wood shear wall specimens under two different loading protocol to investigate the limit strength. The study outcome shows very similar yield strength for different nail schedules which supports the proposed correlation by Van De Lindt. Additionally, this study by Pei et al. also suggests that vertical load has very insignificant impact on equivalent yield force determination which reasonably justifies the adoption of this proposed relationship with nail spacing for shear walls at different story level for multistory wood building. A separate study (He et al., 1999) for monotonic loading on wood shear wall with varying amount of opening and nail spacing (76, 102 and 152 mm) has also shown similar result for both displacement and yield force as the proposed relationship. Finally, wood shear wall testing under ATC-71 project (Update Seismic Rehabilitation Guidance Program Definition and Guidance Development: Part -1: Workshop Proceeding, 2008) by Federal Emergency Management Agency (FEMA) suggests and further validates the proposed correlation discussed.

2.3.6 Beta β Parameter

The practicality of the DI model in assessing damage of any building greatly depends on β value. The β value calibrates the DI model and helps to establish a realistic limit state for damage. Study (Y.-J. Park et al., 1987) on concrete and steel building shows reliably constant β value, 0.05 and 0.025 correspondingly. However, β for wood building is highly variable ranging from 0.05 to more than 1.00 (Pan et al., 2020b). Hence, appropriately determining β value for wood shearwall is the biggest challenge in Damage Index (DI) calculation for wood building.

Incremental Dynamic Analysis (IDA) is one way of determining the β value for wood shear walls by identifying collapse intensity levels under earthquakes, marked by the IDA curve slope dropping below 5% (Liang, 2007). Nonlinear dynamic analysis with a damage index (DI) of 1.00 (Liang et al., 2011)integrates hysteretic energy to solve for β according to equation 4.

$$\beta = \frac{\left(DI - \frac{D_{max}}{D_{ult}}\right) * F_y * D_{ult}}{\int dE} \quad (4)$$

2.3.7 Finite Element Modeling of Light Wood Frame Building

Finite Element Modeling (FEM) has been a cornerstone of research in understanding the dynamic behavior of light wood frame buildings under seismic and wind loading. It enables the detailed representation of components such as framing members, sheathing panels, and connections, allowing for the simulation of deformation, energy dissipation, and failure mechanisms. FEM is widely utilized in advanced software like ABAQUS, ANSYS, and SAP2000 to explore the performance of wood structures at both component and system levels.

While FEM provides a powerful tool for analyzing wood frame structures, its application is hindered by several limitations:

a) **Computational Challenges:** Finite element modeling (FEM) requires solving highly nonlinear equations to account for material properties, connection slip behavior, and dynamic interactions. This complexity becomes particularly pronounced when analyzing multi-story buildings or conducting nonlinear time-history simulations. For instance, (Kasal et al., 1994) emphasized the computational burden of capturing detailed nonlinearities in the connections and materials, especially for full-structure simulations. Similarly, Folz and Filiatrault (2001) highlighted the challenges of achieving convergence in dynamic analyses, which often translate into long computation times, making FEM computationally expensive for large-scale applications.

b) **Modeling Challenges:** The inherent nonlinear behavior of wood and its connections, such as nail slip, hold-down deformations, and sheathing-to-framing interactions, is a critical challenge in FEM analysis. Kasal et al. (1994) meticulously modeled these nonlinearities,

providing insight into their significant influence on the global response of wood-frame buildings. However, simplified approaches, such as those noted by Pang and Rosowsky (2010) and Cattari et al. (2014), often struggle to replicate these interactions accurately, leading to potential discrepancies in predicting the overall structural performance.

c) **Mesh Dependency and Scalability:** FEM models are sensitive to mesh quality, with finer meshes needed to capture localized stress concentrations and deformations. This increases computational cost and can lead to numerical instability in dynamic simulations of large systems (Pei et al., 2013).

d) **Boundary and Interaction Assumptions:** Assumptions regarding diaphragm rigidity, base fixity, and interaction between wall panels and diaphragms often simplify the model but reduce accuracy. These assumptions are particularly limiting for light wood frame structures, where semi-rigid behavior significantly affects global performance (van de Lindt et al., 2010).

e) **Practical Limitations in Routine Design:** The complexity and computational demands of FEM make it impractical for routine engineering design. Practitioners often favor simplified methods, as FEM requires significant expertise in defining material models, interaction effects, and boundary conditions (Filiatrault & Folz, 2002).

2.3.8 Global Level Modeling of Light Wood Frame Building

Numerical modeling plays a vital role in understanding the dynamic behavior of light wood-frame buildings and shear walls under seismic loads. These models provide insights into deformation mechanisms, energy dissipation, and failure patterns, enabling better design and retrofit strategies. Early numerical models for wood-frame buildings relied on finite element methods (FEM) to represent the nonlinear response of wood-frame structures. These methods used detailed

representations of studs, sheathing panels, and connections through beam elements, plane-stress elements, and nonlinear springs, respectively (Estrella et al., 2020). Despite their accuracy, such models were computationally expensive, limiting their applicability in routine design.

Simplified models such as SAWS (Seismic Analysis of Light wood frame Structures) emerged to address these limitations. This lumped-mass model assumes rigid diaphragms and uses ten-parameter hysteretic models for shear walls, balancing computational efficiency and accuracy. It has been widely used for low-rise wood-frame buildings (Pei & Van De Lindt, 2009).

Similarly, the CASHEW (Cyclic Analysis of Shear Walls) model introduced an effective means of simulating the nonlinear force-displacement behavior of wood-frame shear walls using simplified spring elements. The subsequent M-CASHEW model expanded on this by adding capabilities to account for cyclic degradation and computational optimization, making it a widely applicable tool for both research and practical design scenarios.

2.3.8.1 MSTEW Model Parameters and Their Effectiveness in Timber3D

The Modified Stewart Hysteretic Model (MSTEW) represents a critical advancement in simulating the nonlinear cyclic behavior of light wood-frame shear walls and diaphragms under seismic loading. Evolving from the foundational work of Stewart (1987), which introduced a hysteretic model for degrading and pinched structures, MSTEW incorporates additional parameters to address the unique mechanical behaviors observed in timber structures, including stiffness degradation, strength degradation, and energy dissipation. Over time, this model has been refined and integrated into structural analysis platforms, such as Timber3D, to accurately simulate the performance of light wood-frame buildings during seismic events.

The MSTEW model's development is rooted in early work on cyclic hysteretic behavior, specifically targeting wood-frame structures. Stewart (1987) laid the groundwork by formulating

a model capable of capturing pinching effects and nonlinear responses in general structural systems. Building on this, (Folz & Filiatrault, 2001) extended these concepts to light wood-frame shear walls, introducing hysteretic parameters that accounted for cyclic degradation and load reversals.

Subsequent studies, such as those by (Pang et al., 2007), incorporated evolutionary parameters into hysteretic models, enhancing their applicability to timber shear walls subjected to seismic loading. The MSTEW model emerged as a further refinement, explicitly tailored to simulate the unique mechanical characteristics of wood-frame structures, such as nail slip, rocking mechanisms, and panel interactions. This evolution culminated in its integration into computational tools like Timber3D, which facilitated its use in large-scale analyses, including projects like NEESWood, that investigated seismic resilience in wood-frame buildings (Pang & Rosowsky, 2010).

Key Characteristics of MSTEW Model

a) Backbone Curve:

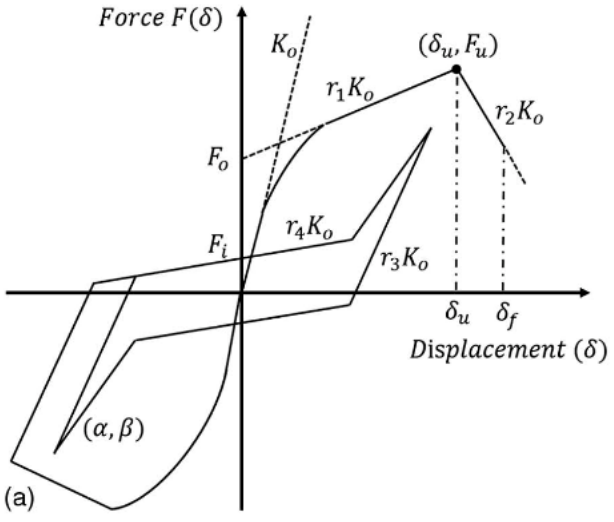

Figure 2. Backbone curves of MSTEW model (Pan et al., 2018)

The backbone curve as shown in the Figure 2, is central to the MSTEW model, defining the primary load-deformation behavior of shear walls. It includes elastic, post-elastic, and ultimate strength regions, ensuring the representation of nonlinear behaviors, including stiffness degradation at higher displacements (Ventura et al., 2021). This curve is calibrated using experimental data from shear wall tests to ensure accuracy in predictions.

b) Cyclic Degradation:

MSTEW introduces parameters to simulate cyclic degradation, accounting for the reduction in stiffness and strength during repeated loading cycles. These parameters are particularly relevant for wood-frame buildings, which exhibit significant hysteretic energy dissipation under seismic forces (Estrella et al., 2020).

c) Pinching Effect:

Pinching in the force-displacement hysteresis loop, caused by the slipping of nails and connectors, is explicitly modeled in MSTEW. This feature is critical for capturing the realistic dynamic response of shear walls, particularly under long-duration ground motions (Pan et al., 2018).

d) Energy Dissipation:

Energy dissipation is a key parameter that measures the cumulative energy absorbed by the shear walls during seismic events. MSTEW effectively models this parameter, providing insights into the structure's ability to resist collapse under severe cyclic loading (Ventura et al., 2021) .

Parameters of the MSTEW Model:

The Modified Stewart Hysteresis Model (MSTEW) incorporates a comprehensive set of parameters that enable it to simulate the nonlinear and cyclic behaviors of light wood-frame shear walls and diaphragms under seismic loading with precision. These parameters are designed to

represent critical aspects of material and connection behavior, including stiffness degradation, energy dissipation, and pinching effects, which are common in light wood-frame construction.

Key Parameters of the MSTEW Model

a) Initial Stiffness, K_0

Represents the stiffness of the spring at the beginning of loading.

b) Reloading Stiffness, K_p

Governs stiffness during reloading phases after unloading.

c) Maximum Backbone Force, F_u

Peak force on the backbone curve.

d) Force Intercept of Backbone, F_0

y-Intercept of the initial linear stiffness line on the backbone.

e) Displacement at F_u

Displacement where the maximum backbone force F_u is reached.

f) Pinching Parameters – r_1, r_2, r_3 and r_4

Control the degree of pinching in the hysteresis loop and the shapes of unloading/reloading paths:

- r_1: Pinching during unloading.
- r_2: Pinching during reloading.
- r_3: Controls backbone curve stiffness changes.
- r_4: Adjusts post-yield stiffness.

g) Strength Degradation Factor, α

Controls how the strength reduces after repeated cyclic loading.

h) Stiffness Degradation Factor, β

Governs the reduction in stiffness with increasing cyclic deformation.

2.3.8.2 Out-of-plane Stiffness of Light Wood Frame Buildings

The out-of-plane stiffness of light-frame buildings, particularly shear walls, is a critical aspect of their structural behavior, especially in seismic zones. While in-plane stiffness determines the shear wall's ability to resist lateral loads, out-of-plane stiffness is essential for ensuring the overall stability and load transfer mechanisms of the building. This is particularly relevant in light-frame wood buildings, which are characterized by their relatively low stiffness compared to other construction systems like reinforced concrete or steel (Véliz et al., 2023).

Out-of-plane stiffness contributes significantly to the holistic performance of a building under seismic loads. It influences load redistribution between structural and non-structural components and ensures that diaphragms and shear walls interact effectively to resist complex loading scenarios. Neglecting or inaccurately representing this parameter can lead to underestimated deformations and unsafe design outcomes. The bending stiffness component, which governs out-of-plane deformation, can be represented mathematically as (Véliz et al., 2024):

$$K_{\text{bending}} = \frac{2H^3}{3EA_{\text{ext}}L^2}$$

Here:

K_{bending} : Bending stiffness, representing the wall's resistance to out-of-plane deformation.

H : Height of the shear wall.

E : Elastic modulus of the material (e.g., sheathing or framing components).

A_{ext} : Effective cross-sectional area of the shear wall in the bending plane.

L : Span length of the wall.

This equation, derived from the principles of mechanics of materials, captures the flexural rigidity of the wall system under out-of-plane loads. The height (H) and span length (L) are critical geometric parameters that define the wall's susceptibility to bending deformations, while the elastic modulus (E) and cross-sectional area (A_{ext}) account for the material and geometric properties that influence stiffness.

2.3.9 Mass Distribution in Numerical Modeling

The distribution of mass within light-frame timber diaphragm systems plays a crucial role in accurately modeling their dynamic behavior under seismic loads. In numerical modeling, mass is often assigned using a lumped mass approach to simplify the analysis while maintaining fidelity to the structural behavior. This method involves distributing seismic weights to critical points, such as diaphragm nodes or shear wall connections, to represent the inertia forces during seismic events (Pang & Rosowsky, 2010).

Typically, master nodes are introduced at key diaphragm locations, with masses distributed proportionally based on the structural and non-structural components. These master nodes are connected to slave nodes through rigid elements, ensuring that the mass is transferred and engaged in the overall system response. The seismic weights are calculated based on the total structural and applied loads, accounting for variations across different building components and construction phases (Folz & Filiatrault, 2001).

The diaphragm's mass distribution affects how loads are transferred between diaphragms and shear walls, influencing the interaction between in-plane and out-of-plane forces. An effective

mass distribution model must consider both horizontal and vertical load paths, ensuring that the simulated seismic response closely matches real-world behavior (Véliz et al., 2024).

2.4 Incremental Dynamic Analysis

Incremental Dynamic Analysis (IDA) is a crucial methodology in seismic performance assessment, providing a systematic framework to evaluate structural response under increasing levels of ground motion intensity. In this study, IDA plays a key role in determining collapse intensity, which is essential for calibrating the β parameter in the Park and Ang Damage Index (DI) framework for light wood-frame buildings. The collapse intensity defines the seismic demand level at which the structure reaches its ultimate limit state, allowing for a more accurate global-level damage assessment.

By incrementally scaling a suite of ground motion records and performing nonlinear dynamic analyses, IDA provides a comprehensive understanding of structural behavior under extreme loading conditions. This methodology enables the identification of critical intensity measures, such as peak ground acceleration (PGA) and spectral acceleration (Sa(T)), that correspond to key performance thresholds, including yielding, peak strength, and collapse. Given the unique characteristics of light wood-frame structures—such as load redistribution, nonlinear energy dissipation, and complex failure mechanisms—IDA serves as an indispensable tool for establishing realistic collapse criteria.

Incremental Dynamic Analysis (IDA) is a performance-based seismic assessment method that involves subjecting a structural model to a series of ground motion records, incrementally scaled

to increasing intensity levels. This procedure provides a detailed picture of how structures transition from elastic to inelastic behavior and ultimately to collapse.

The IDA methodology was pioneered by Vamvatsikos and Cornell (2002) in their seminal work on performance-based earthquake engineering. It has since been widely adopted for seismic vulnerability assessment, particularly in conjunction with FEMA guidelines for evaluating structural collapse capacity (FEMA P695, 2009). IDA produces a set of response curves, known as IDA curves, which depict the relationship between ground motion intensity and structural response parameters such as maximum inter-story drift, base shear, or roof displacement.

2.4.1 FEMA Guidelines for Conducting IDA

The Federal Emergency Management Agency (FEMA) has played a pivotal role in shaping the methodological framework for seismic performance assessment through its detailed publications—FEMA P695 (2009) and FEMA P58 (2012). These documents outline rigorous procedures for conducting Incremental Dynamic Analysis (IDA), a core technique used in performance-based earthquake engineering (PBEE). IDA facilitates a nuanced understanding of how structures behave under progressively increasing seismic intensities, culminating in the identification of their collapse capacities.

The strength of the FEMA guidelines lies in their ability to standardize the IDA process, ensuring consistency, comparability, and reliability across various studies and engineering applications. By following these protocols, researchers and engineers can systematically quantify structural vulnerabilities and calibrate damage metrics using a scientifically grounded approach.

The key steps in the IDA process, as outlined in the FEMA P695 and P58 documents, are elaborated below:

2.4.1.1 Selection of Ground Motion Records

The first and foundational step in IDA is the careful selection of earthquake ground motion records that are representative of the seismic hazard at the target site. This involves curating a suite of ground motions that spans a broad spectrum of earthquake characteristics, including:

- Magnitude range
- Source-to-site distances
- Fault types (e.g., strike-slip, reverse, normal)
- Site soil conditions and spectral content

These records should be chosen based on probabilistic seismic hazard analysis (PSHA) results and in accordance with criteria recommended by FEMA and the Pacific Earthquake Engineering Research (PEER) Center. The goal is to ensure statistical representativeness, spectral compatibility, and hazard consistency, which are critical for achieving robust and generalizable IDA outcomes.

2.4.1.2 Scaling of Ground Motions

Once selected, each ground motion is incrementally scaled to various intensity levels—typically using spectral acceleration (Sa) at a specific period or peak ground acceleration (PGA) as the intensity measure (IM). This scaling allows for the exploration of the structure's behavior across a wide range of seismic demands.

Through this process, analysts can trace the transition from elastic to nonlinear and inelastic responses, ultimately reaching the point of global or local collapse. The progressive scaling is crucial for constructing IDA curves that plot the chosen IM against an Engineering Demand Parameter (EDP) such as inter-story drift ratio or roof displacement, offering a visual representation of performance degradation.

2.4.1.3 Nonlinear Dynamic Analysis

The core of IDA lies in performing nonlinear time-history analyses (NLTHA) on a detailed structural model subjected to each scaled ground motion. These models, often built using finite element methods (FEM) or equivalent simulation techniques, must capture a comprehensive range of response behaviors, including:

- Material and geometric nonlinearities
- Stiffness and strength degradation
- Energy dissipation through hysteresis
- Damage propagation and failure mechanisms

This analytical phase produces rich datasets from which IDA curves are generated. The shape and critical points of these curves—especially the collapse point—provide direct insight into the structure's seismic resilience, damage tolerance, and fragility. Moreover, these outputs serve as essential inputs for collapse fragility curves and for validating damage indices used in performance-based design.

3 Shaking Table Tests Used for Damage Observation and Model Validation

3.1 Background of the Project

Light wood frame structures have long been a staple of residential construction, particularly in regions of moderate to high seismicity. Historically, these structures have demonstrated commendable life safety performance during earthquakes. However, significant structural and non-structural damage has often been observed, even in low-rise configurations, highlighting vulnerabilities in their seismic behavior. The height of light wood frame buildings has traditionally been limited to four to six stories due to several factors, including:

a) **Dynamic Response Uncertainties**: A limited understanding of the seismic response of mid-rise light wood frame structures has posed challenges to their adoption in active seismic zones.

b) **Non-Structural Limitations**: Issues such as fire safety requirements and damage to non-structural finishes have restricted the widespread use of taller light wood frame construction.

c) **Lack of Global Seismic Design Philosophy**: Existing building codes for engineered wood construction are component-based, focusing on individual elements rather than adopting a global approach that considers the interactions between structural components.

These factors, compounded by the lack of clarity in load paths during earthquake shaking, have constrained the use of wood to low-rise buildings. This limitation has reduced the competitiveness of the wood construction industry relative to steel and concrete alternatives, particularly in the U.S. and international markets.

Recognizing these challenges, the NEESWood Project was conceived as part of the National Science Foundation's George E. Brown Jr. Network for Earthquake Engineering Simulation (NEES). The project's mission is to advance the seismic design of light wood frame structures, enabling their use in mid-rise buildings while addressing vulnerabilities in low-rise configurations. This study builds upon previously conducted research by incorporating benchmark data from the NEESWood two-story light wood frame shake table test. While the experiment itself was not part of this study, its data played a key role in validating the numerical analyses and shaping the methodology developed herein.

3.2 Test Building Architecture

The test structure utilized in the NEESWood benchmark testing is a two-story townhouse, representing one unit of a three-unit townhouse configuration, as illustrated in Figure 3 and Figure 5. This design provides approximately 1800 square feet of living space with an attached two-car garage. The structure is modeled as a "production house," reflecting typical construction practices of the 1980s and 1990s in Northern or Southern California.

The townhouse follows engineered construction principles compliant with the seismic provisions of the 1988 Uniform Building Code. The overall height of the building, from the first-floor slab to the roof eaves, is 18 feet, and its total weight is approximately 40 tons (80 kips). These architectural details make the structure a representative sample for assessing light wood frame behavior under seismic loads.

The exterior walls of the structure consist of a layered system, including:

a) Exterior finish: 7/8-inch stucco.

b) Sheathing: 7/16-inch oriented strand board (OSB).

c) Interior finish: 1/2-inch gypsum wallboard.

(a)

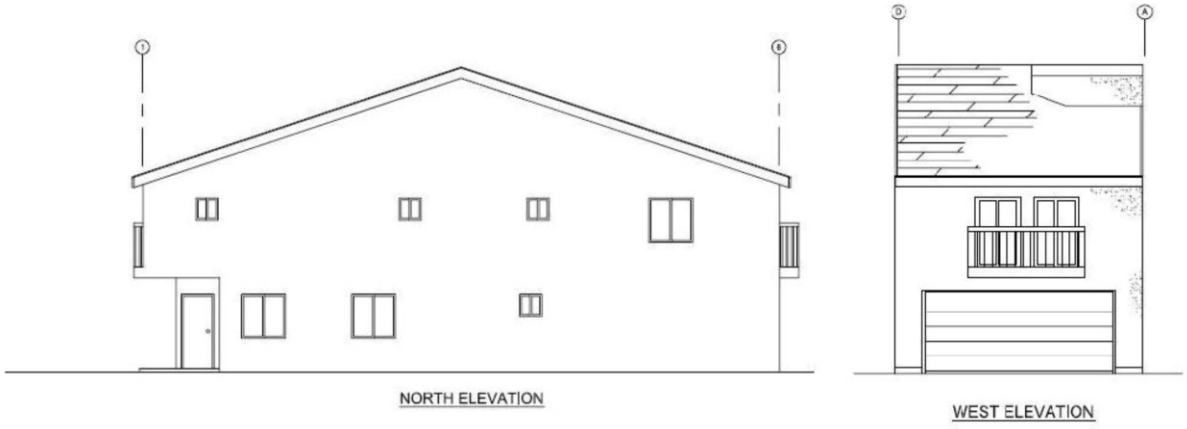

(b)

Figure 3 Elevation view of the NEESWood two-story residential project building (Christovasilis et al., n.d., 2009)

The structural framing of the shear walls employs 2x4 dimensional lumber, except for the first level of the garage, which uses 2x6 lumber. The framing includes double members for the top plates and end studs, while the sole plate and interior studs are single members. Stud spacing is maintained at 16 inches on-center. Conventional corner hold-downs are used to mitigate overturning and ensure the racking mode of deformation during seismic events.

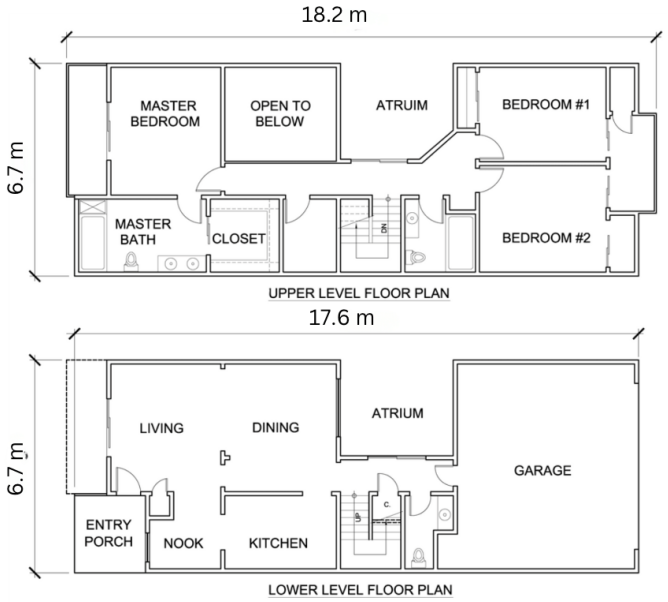

Figure 4 Floor plan layour of the NEESWood project building (Christovasilis et al., n.d., 2009)

The floor plan includes functional spaces such as living, dining, and bedroom areas as shown in the Figure 4, demonstrating typical residential configurations.

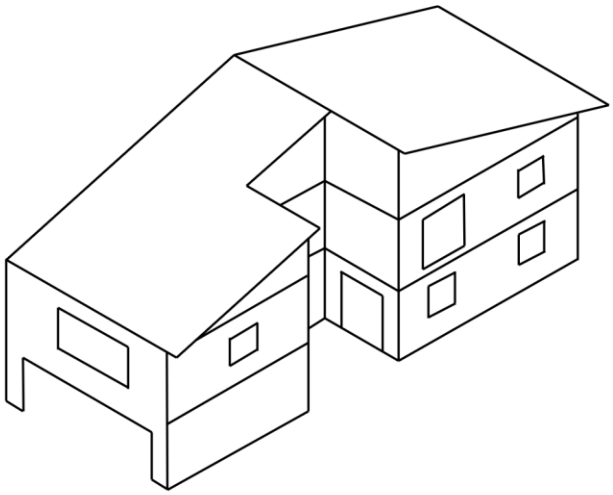

Figure 5 Isometric view of the project building

3.3 Shake Table Setup

The experimental test setup for the NEESWood benchmark structure was carried out at the Structural Engineering and Earthquake Simulation Laboratory (SEESL) at the University at Buffalo. Utilizing two tri-axial shake tables, the testing accommodated the full-scale two-story townhouse to simulate dynamic earthquake loading. Each shake table, weighing approximately 50 tons, was extended with 7 m x 7 m steel frames and connected through a rigid steel link structure to support the building's weight while minimizing vertical deflection as depicted in the Figure 6. This setup ensured the accurate simulation of seismic responses over a continuous platform.

The foundation of the test building was constructed with threaded A-307 steel rods that were bolted to the existing hole patterns in the extension frame. Anchor bolts were placed at critical locations, reinforced with 2-1/4 in. x 2-1/4 in. x 1/4 in. steel plate washers. At hold-down device locations, 5/8 in. diameter rods were employed, while 1/2 in. diameter rods were used elsewhere. A 2-1/4 in. layer of grout was installed beneath pressure-treated sill plates to emulate a true concrete foundation. The friction between the sill plate and the grout was intended to represent realistic base resistance conditions.

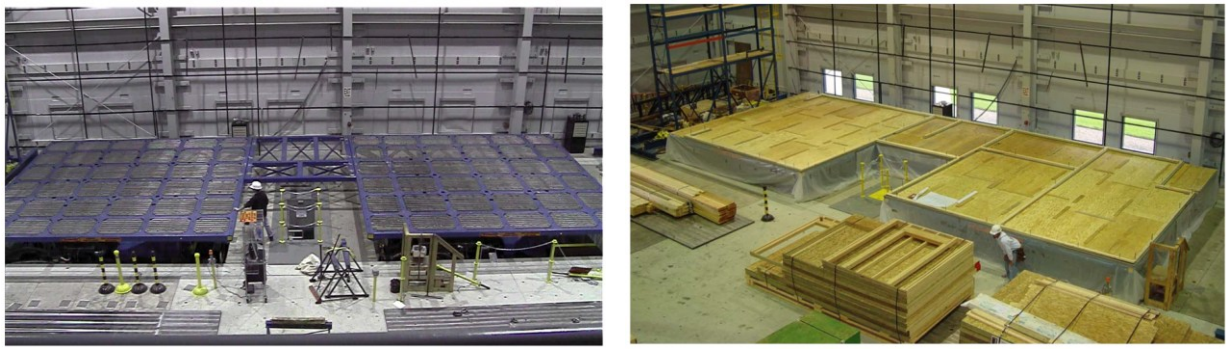

(a) (b)

Figure 6 (a) Extension frame of shake tables connected by steel link structure, and (b) Foundation of Test Building under Construction building (Christovasilis et al., n.d., 2009)

This experimental setup was designed to evaluate the dynamic response of the full-scale townhouse structure under seismic loading conditions. The setup also served as a benchmark for calibrating numerical models and for understanding load path behavior and structural interactions during earthquake events

3.4 Test Phases

The NEESWood benchmark testing program consisted of five distinct test phases, each representing a specific construction configuration of the two-story light wood frame townhouse. These phases were designed to systematically evaluate the dynamic behavior of the structure as various construction components and supplemental systems were incorporated. Table 1 provides a summary of these phases:

Phase 1: Wood Structural Elements Only

This phase included only the wood structural elements without any additional sheathing or supplemental damping systems. The focus was on establishing a baseline understanding of the bare structural response of the light wood frame system under seismic loading conditions.

Phase 2: Incorporation of Passive Fluid Dampers

Phase 2 involved the addition of passive fluid dampers integrated into selected wood shear walls. This configuration was tested to assess the influence of supplemental damping systems on energy dissipation and overall seismic performance.

Phase 3: Addition of Gypsum Wallboard (Load-Bearing Walls Only)

In this phase, the structure from Phase 1 was supplemented with 1/2-inch thick gypsum wallboard fastened to the structural (load-bearing) walls using #6-1-1/4 inch long screws at 16 inches on-center (O.C.). The testing aimed to determine the contribution of interior finishes to the stiffness and damping characteristics of the structure.

Phase 4: Gypsum Wallboard on All Walls and Ceilings

Building on Phase 3, this phase involved the installation of 1/2-inch thick gypsum wallboard on all walls (16 inches O.C.) and ceilings (12 inches O.C.). This configuration was tested to further evaluate the role of extensive interior sheathing in modifying the dynamic behavior of the structure.

Table 1 Summary of test phases and building configurations

Test Phase	Test Building Configuration
Phase 1	Wood structural elements only
Phase 2	Test Phase 1 structure with passive fluid dampers incorporated into selected wood shear walls
Phase 3	Test Phase 1 structure with 1/2 in. thick gypsum wallboard installed with #6-1-1/4 in. long screws @ 16 in. O.C. on structural (load-bearing) walls
Phase 4	Test Phase 3 structure with 1/2 in. thick gypsum wallboard installed with #6-1-1/4 in. long screws on all walls (16 in. O.C.) and ceilings (12 in. O.C.)
Phase 5	Test Phase 4 structure with 7/8 in. thick stucco installed with 16-gauge steel wire mesh and 1-1/2 in. long leg staples @ 6 in. O.C. on all exterior walls

Phase 5: Full Building Configuration with Stucco Exterior

The final phase represented the complete construction of the building with all inclusive components. The structure included 7/8-inch thick stucco on the exterior walls, reinforced with

16-gauge steel wire mesh and 1-1/2 inch long leg staples at 6 inches O.C. This phase also retained the gypsum wallboard configuration from Phase 4. Phase 5 provided the most realistic representation of the building's full-scale performance under seismic loading, capturing the combined effects of structural, non-structural, and exterior finishes.

In this study, Phase 5 is the primary focus as it reflects the complete configuration of the test building, incorporating all structural and non-structural elementsGround Motions

In the experimental phase of the NEESWood project, a comprehensive suite of ground motion records was employed to evaluate the seismic performance of a two-story light-frame wood structure under progressively increasing levels of earthquake excitation. This test series was conducted at the University at Buffalo, and the building was constructed in phases to allow for sequential assessment of structural performance with and without various architectural finishes and retrofits. Notably, only data from Phases 3, 4, and 5 were considered for this study, as the structure was not fully completed during Phases 1 and 2, rendering those early datasets unsuitable for reliable damage assessment and dynamic response analysis.

3.4.1 Ground Motion Selection

The seismic excitations used in these tests were derived from two real historical earthquake records, both originating from the 1994 Northridge Earthquake in California:

- **Canoga Park (CP)**: Representing ordinary ground motion, recorded approximately 15.8 km from the fault rupture (Topanga Canyon, USC Station 90053). This record served as a primary input for mid-to-moderate seismic intensities. It includes three orthogonal components (east-west, north-south, and vertical), although only the horizontal components were considered in this study, in accordance with the modeling and validation strategies adopted in Chapter 4.

- **Rinaldi (RN)**: Representing near-fault motion, recorded just 7.1 km from the fault rupture (Rinaldi Receiving Station, DWP Station 77). This record embodies a more intense shaking profile, characteristic of maximum credible earthquake (MCE) scenarios, typically associated with a 2% probability of exceedance in 50 years (return period of 2475 years).

3.4.2 Ground Motion Scaling

The Canoga Park records were systematically scaled using amplitude-scaling factors ranging from 0.12 to 1.20, simulating a wide range of seismic intensities—from minor shaking to design-basis earthquake (DBE) levels and beyond. Specifically, a scaling factor of 1.20 was adopted to simulate DBE-level shaking (equivalent to a 10% probability of exceedance in 50 years, or a 475-year return period). The progression of ground motion intensities allowed for the observation of the structure's transition from elastic to nonlinear behavior, and ultimately towards localized and global damage accumulation.

The Rinaldi record was scaled to a factor of 1.0, corresponding to MCE-level ground motion, with Peak Ground Accelerations (PGAs) substantially higher than those observed in Canoga Park cases. This provided the necessary stimulus to evaluate performance under severe seismic demands, thereby offering a basis for benchmarking collapse-level or near-collapse structural behavior.

The Table 2 below provides a detailed breakdown of the applied ground motions, including the test ID, ground motion source, scaling factors, and corresponding PGAs in both the X and Y directions. These ground motions, in conjunction with detailed instrumentation (including accelerometers and string potentiometers), enabled the research team to evaluate component-level, story-wise, and global-level damage indices under a range of seismic demands. The rigorous application of these records also conforms with FEMA guidelines for IDA (Incremental Dynamic

Analysis), making the study's findings robust and generalizable across a wide spectrum of wood-frame seismic performance assessments.

Table 2 Ground Motion Information for NEESWood Benchmark Tests

Test ID	Ground Motion	X (scale factor)	PGA (g) X Direction	Y (scale factor)	PGA (g) Y Direction
P3S1	Canoga Park	0.12	0.04	0.12	0.05
P3S2	Canoga Park	0.12	0.04	0.12	0.05
P3S3	Canoga Park	0.53	0.19	0.53	0.22
P3S4	Canoga Park	0.53	0.19	0.53	0.22
P4S1	Canoga Park	0.12	0.04	0.12	0.05
P4S2	Canoga Park	0.12	0.04	0.12	0.05
P4S3	Canoga Park	0.53	0.19	0.53	0.22
P4S4	Canoga Park	0.53	0.19	0.53	0.22
P5S1	Canoga Park	0.12	0.04	0.12	0.05
P5S2	Canoga Park	0.12	0.04	0.12	0.05
P5S3	Canoga Park	0.53	0.19	0.53	0.22
P5S4	Canoga Park	0.53	0.19	0.53	0.22
P5S5	Canoga Park	0.86	0.31	0.86	0.36
P5S6	Canoga Park	0.86	0.31	0.86	0.36
P5S7	Canoga Park	1.20	0.43	1.20	0.50
P5S8	Canoga Park	1.20	0.43	1.20	0.50
P5S11	Rinaldi	1.00	0.47	0.00	0.00

3.4.3 Description of Test Phase 5 Protocol

Test Phase 5 was the culminating stage of the NEESWood benchmark testing and aimed to comprehensively evaluate the seismic performance of the fully finished test structure, inclusive of all structural and non-structural components. This phase incorporated the application of exterior stucco wall finishes to simulate construction practices typical of California homes built in the 1980s or 1990s. The stucco application included multiple steps: the installation of a vapor-permeable, water-resistant tar paper, followed by a 16-gauge steel wire mesh attached to the exterior walls using staples spaced 6 inches on center. The plastering process consisted of three

coats: two base coats of 3/8-inch thickness each and a final finishing coat of 1/8 inch. Figure 7 shows the finished benchmark structure before initiation of phase 05.

Figure 7 South-east external view of the benchmark structure after the installation of the exterior stucco finish (Christovasilis et al., n.d., 2009)

Unique to Phase 5, the tri-axial motion represented Seismic Test Level 5, the most severe condition within the experimental protocol, simulating the maximum credible earthquake scenario. To enhance realism and illustrate potential non-structural vulnerabilities, the structure was fully furnished as though occupied by a family of four. Anchored non-structural components, including furniture and appliances, were installed in accordance with established standards. For example, one heater in the garage was anchored to the wall, while the other remained unanchored. These configurations were designed to evaluate the performance of non-structural elements under seismic excitation.

3.5 Instrumentation of Shake Table Tests

Instrumentation is a critical component of experimental studies, providing precise data to evaluate structural responses under dynamic loading. The project building for the NEESWood shake table tests incorporated an array of sensors designed to capture comprehensive measurements, including acceleration, displacement, and force data.

More than 70 accelerometers were installed to monitor the dynamic behavior of the structure. These accelerometers captured data in two horizontal directions (east-west and north-south) and the vertical direction.

To capture absolute and relative displacements, 21 linear string potentiometers were deployed. Their specific uses included:

a) Monitoring absolute displacements between the shake tables and the test structure relative to a stationary reference system.
b) Measuring racking deformations of shear walls through diagonally oriented potentiometers.
c) Capturing inter-story drifts by measuring floor diaphragm displacements.

Force sensors included more than 50 load cells installed to measure tensile axial forces in key structural elements, such as:

a) Shear transfer anchor bolts.
b) Hold-down anchor bolts of first-floor shear walls.

3.6 Observed Damage in Phase 5 Testing

During Phase 5 of the NEESWood benchmark shake table test, the building was subjected to high-intensity seismic loading, resulting in a range of structural and non-structural damage. Notable forms of damage included cracking, spalling, material separation, and deformation, predominantly

in highly stressed regions such as wall bases, corners, and connection interfaces. The observations provide valuable insight into the vulnerability of exterior finishes, sill plates, anchorage zones, and gypsum wallboards under strong lateral and vertical seismic demands.

Cracking and significant spalling of the exterior stucco were observed at the base of the garage wall. This damage likely resulted from concentrated stresses near the foundation during seismic excitation, leading to the detachment of the stucco layer and exposing the underlying surface.

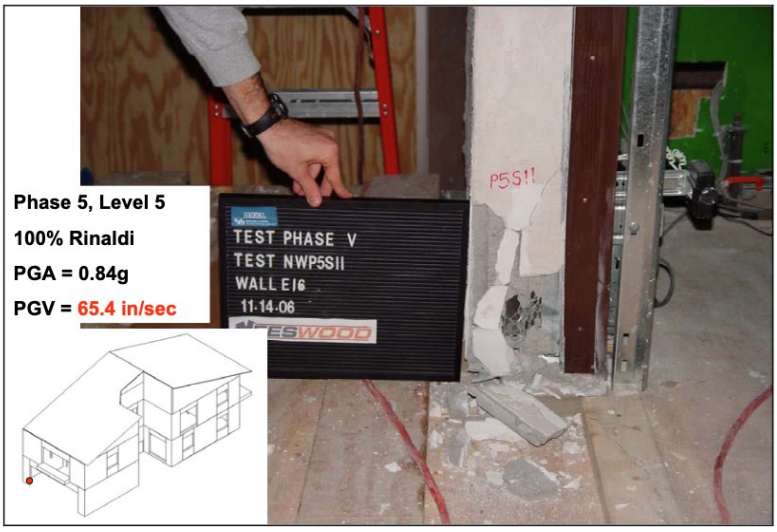

Figure 8 Cracking and Spalling of Stucco at the Bottom of Garage Wall (Christovasilis et al., n.d., 2009)

Severe cracking appeared at the corner of the garage wall opening, accompanied by spalling. The damage concentrated at the structural stress points around the corners, where the forces were amplified due to openings in the wall.

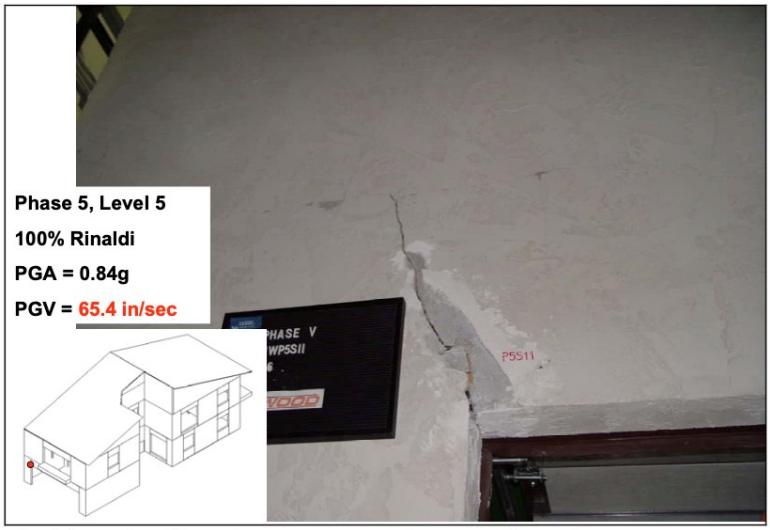

Figure 9 Cracking and Spalling of Stucco at the Corner of Garage Wall Opening (Christovasilis et al., n.d., 2009)

The sill plate at the narrow pier of the garage wall exhibited cracking and separation along its entire length. This resulted from the high inter-story drifts experienced during seismic loading. The observed damage demonstrates the vulnerability of sill plates at narrow wall segments.

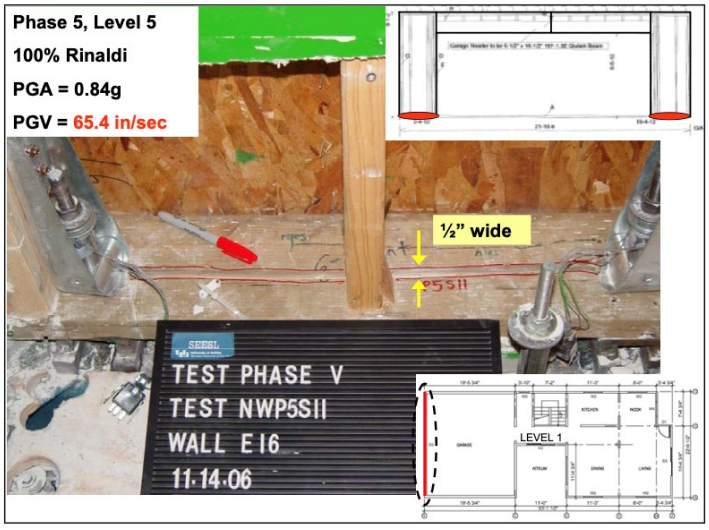

Figure 10 Cracking and separation of sill plate through entire length of garage narrow wall piers (Christovasilis et al., n.d., 2009)

Vertical cracking occurred at the stud immediately above the hold-down anchor. The damage indicates the transfer of seismic forces through the anchoring system, creating tensile stresses in the wood stud that exceeded its capacity.

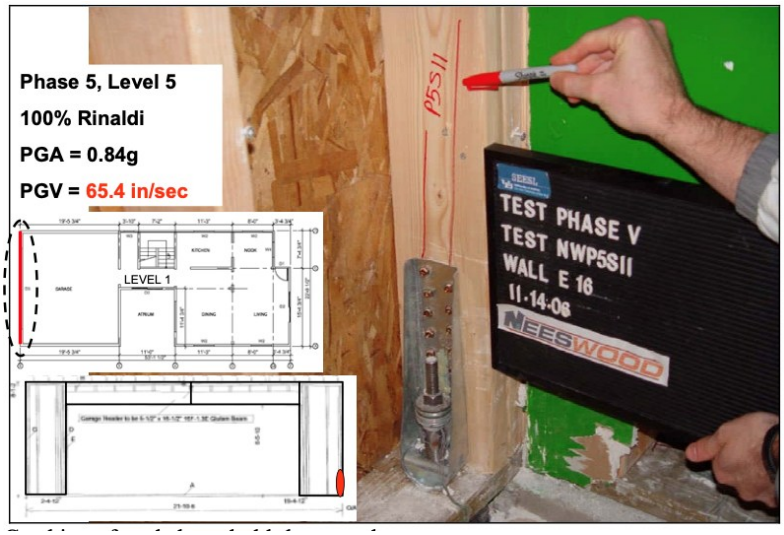

Figure 11 Cracking of stud above hold-down anchor (Christovasilis et al., n.d., 2009)

Large sections of the gypsum wallboard were separated from the ceiling, indicating significant deformation and failure in the ceiling connections. This damage highlights the challenges in maintaining ceiling integrity under tri-axial seismic loads.

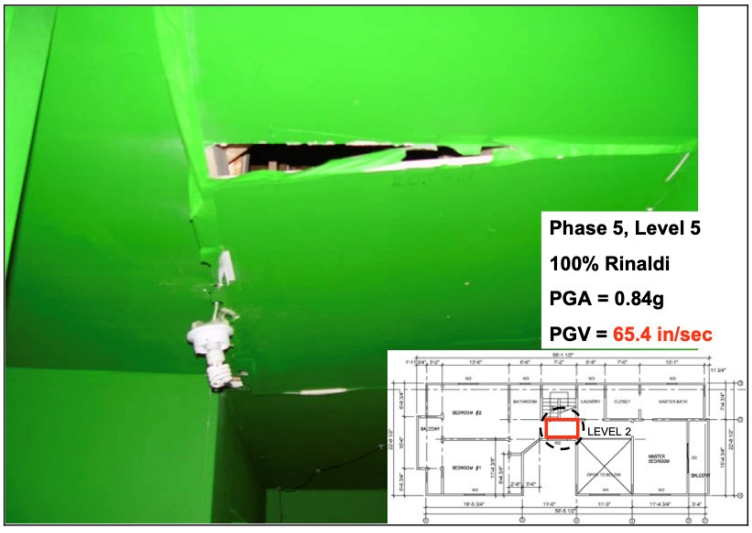

Figure 12 Separation of Gypsum Wallboard from Ceiling (Christovasilis et al., n.d., 2009)

Horizontal cracking was evident along the second-floor level, reflecting the influence of inter-story drift. The cracks followed the drywall seams and were exacerbated by the lateral deformation of the building.

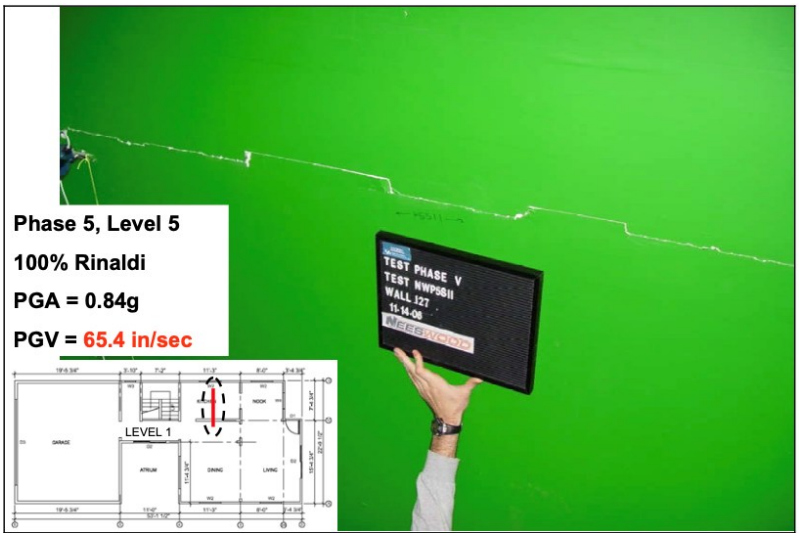

Figure 13 Horizontal Cracking of Gypsum Wallboard (Christovasilis et al., n.d., 2009)

The gypsum wallboard near the door opening exhibited significant cracking and buckling. The structural discontinuity around the opening led to localized stress concentrations, causing the wallboard to deform and fail.

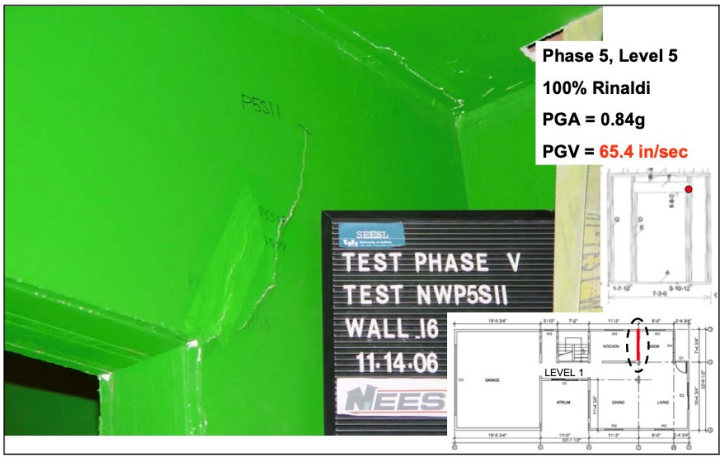

Figure 14 Cracking and Buckling of Gypsum Wallboard at Door Opening (Christovasilis et al., n.d., 2009). Table below summarises the damage observed and shown above:

A detailed summary of the damage types and their locations is presented in Table 3.

Table 3 Summary of Observed Damage in Phase 5

Damage Location	**Description of Damage**
Base of garage wall	Cracking and spalling of exterior stucco
Corner of garage wall opening	Cracking and stucco detachment
Sill plate at narrow wall pier	Full-length cracking and separation
Stud above hold-down anchor	Vertical splitting of the stud
Ceiling (gypsum wallboard)	Separation of gypsum wallboard from ceiling
Second-floor drywall seam	Horizontal cracking along gypsum wallboard seams
Door opening area	Cracking and buckling of gypsum wallboard

4 Numerical Model Development

4.1 Overview of Timber3D and Nonlinear Modeling

Timber3D is a specialized numerical modeling framework tailored for the analysis of light wood frame buildings subjected to lateral loads, such as seismic events. Developed within the MATLAB environment, Timber3D integrates nonlinear hysteretic material models and advanced computational techniques to capture the complex behavior of light wood structures at various scales, from connection details to full building systems.

The framework consists of three interconnected modules:

a) **Connection-Level Analysis**: Focused on deriving nonlinear hysteresis properties of fasteners and connections, such as nails, screws, and hold-downs.

b) **Assembly-Level Analysis**: Designed for simulating the nonlinear behavior of shear walls and diaphragms under cyclic loads.

c) **Building-Level Analysis**: Extends the assembly-level simulation to entire structures, incorporating interactions between diaphragms, walls, and load paths.

This modularity allows for a comprehensive understanding of the behavior of wood frame structures, offering capabilities for both static pushover and dynamic nonlinear time history analyses. By representing physical systems using frame and frame-to-frame link elements (F2F), Timber3D enables accurate predictions of structural performance while accounting for localized deformations and energy dissipation mechanisms.

4.2 Modeling Approach

4.2.1 Structural Representation

The Timber3D numerical model utilizes a hybrid approach, combining frame elements for primary load-bearing members and frame-to-frame link elements (F2F) to capture nonlinear interactions at interfaces:

Frame Elements: Represent components such as studs, beams, and columns, modeled as deformable members connected at master nodes.

Frame-to-Frame Links (F2F): Represent sheathing-to-framing connections and are designed with six degrees of freedom, capturing nonlinear hysteretic behavior for load path interactions.

4.2.2 Master-Slave Nodal System

To optimize computational efficiency, Timber3D employs a master-slave node system:

Master Nodes: Represent key structural points, such as diaphragm centroids and load transfer joints, ensuring accurate global load distribution.

Slave Nodes: Condensed into master nodes via a nodal condensation technique, reducing computational complexity while maintaining localized response accuracy.

4.2.3 Diaphragm and Shear Wall Modeling

Diaphragms: Modeled using rigid beam elements at the base, first floor, and second floor to define their geometry. The diaphragms are assigned predefined stiffness values to replicate semi-rigid behavior and load transfer mechanisms between shear walls and floors.

Shear Walls: Modeled as nonlinear springs calibrated from experimental hysteresis data, incorporating hold-down effects, energy dissipation, and uplift responses.

4.2.4 Dynamic Analysis

Timber3D supports nonlinear dynamic analyses using ground motion records to simulate real-world earthquake scenarios. Time history analyses are conducted using numerical integration method to evaluate global structural responses, such as:

- Roof displacement profiles.
- Hysteretic energy dissipation.
- Base shear forces and moment distributions.

4.2.5 Validation

The Timber3D framework has been validated against experimental benchmarks, including shake table tests and static cyclic analyses. These validations demonstrate close agreement between numerical predictions and experimental results for hysteretic energy dissipation, displacement responses, and global structural behavior.

Through its modular design and robust modeling capabilities, Timber3D provides a powerful tool for understanding and optimizing the performance of light wood frame buildings under seismic and lateral loads.

4.2.6 Spring Parameters

4.2.6.1 In-Plane Shear Spring Parameters

In this study for developing the numerical model of the NEESWood two story light wood frame building, in-plane shear springs are used to represent the load-deformation behavior of the shear walls along the wall lines in a light-frame wood building. The springs are designed to replicate the aggregate stiffness and strength characteristics of each shear wall and are calibrated based on experimental and numerical studies.

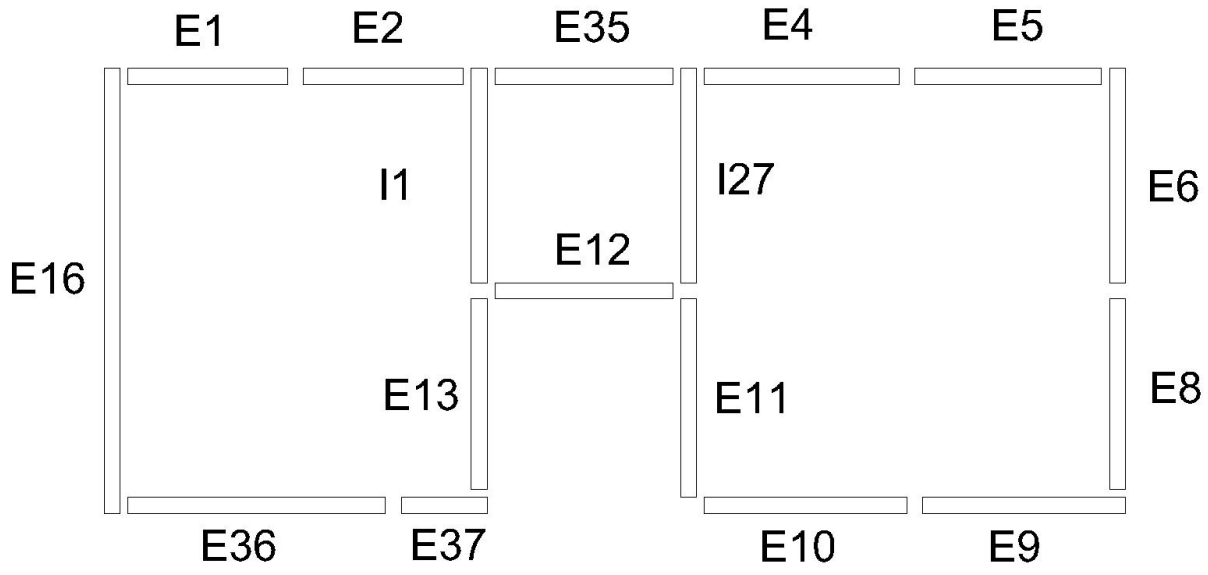

(a)

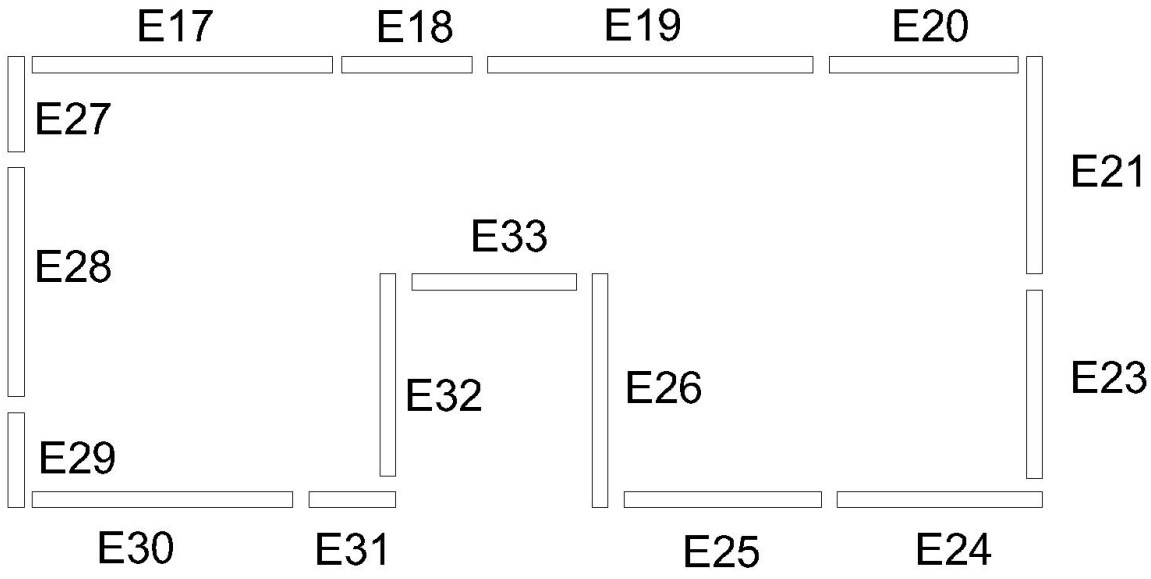

(b)

Figure 15 Shear wall plan for the NEESWood two story light wood frame building (a) First Floor (b) Second Floor

Figure 15 illustrates the shear wall plan of the NEESWood two-story light-frame building, showcasing the layout of the shear walls on both the first and second floors. The figure provides detailed wall IDs, such as E1, E2, E3, and others, which correspond to specific shear walls within the structure. These wall IDs are used for referencing the structural springs in the building for modeling and analysis purposes.

The parameters for the shear walls for the NEESWood two-story building were obtained from the study by (Pang & Rosowsky, 2010). The tables below (Table 4, Table 5, Table 6 and Table 7) outline the key hysteretic parameters for walls across both stories of the structure in the longitudinal and transverse directions. These include essential attributes such as initial stiffness (K_0), force intercepts (F_0, F_i), deformation parameters (Δ, r_1, r_2, r_3, r_4), and maximum forces (F_u). Each of these parameters plays a critical role in capturing the dynamic behavior of the walls under seismic loading.

The parameter values were derived using the MSTEW model, a specialized shear wall analysis tool developed to predict non-linear force-displacement responses for timber shear walls. MSTEW accounts for various factors, including nail slip behavior, shear panel deformation, and anchorage effects.

Table 4 First story in plane shear spring parameters in x direction

Wall ID	Ko (kN/mm)	r1	r2	r3	r4	F0 (kN)	Fi (kN)	Δ (mm)	α	β
E1	2.57	0.04	-0.06	1.01	0.06	18.14	2	57.3	1	1.2
E2	2.59	0.05	-0.05	1.01	0.06	16.75	1.63	54.9	0.9	1.2
E35	2.88	0.04	-0.04	1.01	0.06	23.74	2.58	57.1	1	1.2
E4	2.55	0.04	-0.05	1.01	0.05	22.51	1.88	72.6	1	1.2
E5	1.81	0.05	-0.06	1.01	0.08	15.76	1.54	64.3	1	1.2
E9	2.66	0.04	-0.06	1.01	0.05	28.13	2.29	70.5	1	1.2
E10	2.42	0.03	-0.07	1.01	0.07	29.26	2.38	64.4	1	1.5
E12	0.78	0	-0.08	0.82	0.13	21.39	1.78	102.4	1	1.2
E37	0.83	0.02	-0.03	0.74	0.04	4.44	0.09	42.9	1	1.2
E36	4.04	0.03	-0.04	1.01	0.05	37.01	3.34	64.7	1	1.2

Table 5 Second story in plane shear spring parameters in x direction

Wall ID	Ko (kN/mm)	r1	r2	r3	r4	F0 (kN)	Fi (kN)	Δ (mm)	α	β
E17	2.73	0.026	-0.098	1.01	0.051	29.31	3.5	82.5	0.99	1.37
E18	1.83	0.017	-0.04	1.01	0.049	19.37	1.2	66.3	0.99	1.26
E19	3.68	0	-0.059	1.01	0.04	42.46	2.13	42.8	0.99	1.25
E20	3.71	0	-0.059	1.01	0.057	42.9	3.93	42.8	0.95	1.15
E24	2.22	0.035	-0.079	1.01	0.075	23.66	2.45	51.2	0.99	1.2
E25	1	0.027	-0.03	1.01	0.045	13.16	1.42	95.1	0.95	1.15
E33	1.4	0.081	-0.038	1.01	0.08	11.07	1.33	37.3	0.95	1.15
E31	0.61	0.039	-0.046	1.01	0.024	3.1	0.27	35.3	1	1.29
E30	2.84	0	-0.047	1.01	0.055	34.23	3.19	53.7	0.8	1.2
E22	0.6	0.02	-0.034	1.01	0.03	2.81	0.35	41.8	0.99	1.24

Table 6 First story in plane shear spring parameters in y direction

Wall ID	Ko (kN/mm)	r1	r2	r3	r4	F0 (kN)	Fi (kN)	Δ (mm)	α	β
E6	1.07	0.026	-0.055	0.455	0.062	15.7	1.71	48.6	0.95	1.15
E8	2.6	0.03	-0.041	0.834	0.077	45.39	2.07	106.9	0.95	1.25
E11	1.85	0.071	-0.027	0.699	0.034	12.67	1	88.3	0.91	1.21
E13	2.18	0.031	-0.05	1.4	0.055	23.08	1.93	62.4	0.95	1.2
E16	1.36	0.1	-0.063	0.861	0.053	15.4	1.76	78.9	0.85	1.25
I1	2.26	0.048	-0.005	0.32	0.094	22.08	2.39	43.1	0.95	1.2
I27	1.96	0.046	-0.038	1.01	0.044	19.66	1	88.1	0.94	1.15

Table 7 Second story in plane shear spring parameters in y direction

Wall ID	Ko (kN/mm)	r1	r2	r3	r4	F0 (kN)	Fi (kN)	Δ (mm)	α	β
E21	0.51	0.01	-0.04	0.88	0.08	5.42	0.43	39.3	1	1.3
E23	1.54	0.01	-0.02	1.01	0.06	23.48	1.24	39.8	1	1.2
E26	1.85	0.02	-0.05	0.48	0.08	22.23	2.5	37.9	1	1.4
E32	1.93	0.06	-0.06	0.72	0.06	12.31	1.19	34.1	0.9	1.3
E29	1.27	0.01	-0.02	1.01	0.01	2.96	0.24	38.6	1	1.2
E28	1.11	0.04	-0.01	0.52	0.03	6.83	0.61	70.3	1	1.3
E27	1.27	0.01	-0.02	1.01	0.01	2.96	0.24	38.6	1	1.2

However, in seismic modeling of light-frame shear walls, accurately capturing the behavior of different components such as structural studs, gypsum wallboards, and stucco is crucial. Each of these elements contributes to the wall's overall in-plane stiffness and strength, with unique mechanical properties and hysteresis behavior.

The data presented in the tables above corresponds to Phase 3 of the two-story building tested during the shake table experiments.

The complete seismic behavior of the building as a whole, incorporating additional elements such as stucco in later phases, cannot be accurately captured without a comprehensive approach that accounts for the interactions between all components across all phases. Specifically:

- In Phase 4, the GWBs were extended to cover all walls and ceilings, introducing additional stiffness and damping contributions.
- In Phase 5, the inclusion of 22.2 mm thick stucco on the exterior further enhanced the structural capacity by significantly increasing the lateral stiffness and energy dissipation of the system.

To model the full-scale seismic behavior of the building across all phases, it becomes necessary to develop a framework that integrates the contributions of all components—including structural elements, GWBs, and stucco—into a unified representation. This is essential for understanding the interaction between these layers and predicting the global response of the structure under seismic loading.

To that purpose, spring theory provides an efficient and reliable solution. By representing each component as a nonlinear spring with calibrated parameters and combining them in parallel (Zhou, n.d.), the collective behavior of the building can be modeled effectively. To create a representative model of the combined wall behavior, we employed the parallel spring theory, which assumes that the stiffness of multiple components connected in parallel adds linearly.

4.2.6.2 Parallel Spring Theory

The parallel spring theory is based on the principle that when multiple spring elements are connected in parallel as shown in the Figure 16, their combined stiffness is the sum of their individual stiffness values.

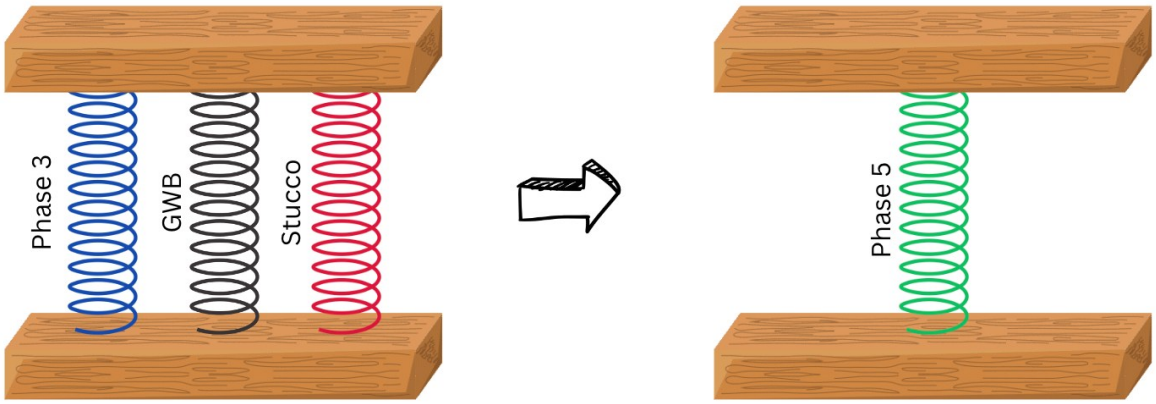

Figure 16 Equivalent in-plane shear spring system

This approach assumes that all the spring components experience the same deformation under applied loads, which is consistent with the physical behavior of a composite shear wall. The total stiffness K_{total} is given by:

$$\mathrm{K_{total}} = \mathrm{K_{studs}} + \mathrm{K_{gypsum}} + \mathrm{K_{stucco}}$$

For other parameters, such as yield force (F_0) and deformation (Δ), a weighted average approach was used. This weighting ensures that the contributions of each material are proportional to their stiffness, reflecting their relative influence on the overall wall behavior. The weighted average is calculated as:

$$\mathrm{P_{combined}} = \frac{\mathrm{K_{studs}P_{studs}} + \mathrm{K_{gypsum}P_{gypsum}} + \mathrm{K_{stucco}P_{stucco}}}{\mathrm{K_{total}}}$$

Where, P represents the parameter being combined (e.g., F_0, Δ).

For the purpose of developing the numerical model in this study, the parameters for gypsum wallboard (GWB) and stucco were obtained from the literature by Pan et al. (2018). This study provided the necessary MSTEW model parameters for these materials, which were then combined with the spring parameters given in the table for Phase 3 of the NEESWood two-story light-frame

building. The GWB and stucco parameters were effectively treated as parallel springs, combined with the Phase 3 springs to represent the in-plane shear behavior of the composite wall system in the numerical simulations.

The E27 shear wall has been investigated as a demonstration of how the combined parameters were utilized in the numerical modeling on this study. Its phase 03 parameters (Table 07) were combined with those of gypsum wallboard and stucco to create a representative model of the composite wall system. The table below provides the tabulated values for the individual components and their combined parameters, reflecting their in-plane shear behavior.

Table 8 Case Study: E27 Wall and Combined Parameters

Component	**Ko (kN/mm)**	**r1**	**r2**	**r3**	**r4**	**F0 (kN)**	**Fi (kN)**	**Δ (mm)**	**α**	**β**
E27 Wall	1.27	0.01	-0.02	1.01	0.01	2.96	0.24	38.6	1	1.2
Stucco	1.09	0.07	-0.27	1	0.01	32.6	3.6	71.88	0.8	1.1
Gypsum	0.45	0.05	-0.02	1.01	0.01	2.76	0.44	39.62	0.9	1.65
Combined	2.81	0.046	-0.109	1.01	0.009	15.28	1.46	55.75	0.9	1.32

Figure 17 illustrates the MSTEW hysteresis backbone curves for the individual components used in this study for numerical model development. Figure 17(a) represents the backbone curve of the E27 wall for Phase 3, while Figure 17(b) and Figure 17(c) display the backbone curves for gypsum wallboard and stucco, respectively, derived from Pan et al. (2018). These curves characterize the force-displacement relationship and highlight the distinct hysteretic behaviors of each component.

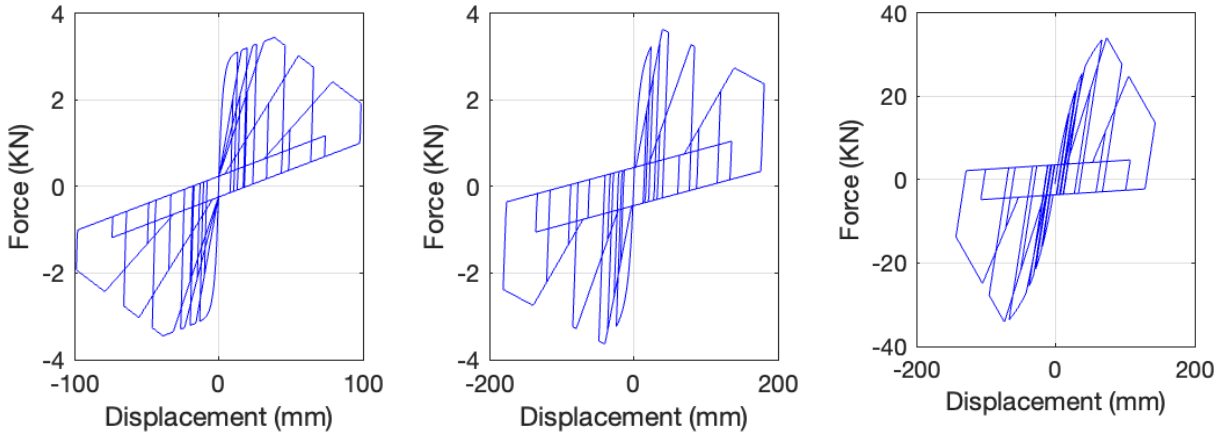

(a) (b) (c)

Figure 17 MSTEW hysteresis backbone curve used in this study for numerical model development (a) E27 wall - Phase 03 (b) Gypsum wall board (Pan et al., 2018) (c) Stucco (Pan et al., 2018)

Figure 18, in contrast, depicts the backbone curve for the combined wall system, which integrates the contributions of the E27 wall (phase 03), gypsum wallboard, and stucco. The combined backbone curve demonstrates the aggregated response, incorporating the stiffness and hysteretic properties of all three components, effectively representing the global behavior of the composite shear wall under seismic loading.

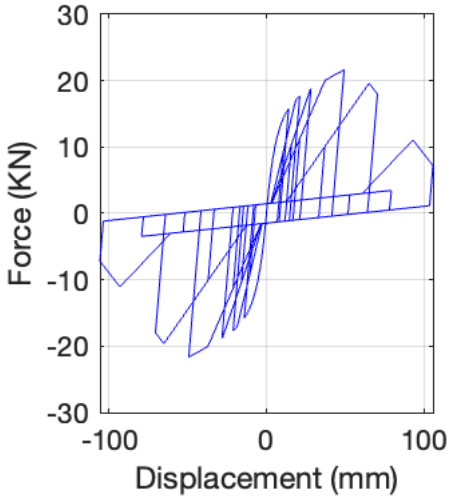

Figure 18 MSTEW back bone curve for combined action of Phase 3 shear wall, GWB and Stucco

Table 9 Combined MSTEW backbone parameters for in-plane shear springs

Wall ID	K0 (kN/mm)	r1	r2	r3	r4	F0 (kN)	Fi (kN)	Δ (mm)	α	β
E1 Combined	4.11	0.042	-0.073	1.01	0.053	20.14	2.68	59.48	0.92	1.32
E2 Combined	4.13	0.052	-0.063	1.01	0.053	18.85	2.31	57.81	0.82	1.32
E35 Combined	4.42	0.042	-0.053	1.01	0.053	25.65	3.11	58.47	0.92	1.32
E4 Combined	4.09	0.042	-0.063	1.01	0.043	24.17	2.47	73.3	0.92	1.32
E5 Combined	3.35	0.052	-0.073	1.01	0.073	18.22	2.11	65.43	0.92	1.32
E9 Combined	4.2	0.042	-0.073	1.01	0.043	31.05	3.14	71.78	0.92	1.32
E10 Combined	3.96	0.032	-0.083	1.01	0.063	32.18	3.23	66.68	0.92	1.62
E12 Combined	2.32	0.002	-0.093	0.82	0.103	23.52	2.17	102.9	0.92	1.32
E37 Combined	2.37	0.022	-0.043	0.74	0.023	10.89	1.17	46.84	0.92	1.32
E36 Combined	6.58	0.032	-0.053	1.01	0.043	40.1	4.74	66.35	0.92	1.32
E17 Combined	4.27	0.034	-0.085	1.01	0.044	24.88	3.18	77.78	0.92	1.32
E18 Combined	3.37	0.031	-0.067	1.01	0.046	17.11	1.88	64.07	0.92	1.32
E19 Combined	5.22	0.019	-0.072	1.01	0.037	31.88	2.54	47.69	0.92	1.32
E20 Combined	5.25	0.019	-0.072	1.01	0.045	31.9	3.72	47.69	0.91	1.28
E24 Combined	4.76	0.041	-0.085	1.01	0.061	22.18	2.96	52.87	0.92	1.32
E25 Combined	3.54	0.038	-0.054	1.01	0.039	13.46	1.92	84.3	0.91	1.28
E33 Combined	2.94	0.053	-0.048	1.01	0.062	11.92	1.63	46.96	0.91	1.28
E31 Combined	2.15	0.049	-0.046	1.01	0.021	4.13	0.92	41.32	0.92	1.35
E30 Combined	4.38	0.016	-0.054	1.01	0.043	26.57	3.12	53.98	0.86	1.28
E22 Combined	2.13	0.028	-0.041	1.01	0.024	3.69	0.87	45.92	0.92	1.31
E6 Combined	2.61	0.042	-0.055	0.627	0.054	19.75	2.09	53.7	0.92	1.28
E8 Combined	4.14	0.038	-0.045	0.922	0.063	32.7	2.61	84.47	0.91	1.33
E11 Combined	3.39	0.055	-0.037	0.795	0.035	17.11	1.58	80.94	0.91	1.31
E13 Combined	3.72	0.041	-0.046	1.24	0.053	21.63	2.28	63.77	0.91	1.28
E16 Combined	2.9	0.059	-0.05	0.939	0.049	17.85	2.14	74.49	0.89	1.33
I1 Combined	4.18	0.049	-0.025	0.701	0.065	25.54	2.83	53.27	0.91	1.3
I27 Combined	3.88	0.046	-0.04	0.934	0.046	20.99	1.83	73.63	0.91	1.26
E21 Combined	2.05	0.026	-0.058	0.818	0.058	10.16	1.26	55.27	0.92	1.32
E23 Combined	3.08	0.032	-0.038	0.936	0.053	17.68	2.18	52.5	0.92	1.28
E26 Combined	3.39	0.038	-0.054	0.726	0.059	17.24	2.85	51.55	0.92	1.35
E32 Combined	3.47	0.051	-0.061	0.804	0.053	12.56	1.63	47.66	0.89	1.32
E29 Combined	2.81	0.027	-0.033	0.936	0.033	8.38	1.29	50.58	0.92	1.28
E28 Combined	2.65	0.045	-0.017	0.697	0.038	9.54	1.24	64.6	0.93	1.32
E27 Combined	2.81	0.027	-0.033	0.936	0.033	8.38	1.29	50.58	0.92	1.28

Similarly, the same methodology employed for the E27 shear wall, involving the integration of spring parameters for the structural studs, gypsum wallboard, and stucco, was also applied to the remaining shear walls. For each wall, the parameters were combined using the parallel spring

theory, where individual contributions were aggregated to capture the global in-plane shear behavior of the composite system. The combined parameters for the walls are listed in Table 9.

4.2.6.3 Out-of-Plane Bending Spring Parameters

In this study, linear springs were employed in the out-of-plane direction to replicate the bending behavior of each shear wall. The out-of-plane bending stiffness of the each shear walls, K_{bending}, was calculated using the equation (Véliz et al., 2024):

$$K_{\text{bending}} = \frac{2H^3}{3EA_{\text{ext}}L^2}$$

Here:

$\mathrm{H} = 3048\,\mathrm{mm}$ (wall height),

$\mathrm{E} = 10{,}000\,\mathrm{N/mm^2}$(elastic modulus of wood and sheathing materials),

The effective cross-sectional area (A_{ext}) was calculated based on the contributions of different wall components, including studs, sheathing (gypsum wallboard and stucco), and framing elements. The total $A_{\text{ext}} = 18.01\,\mathrm{mm^2/mm}$ was derived as follows:

Studs Contribution: $A_{\text{studs}} = 9.68\,\mathrm{mm^2/mm}$, based on the stud spacing (400 mm) and their cross-sectional area ($38 \times 89\,\mathrm{mm}$).

Sheathing Contribution: The effective thicknesses of gypsum wallboard and stucco were used to calculate their respective contributions. For gypsum, $t = 12.7\,\mathrm{mm}$, and for stucco, $t = 22.2\,\mathrm{mm}$, resulting in combined contributions of $8.33\,\mathrm{mm^2/mm}$.

Table 10 lists out the bending stiffness of the linear spring that is used in the numerical model in this study to incorporate the out-of-plane stiffness of the shear walls.

Table 10 Out-of-plane stiffness of the shear walls

Wall ID	Length (mm)	$K_{bending}$ (kN/mm)
E1	2950	0.02804
E2	2930	0.02825
E35	3350	0.0226
E4	3430	0.02156
E5	2440	0.04535
E6	990	0.27324
E9	3430	0.02156
E10	3430	0.02156
E12	3430	0.02156
E13	3430	0.02156
E16	2930	0.02825
E36	3350	0.0226
E37	2520	0.04302
I27	3430	0.02156
I1	3350	0.0226
E17	5870	0.00169
E18	3350	0.01071
E19	4620	0.00058
E20	6870	0.00172
E21	990	0.00172
E22	990	0.00117
E23	4650	0.00185
E24	3350	0.00112
E25	3430	0.00104
E26	3430	0.00104
E27	2930	0.00174
E28	1500	0.00174
E29	1500	0.00268
E30	5870	0.00169
E31	2520	0.00456
E32	2520	0.00456
E33	3430	0.00104
E34	2290	0.00185

4.2.6.4 Nodal Restraints

In this study, the vertical stiffness of the building model was constrained by fixing the degree of freedom in the Z direction for master nodes, ensuring no vertical deformation in the model. This approach aligns with the methodology outlined in Pang and Rosowsky (2010), where master nodes were assigned only two in-plane translational degrees of freedom (X and Y directions) and one rotational degree of freedom. The absence of a vertical degree of freedom in the model reflects the assumption of rigid vertical connectivity, effectively simulating the shear wall's behavior under in-plane loading.

4.2.6.5 Diaphragm Beam

The semi-rigid behavior of the diaphragms in the NEESWood benchmark structure was modeled using linear two-node beam elements. The layout of the beam elements are depicted in the Figure 20. These elements connect master nodes placed along transverse wall lines (2, 4, 5, and 6) as shown in Figure 19 on the floor and roof diaphragms, allowing for relative movement in the transverse (N–S) direction. Each master node retains one rotational and two in-plane translational degrees of freedom, simulating the semi-rigid diaphragm behavior.

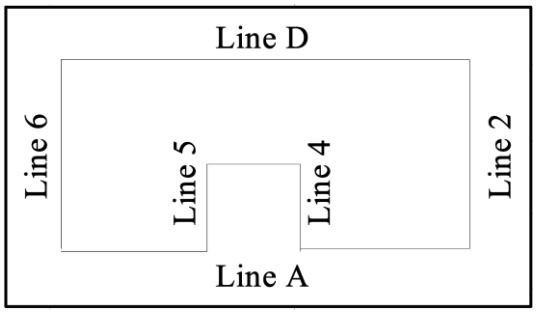

Figure 19 Wall line plan of the NEESWood two story building

The stiffness matrix for the two-node beam elements was derived using classical beam theory:

$$\mathrm{K}_{\mathrm{beam}} = \frac{E}{L^3}\begin{bmatrix} AL^2 & 0 & -AL^2 & 0 \\ 0 & 12I & 0 & -12I \\ -AL^2 & 0 & AL^2 & 0 \\ 0 & -12I & 0 & 12I \end{bmatrix}\begin{Bmatrix} u_1 \\ v_1 \\ u_2 \\ v_2 \end{Bmatrix}$$

where:

E: Elastic modulus (12,410 MPa for Douglas Fir),

L: Length of the beam element (see Table 4 for specific lengths),

A: Cross-sectional area,

I: Moment of inertia.

The moment of inertia (I) for each diaphragm segment was calculated using the diaphragm stiffness obtained from its backbone curve. The backbone curve was generated through monotonic pushover analysis of diaphragm segments Pang and Rosowsky (2010), yielding a stiffness parameter (K_d) corresponding to the slope of the linear portion of the curve.

The relationship for I is:

$$I = \frac{K_d L^3}{E}$$

Using K_d = 0.0742 kN/mm (example value for B2, middle floor segment):

1. Convert K_d to consistent units: K_d = 74.2 N/mm.
2. Substitute into the equation:

$$I = \frac{74.2 \times (3.35 \times 10^3)^3}{12{,}410 \times 10^6}$$

3. Compute I: $I = 22{,}476\ \mathrm{cm}^4$.

This process was repeated for each diaphragm segment using their respective K_d values obtained from pushover analyses.

Table 11 summarizes the beam properties, including elastic modulus, effective moment of inertia (I), and length (L):

Table 11 Equivalent diaphragm beam element properties

Element ID	Location	E (MPa)	I (cm^4)	L (m)
B1	Floor west	12410	265556	5.87
B2	Floor middle	12410	22476	3.35
B3	Floor east	12410	261810	6.86
B4	Roof west	12410	224765	5.87
B5	Roof middle	12410	16649	3.35
B6	Roof east	12410	191466	6.86

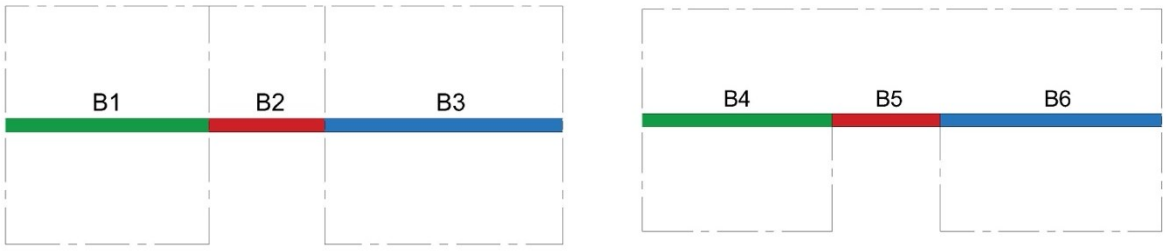

(a) (b)

Figure 20 Diaphragm equivalent beam (a) first floor level (b) second floor level

The calculated I values provided an accurate representation of the diaphragm's bending resistance. By incorporating these beam elements, the model effectively captured the semi-rigid behavior of the diaphragms, including load redistribution and transverse deformations. The stiffness properties derived from the backbone curves ensured realistic simulation of diaphragm behavior under seismic loading conditions.

4.2.6.6 Mass Distribution

For the numerical modeling of the benchmark structure in Phase 05, the mass distribution was implemented to accurately reflect the building's dynamic behavior. The weights for the diaphragms on the first and second floors were allocated based on the structural configuration and applied uniformly across the master and slave nodes.

The total weight assigned to the first-floor diaphragm was 133.45 kN. This weight was distributed uniformly along the master nodes of the first-floor diaphragm. The allocation ensured that the in-plane behavior of the first-floor diaphragm was accurately captured, enabling proper interaction with the supporting shear walls.

The second-floor diaphragm included a total weight of 186.34 kN, composed of 103 kN from the second-floor level and 83.34 kN from the roof diaphragm load. This combined weight was distributed across the master nodes on the second-floor diaphragm to account for its in-plane behavior and on the slave nodes to represent the roof load effects.

4.2.6.7 Timber 3D Modeling

The numerical model of the NEESWood two-story light wood-frame building (Test Phase 05) was developed in Timber 3D as shown in the Figure 21 to simulate the dynamic response and seismic behavior of the structure. This section outlines the modeling approach and high-level design considerations.

Rigid beam elements (with very high modulus of elasticity) were used to define the diaphragm geometry at three distinct levels: the base, first floor, and second floor. These rigid beam elements served to transfer loads from the slave nodes to the diaphragm beam and the shear walls, ensuring effective load redistribution within the system. The diaphragm stiffness itself was not governed by these rigid beam elements but was instead defined by six dedicated beam elements running in the

longitudinal direction. These longitudinal beams captured the semi-rigid behavior of the diaphragms during seismic events and accounted for their deformation characteristics.

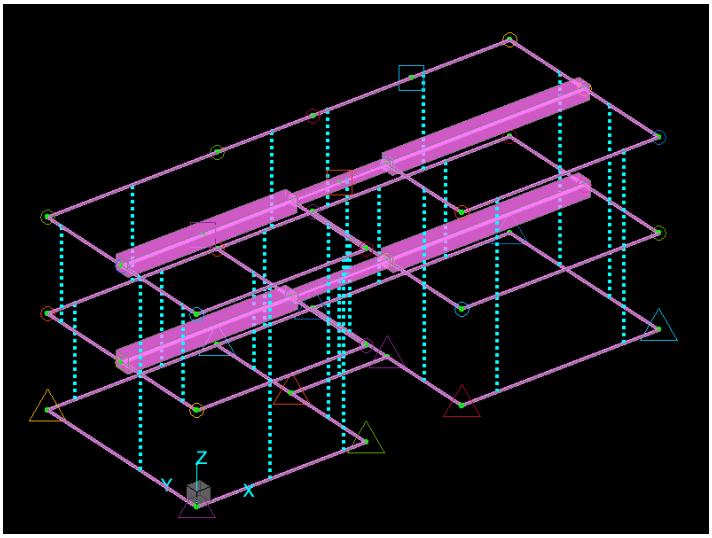

Figure 21 Timber 3D numerical model of NEESWood two-story light wood frame building

Frame-to-frame 3D spring elements were employed to connect the diaphragms across the floors, simulating the interaction between structural components. The spring elements accounted for the in-plane shear stiffness of the shear walls and their interaction with the diaphragms. For the out-of-plane behavior, bending stiffness values were incorporated into the spring elements, reflecting the wall components' ability to resist out-of-plane loads.

Master nodes were assigned at critical locations in the diaphragm to represent the center of mass and capture the diaphragm's overall translational and rotational behavior. Slave nodes were distributed along the edges of the diaphragm and connected to the master nodes, ensuring accurate load redistribution and maintaining the building's structural integrity.

For simulating vertical stiffness, the degrees of freedom in the Z-direction were fixed at both floor levels. This ensured that the vertical stiffness did not influence in-plane load transfer but allowed accurate modeling of gravity and axial loads on the shear walls and diaphragm connections.

4.2.7 Damping Ratios in Phase 5

Damping ratios for Phase 5—the final and fully constructed stage of the two-story wood-frame building—provide key insights into the system's energy dissipation capacity under near-complete structural and non-structural configurations. This phase included all architectural finishes such as gypsum board and stucco, which are known to significantly influence dynamic behavior. The table below presents the initial damping ratios for the first three vibration modes during Phase 5:

Table 12. Damping ratio of Phase 5 structure used in the numerical model

Mode	Damping Ratio (%)
1	17.9
2	17.1
3	5.0

4.3 Model Validation

4.3.1 Modal Analysis

The modal periods obtained from the Timber 3D numerical model for Phase 5 are compared to the experimental periods recorded during the shake table test (benchmark test).

Table 13 provides a modal period comparison and

Figure 22 compares their corresponding mode shapes for the first three modes of vibration. These modal periods serve as an essential measure of dynamic behavior, reflecting the structural stiffness and mass distribution.

Mode 1: The benchmark full scale model and numerical model periods for the first mode show a close agreement, with the numerical model slightly overestimating the period. This discrepancy is attributed to minor variations in the diaphragm stiffness and nodal fixity in the numerical model.

Mode 2: The second mode, representing torsional behavior, exhibits an excellent match between the experimental and numerical periods, with a negligible difference of only -2.5%. This validates the semi-rigid diaphragm assumptions and mass distribution accuracy used in the Timber 3D model.

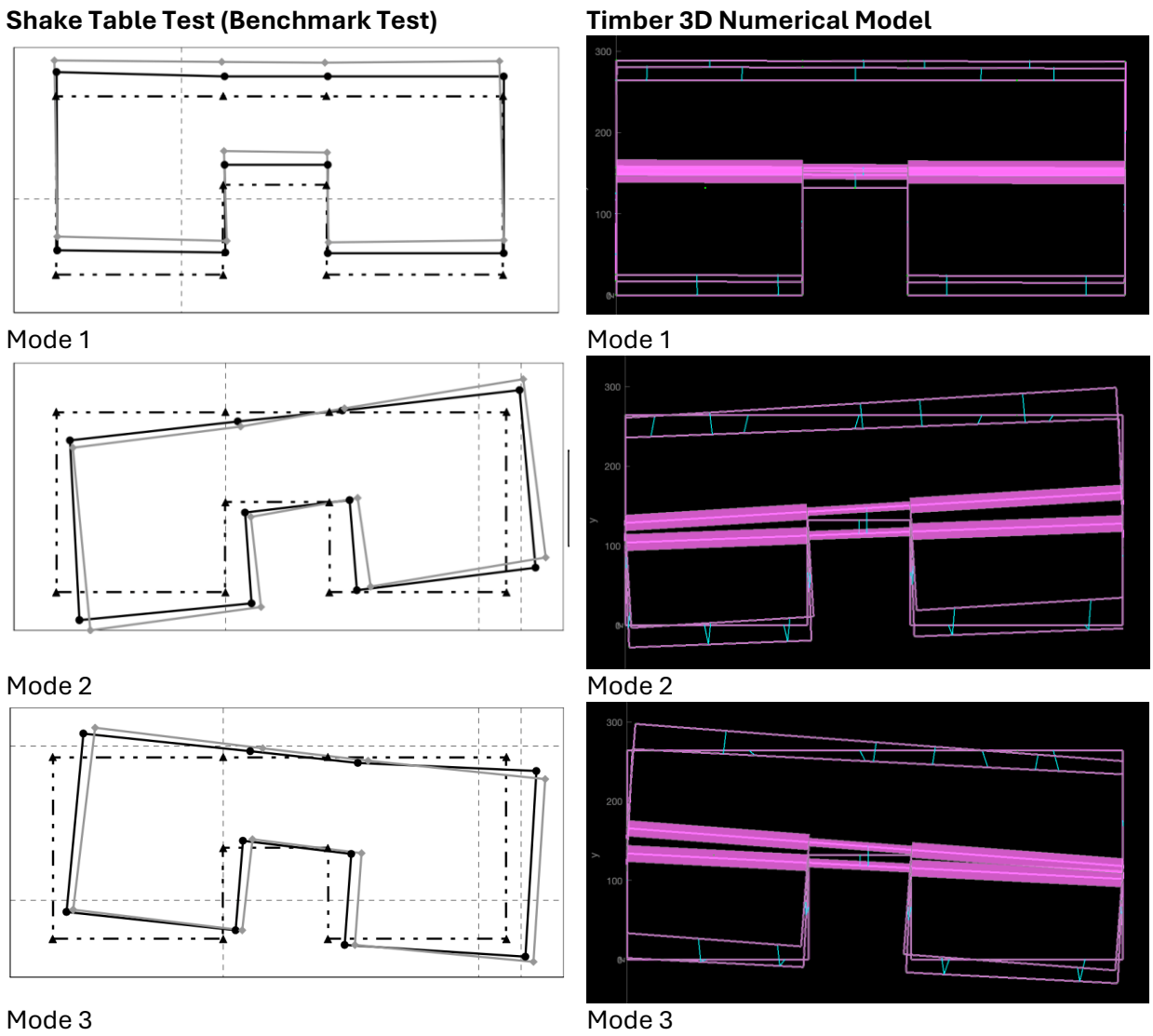

Figure 22 Comparison of mode shapes obtained from the shake table test (benchmark test) and the Timber 3D numerical model for the NEESWood two-story light wood-frame building.

Mode 3: The third mode shows the largest deviation, with the numerical model overestimating the period by approximately 12.60%. This difference may stem from simplifications in modeling local shear wall deformations or assumptions in the distribution of stiffness along the building.

Table 13 Comparison of modal periods between the benchmark test model and numerical model

Mode	Shake Table Test(sec)	Numerical Model Period (sec)
1	0.286	0.31
2	0.198	0.193
3	0.127	0.143

The numerical model captures the essential dynamic characteristics of the NEESWood two-story light wood-frame building, as evidenced by the close agreement between the experimental and numerical modal periods. These results demonstrate the Timber 3D model's robustness in predicting the behavior of light wood-frame structures under seismic loads.

The slight deviations observed highlight the influence of modeling assumptions, including diaphragm stiffness, mass distribution, nodal fixity and material properties. Overall, the comparison validates the numerical modeling approach adopted in this study for Phase 5 of the structure. This alignment reinforces confidence in the use of the Timber 3D framework for accurately simulating seismic performance in light wood-frame buildings.

4.3.2 Structural Response

4.3.2.1 Displacement Response

The displacement responses shown in Figure 23 to Figure 26 illustrate a comparative analysis of nodal displacement time-history for the benchmark shake table test and the numerical model. The responses correspond to specific shear walls, as indicated in Figure 19, and represent the behavior of the structure at selected nodes under seismic excitation.

Observations:

a) Figure 23: The numerical simulation exhibits strong agreement with the benchmark shake table test results, effectively replicating both the amplitude and phase characteristics of the observed dynamic behavior. The oscillatory patterns and gradual decay of motion after the peak seismic input are well captured by the model. Notably, the residual displacement—visible after approximately 30 seconds—settles around -20 mm, indicating permanent deformation in the structural system due to inelastic response. This residual drift confirms energy dissipation and plastic behavior within the structural components, aligning with expectations for damage accumulation during strong seismic excitation.
b) Figure 24: The displacement response of shear wall E1 in the X-direction (1st-floor roof) demonstrates a slight deviation in peak displacement magnitudes between the numerical and test responses. However, the overall trend and oscillation frequency are consistent, validating the robustness of the numerical model in this direction.
c) Figure 25: For shear wall E28 in the Y-direction (2nd-floor roof), the numerical model captures the general displacement trend but exhibits slight underprediction in the amplitude of peak displacements. This variance might be attributed to minor simplifications in the model assumptions for the semi-rigid diaphragm interaction.
d) Figure 26: The displacement response for shear wall E17 in the X-direction (2nd-floor roof) shows strong alignment between the numerical predictions and the benchmark test. Both responses follow similar oscillatory patterns with closely matching peak values, indicating that the model effectively represents the system's dynamics in this direction.

The numerical model effectively replicates the benchmark shake table test results for all analyzed cases, despite minor discrepancies in amplitude. These deviations can be linked to assumptions in

material damping, semi-rigid diaphragm behavior, and connection modeling within the numerical framework.

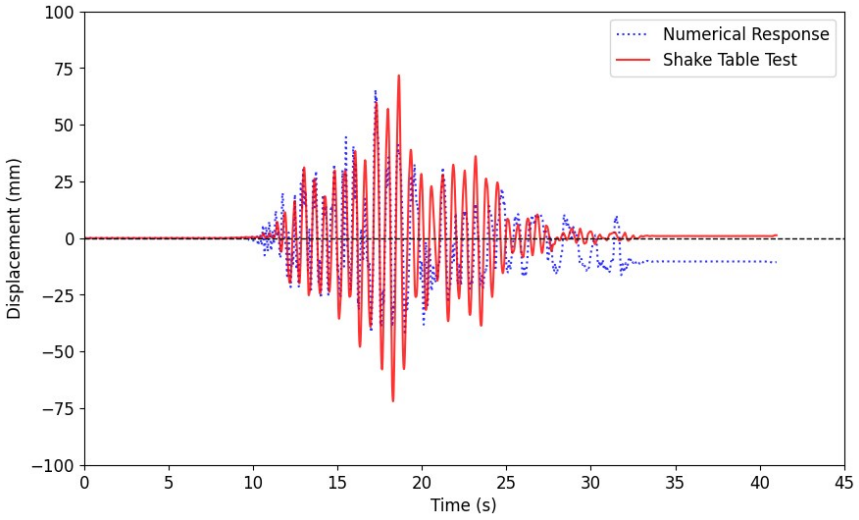

Figure 23 Comparison of nodal displacement time history between the benchmark structure shake table test response and numerical model response for Phase 05 Test 08 – Shear wall E16 in Y direction in 1st floor roof

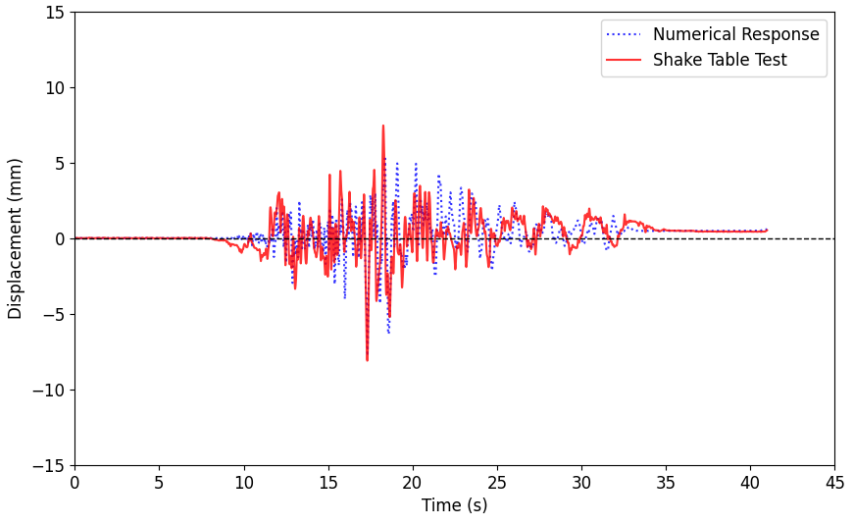

Figure 24 Comparison of nodal displacement time history between the benchmark structure shake table test response and numerical model response for Phase 05 Test 08 – Shear wall E1 in X direction in 1st floor roof

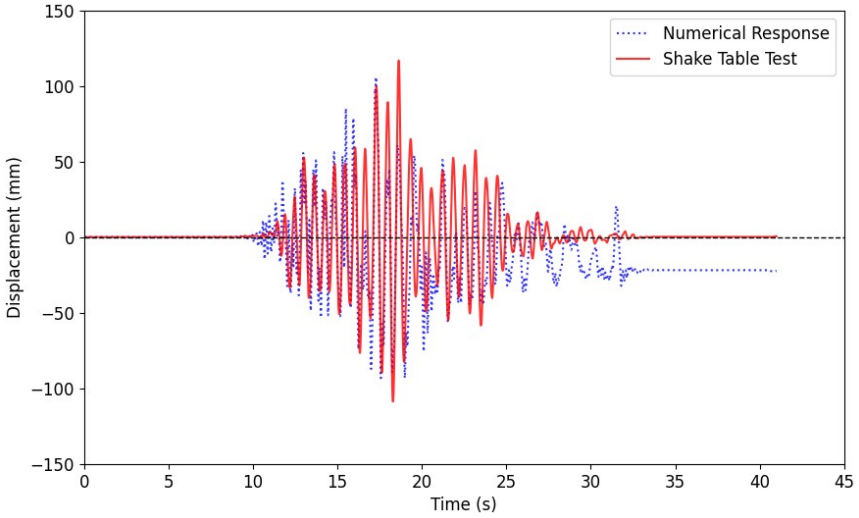

Figure 25 Comparison of nodal displacement time history between the benchmark structure shake table test response and numerical model response for Phase 05 Test 08 – Shear wall E28 in Y direction in 2nd floor roof

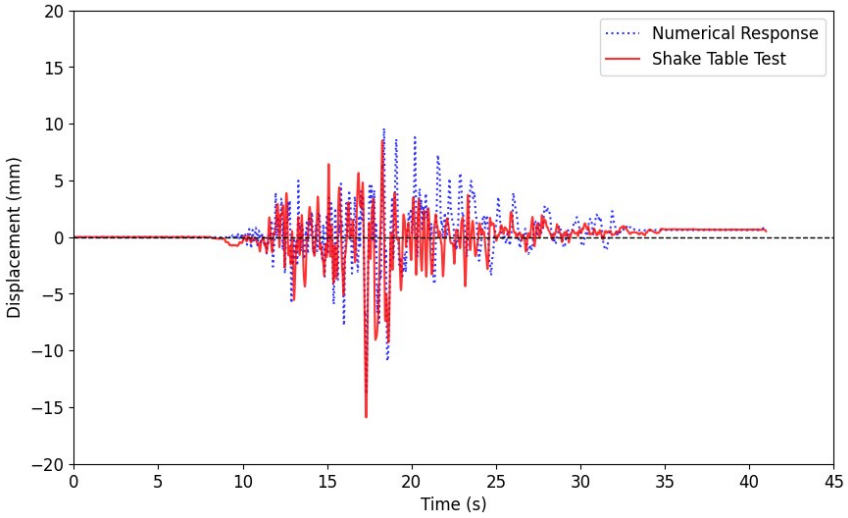

Figure 26 Comparison of nodal displacement time history between the benchmark structure shake table test response and numerical model response for Phase 05 Test 08 – Shear wall E17 in X direction in 2nd floor roof.

4.3.2.2 Force Time History

The base shear force time-history comparisons between the benchmark test (Phase 05 – Test 08) and the numerical model are presented in Figure 27 and Figure 28 for the longitudinal (X-axis) and transverse (Y-axis) directions, respectively. In the benchmark test, the base shear force was calculated by considering the average acceleration response from the building corners, as captured by accelerometers strategically placed at these locations. These average accelerations were multiplied by the tributary mass to compute the base shear forces in both longitudinal and transverse directions.

As shown in Figure 27, the peak base shear force in the benchmark test was close to 130 kN, while the numerical model predicted a peak value of 135 kN. The timing of these peaks is closely aligned, occurring within less than a millisecond of each other during the most significant seismic motion. The numerical model effectively replicates the amplitude and frequency characteristics observed in the benchmark test, with minor deviations attributed to simplifications in the modeling assumptions.

In the transverse direction, as illustrated in Figure 28, the peak base shear force in the benchmark test reached just over 305 kN, compared to the numerical model's prediction of 310 kN. Similar to the longitudinal axis, the timing of the peaks aligns closely. The numerical model captures the primary dynamic behavior, including the oscillation trends and energy dissipation observed in the benchmark test data.

The comparison reveals that the numerical model not only replicates the peak values with a margin of error of less than 5%, but it also captures the general trends, including the oscillation frequency and decay patterns. These results validate the robustness of the modeling approach and its ability to simulate the complex interactions of diaphragm, shear wall, and gravity load components under

seismic loading. However, minor discrepancies in the amplitude and phase may be attributed to idealized boundary conditions and simplifications in material properties in the numerical model.

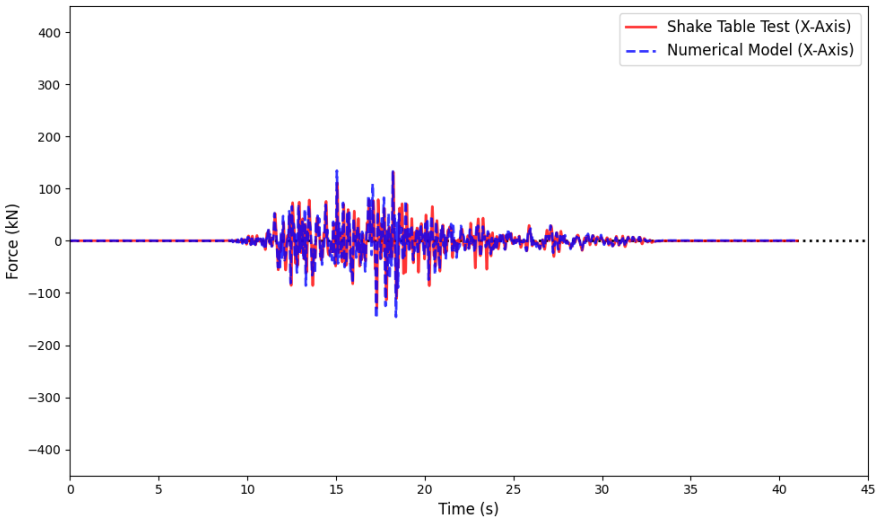

Figure 27 Base shear force time history comparison between the benchmark test (Phase 05 - Test 08) and the numerical response in X direction (longitudinal direction)

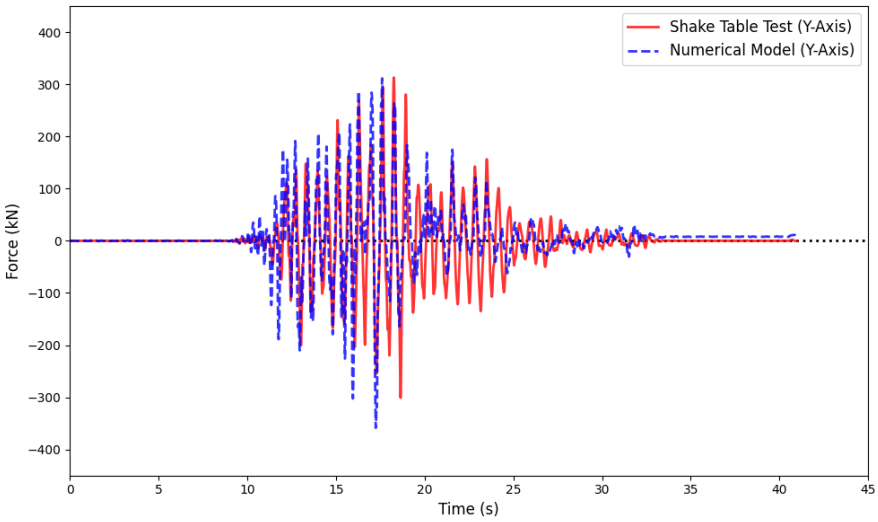

Figure 28 Base shear force time history comparison between the benchmark test (Phase 05 - Test 08) and the numerical response in Y direction (transverse direction)

4.3.2.3 Global Hysteresis

The hysteresis loops shown in Figure 29 depict the relationship between base shear force and central roof displacement for Phase 05 – Test 08, comparing results from the benchmark shake table test and the numerical model.

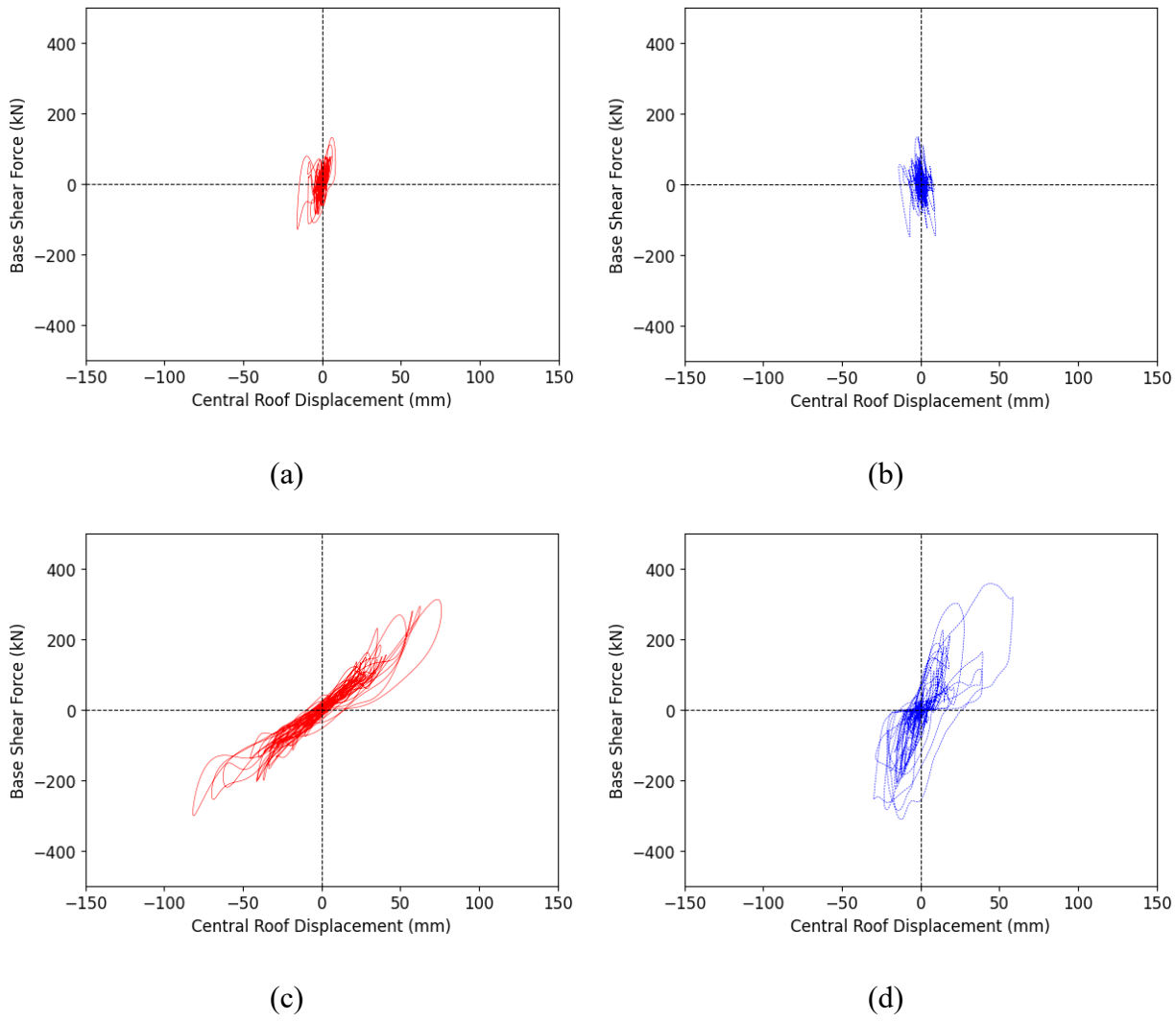

Figure 29 Base shear force versus central roof displacement hysteresis loops for Phase 05 – Test 08. Panels (a) and (c) correspond to the benchmark shake table test results in the X (longitudinal) and Y (transverse) directions, respectively. Panels (b) and (d) represent the corresponding numerical model predictions for the X and Y directions.

Figure (a) and (c) represent the benchmark test results for the X (longitudinal) and Y (transverse) directions, respectively, while panels (b) and (d) show the corresponding numerical model predictions. The central roof displacement was derived by averaging the displacements measured at the roof corners for both the benchmark structure and the numerical model. The base shear force reflects the global structural resistance against the applied seismic loads. The loops indicate the energy dissipation and non-linear behavior of the system under cyclic loading, which is essential for understanding the structural response.

The shape and area enclosed by the loops highlight the structure's capacity for energy dissipation. The similarity in loop shapes between the benchmark test and numerical model demonstrates the accuracy of the modeling approach in capturing global hysteretic behavior.

4.3.2.4 Energy Dissipation

Figure 29 illustrates the base shear force versus central roof displacement hysteresis loops for both the benchmark shake table test and the numerical model in the longitudinal (X) and transverse (Y) directions. These loops provide critical insights into the global hysteretic behavior of the structure, which forms the basis for analyzing the energy dissipation patterns shown in Figure 30 and Figure 31.

Panels (a) and (c) in Figure 29 represent the hysteresis loops derived from the benchmark shake table test for the X and Y directions, respectively. The broader shapes of these loops indicate significant energy dissipation due to the non-linearities in the physical structure, such as material yielding and connection deformation under seismic loading. Panels (b) and (d) correspond to the numerical model's predictions for the same directions. The slightly narrower loops in these panels reflect the calibrated stiffness and damping properties assumed in the numerical model, yet they still capture the overall global behavior with high fidelity.

In Figure 30, the global hysteretic energy dissipation in the longitudinal direction shows agreement between the shake table test results and the numerical model predictions. The benchmark test indicates a slightly faster rate of energy dissipation at the initial stages, primarily due to the direct interaction between the structural elements and seismic inputs. However, by the mid-to-late stages of the simulation, both the test and the numerical model converge, displaying comparable energy dissipation patterns. The peak energy dissipation observed in the numerical model closely follows the benchmark test, validating the model's effectiveness in capturing the global hysteretic behavior.

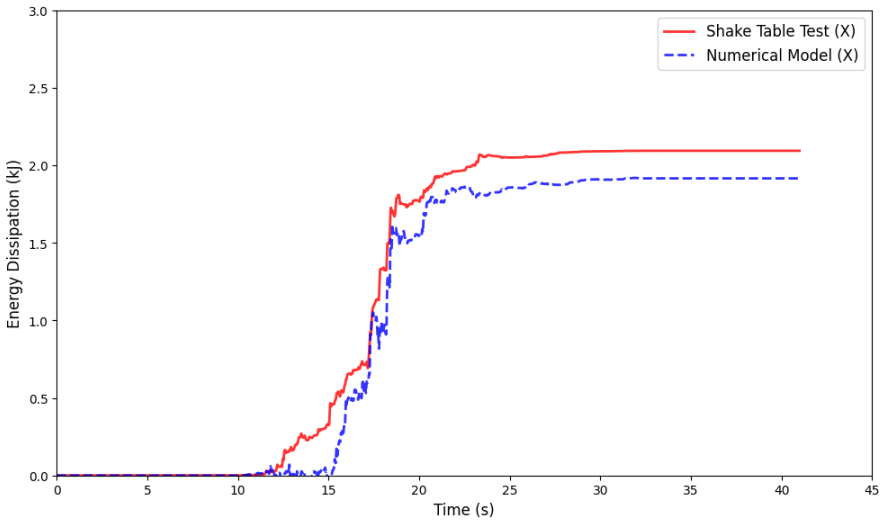

Figure 30 Comparison of global hysteretic energy dissipation of the benchmark test structure and the numerical model in X (longitudinal) direction

Figure 31 provides a similar comparison for the transverse direction. Here, the numerical model successfully replicates the energy dissipation trends observed in the benchmark test. Both curves follow a steady increase, particularly after the 15-second mark, when the seismic inputs reach peak amplitudes. The observed variance in the rate of dissipation during the initial phase might attributed to the assumptions regarding semi-rigid diaphragm behavior in the numerical model.

Despite this, the peak energy dissipation values and the overall cumulative energy trends closely align, demonstrating the robustness of the model in the transverse direction.

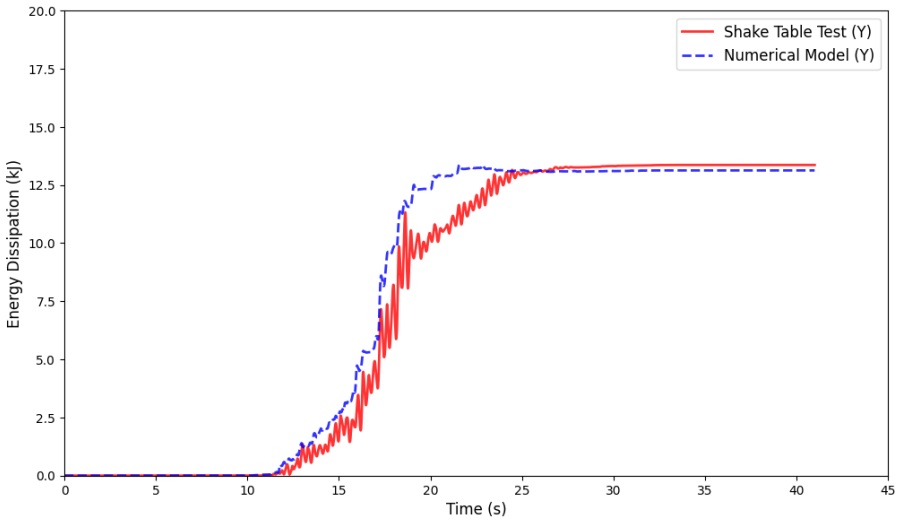

Figure 31 Comparison of global hysteretic energy dissipation of the benchmark test structure and the numerical model in Y (transverse) direction

4.3.2.5 Roof Displacement Profile

The roof displacement profiles of the benchmark test and the numerical model provide essential insights into the structural performance under seismic loading, as depicted in Figure 33 and Figure 34. Figure 32 showcases the deformed shape of the numerical model under the seismic excitation for Phase 05 Test 08 shaking level.

Figure 33 and Figure 34 compare the maximum roof displacement profiles between the shake table test and the numerical model in the X (longitudinal) and Y (transverse) directions. In the X direction, both experimental and numerical results display a consistent linear displacement gradient, with the highest displacement occurring at the roof level. The alignment of the two profiles demonstrates the model's ability to replicate the benchmark structure's global

deformation. Slight differences observed near the second-floor level might attributed to the simplified assumptions about diaphragm stiffness in the numerical representation.

Similarly, in the Y direction, the displacement profiles maintain a comparable trend, with the numerical model closely following the experimental results. Minor deviations are observed in the roof displacement at the second-floor level, likely resulting from the assumptions regarding semi-rigid diaphragm behavior in the numerical model. Despite these differences, the overall displacement patterns agree well, confirming the model's ability to capture the transverse structural response.

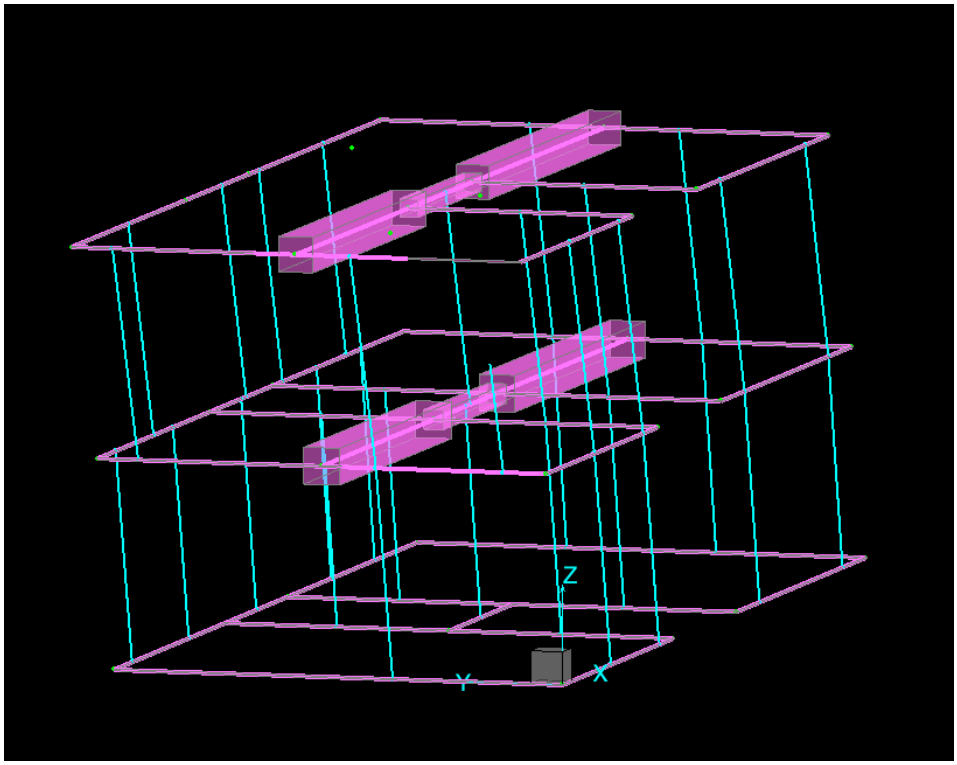

Figure 32 Numerical model time history analysis deformed shape (15th sec) at scale 100 for Phase 05 Test 08

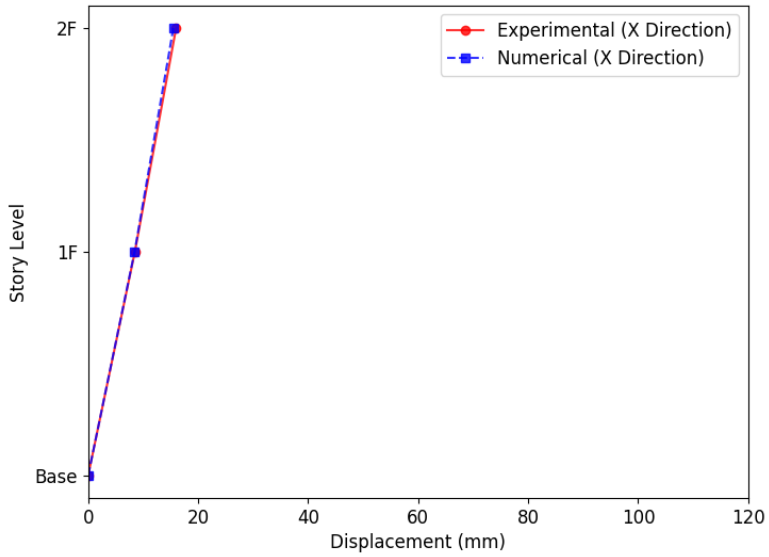

Figure 33 Comparison of maximum roof displacement profile between the benchmark test structure and the numerical model in X direction for Phase 05 Test 08

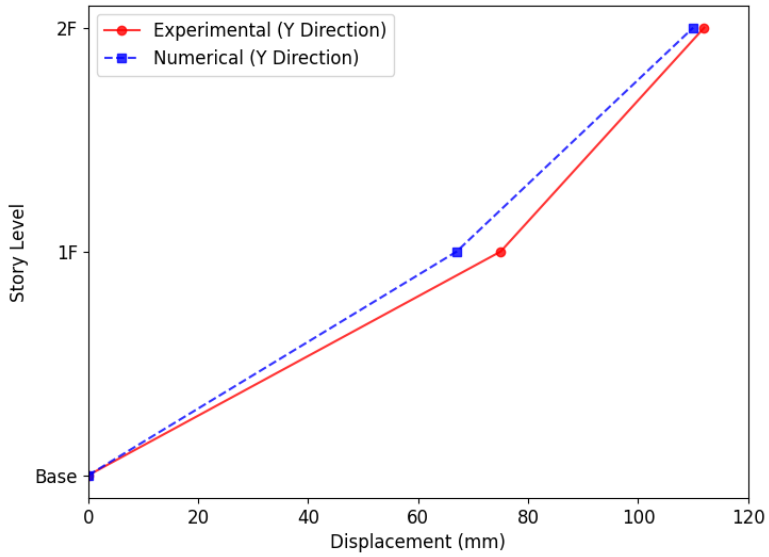

Figure 34 Comparison of maximum roof displacement profile between the benchmark test structure and the numerical model in Y direction for Phase 05 Test 08. The table below summarizes the validation briefly.

Table 14. Summary of Validation Results – Phase 05 Test 08

Validation Item	Benchmark Value	Numerical Model	Difference	% Difference / Match
Modal Period – Mode 1 (sec)	0.286	0.310	+0.024 sec	+8.4%
Modal Period – Mode 2 (sec)	0.198	0.193	-0.005 sec	-2.5%
Modal Period – Mode 3 (sec)	0.127	0.143	+0.016 sec	+12.6%
Residual Displacement (E16 - Y dir)	~-20 mm	~-20 mm	0 mm	100% match
Peak Displacement (E1 - X dir)	~55 mm	~50 mm	-5 mm	~9% underprediction
Base Shear – X Direction	~130 kN	~135 kN	+5 kN	~3.8% overprediction
Base Shear – Y Direction	~305 kN	~310 kN	+5 kN	~1.6% overprediction
Peak Base Shear Timing (X/Y)	~18.2 sec	~18.2 sec	< 1 ms	Excellent match
Energy Dissipation – Final (X Direction)	~2.4 kJ	~2.3 kJ	-0.1 kJ	~4% deviation
Energy Dissipation – Final (Y Direction)	~18.7 kJ	~18.2 kJ	-0.5 kJ	~2.7% deviation
Roof Displacement Profile (X Direction)	Linear gradient	Linear gradient	Minor difference at 2nd fl.	<10 mm deviation
Roof Displacement Profile (Y Direction)	Linear gradient	Linear gradient	Minor difference at 2nd fl.	<10 mm deviation
Global Hysteresis Loop Shape	Full, nonlinear cycles	Closely matching shape	Slightly narrower	High visual agreement

5 Damage Index Model Calibration

The calibration of key parameters is a critical step in implementing the Park and Ang Damage Index (DI) framework for light wood-frame buildings. Unlike steel or reinforced concrete structures, light wood-frame buildings exhibit unique seismic behaviors due to their distributed load paths, reliance on non-structural components, and inherent material variability. These factors necessitate a tailored approach to parameter calibration, ensuring the DI equation accurately reflects the collective seismic response of the building.

When discussing parameter calibration, it is important to distinguish between two types of parameters: the global beta (β) model parameter and the global-level structural parameters, namely global ultimate displacement (D_{ult}) and equivalent yield force (F_y). For global beta calibration, these parameters must be determined specifically for the entire structural system, as opposed to the component-level values commonly derived from shear wall testing. While existing literature provides significant data on component-level ultimate displacement and yield force through shear wall testing, these values are insufficient for system-level calibration. Instead, global parameters must be obtained through pushover analysis of the entire structure, capturing its holistic response under lateral loading.

Figure 35 outlines the systematic process for calibrating these global parameters and the beta model. The process begins with the development and validation of a high-fidelity numerical model of the structure. Pushover analysis is then conducted to identify the global D_{ult} and F_y. Incremental Dynamic Analysis (IDA) follows to determine the collapse intensity of the building, and dynamic analysis is performed to generate global hysteresis responses, in the weaker direction of the building where critical seismic vulnerabilities are most pronounced. These steps culminate in the

calculation of a single β value for the entire system, ensuring consistency and reliability in damage assessments.

This chapter provides a detailed overview of this calibration process, emphasizing its significance in advancing the Damage Index framework to account for the unique challenges posed by light wood-frame buildings.

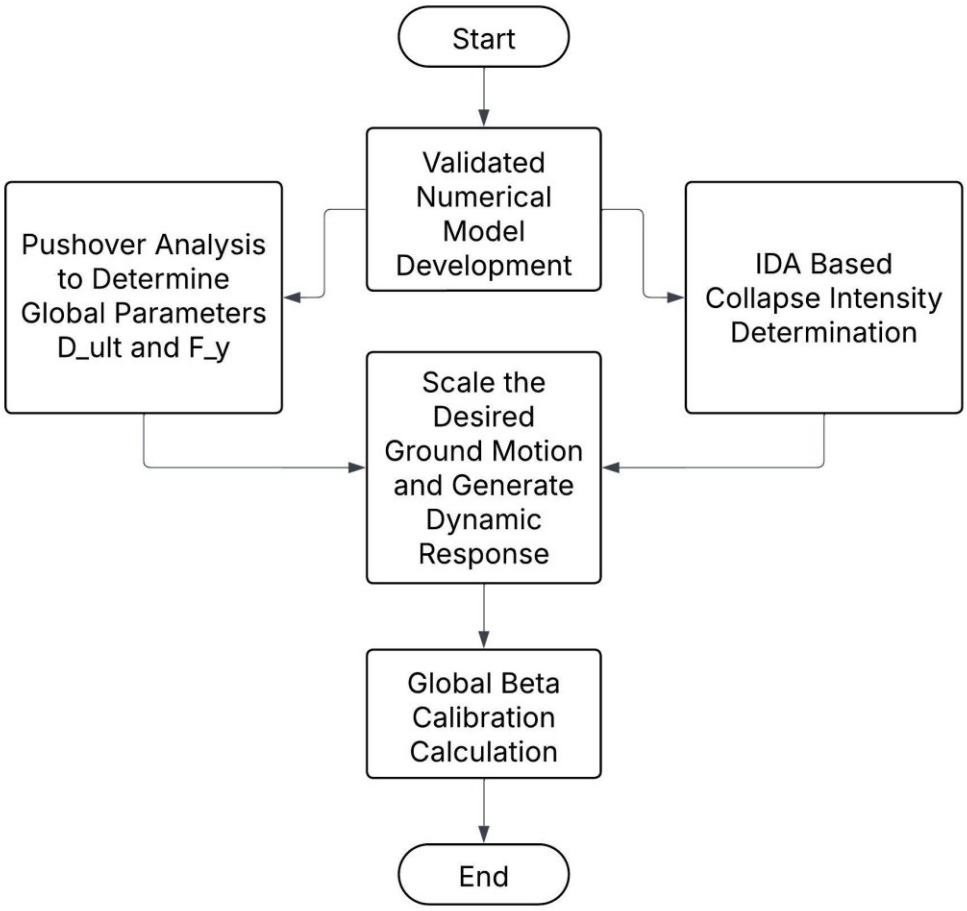

Figure 35. Flowchart illustrating the systematic process for Damage Index (DI) model calibration, including the development and validation of a numerical model, determination of global parameters via pushover analysis, collapse intensity identification through Incremental Dynamic Analysis (IDA), and global beta calibration based on global hysteresis responses.

5.1 Incremental Dynamic Analysis (IDA) of the NEESWood Building

Incremental Dynamic Analysis (IDA) is a powerful method used to assess the seismic performance of structures by subjecting them to a suite of ground motions scaled incrementally in intensity. For this study, the NEESWood light wood frame building numerical model, developed in Timber 3D, was utilized to perform the IDA under 11 distinct ground motion records (Pacific Earthquake Engineering Research Center, 2013) from earthquakes of varying characteristics. These ground motions, listed in the Table 15, include a range of magnitudes, locations, and notable seismic features, reflecting diverse seismic behaviors.

The purpose of Incremental Dynamic Analysis (IDA) is to capture the nonlinear response of a structure as the earthquake intensity increases. This method provides a detailed understanding of how a structure transitions from elastic to inelastic behavior, eventually reaching failure under extreme seismic loads. The analysis helps identify critical seismic parameters which are essential for performance-based design and for quantifying the global Damage Index (DI).

The IDA process employs a diverse set of earthquake ground motions with varying magnitudes, site conditions, and seismic characteristics to provide a robust and comprehensive evaluation of structural behavior under different scenarios. This variability ensures accurate assessment of performance, resilience, and safety across a range of earthquake intensities. The primary goal of IDA is to produce plots that graphically represent spectral acceleration versus structural response, such as drift. These plots are instrumental in evaluating structural performance, calibrating the beta parameter for damage index equations through energy dissipation and displacement trends, and

identifying critical thresholds like maximum drift and displacement to inform performance objectives and failure criteria.

The 11 ground motions were selected to encompass a wide range of seismic events with diverse characteristics, including:

a) **Magnitude and Duration**: Covering small to large-magnitude earthquakes (e.g., 5.9 for Saguenay to 7.4 for Manjil Earthquake), reflecting both short and long-duration shaking.
b) **Geographic and Soil Variations**: Events from different locations, such as Mexico City (amplified effects due to soil conditions) and Kobe, Japan (severe urban ground shaking), capture variations in soil conditions, seismic sources, and geographic regions.
c) **Near-Field vs. Far-Field Effects**: Including near-field events like Northridge and Chi-Chi earthquakes and far-field events such as Val-des-Bois to account for differences in rupture characteristics.
d) **Spectral Characteristics**: Events with varied frequency content and energy dissipation profiles, enabling comprehensive assessment of the structure's dynamic properties.

These ground motions simulate a wide spectrum of seismic scenarios, ensuring that the results from the IDA analysis are representative and encompass real-world conditions. The diverse ground motions provide a basis for understanding the structural response under varying seismic demands.

Table 15. Key information on 11 significant earthquakes used in the IDA analysis, including their year of occurrence, magnitude, location, and notable features.

Earthquake	Year	Magnitude	Location	Notable Features
Northridge Earthquake	1994	6.7	Los Angeles, California, USA	Caused extensive damage and high accelerations; one of the costliest earthquakes.
Christchurch Earthquake	2011	6.2	Christchurch, New Zealand	Severe ground shaking in urban areas; major liquefaction.
Mexico Earthquake	1985	8	Mexico City, Mexico	Amplified effects due to soil conditions; significant loss of life and infrastructure.
Val-des-Bois Earthquake	2010	5	Quebec, Canada	Moderate ground motion; rare event for eastern Canada.
Saguenay Earthquake	1988	5.9	Quebec, Canada	High-frequency shaking; unusual location for significant seismic activity.
Manjil Earthquake	1990	7.4	Iran	Devastating impact in rural areas; significant loss of life.
Loma Prieta Earthquake	1989	6.9	San Francisco, California, USA	Occurred during World Series; caused collapse of freeway structures.
Landers Earthquake	1992	7.3	California, USA	Large surface ruptures; influenced future seismic design.
Chi-Chi Earthquake	1999	7.6	Taiwan	Extensive fault rupture; caused significant structural and geotechnical failures.
Kobe Earthquake	1995	6.9	Kobe, Japan	Severe ground shaking in urban areas; highlighted the importance of seismic retrofits.
Cape Mendocino Earthquake	1992	7.2	Northern California, USA	Significant shaking and surface faulting; caused landslides and infrastructure damage.

5.2 IDA Curve

The IDA scatter plot in the Figure 36 represents the spectral acceleration (S_a) plotted against the drift ratio (%) for the NEESWood two-story light wood frame building model, subjected to a diverse range of 11 earthquake ground motions. The results from 174 dynamic analyses are presented, showcasing a clear trend in structural response under increasing seismic intensity.

5.2.1 Scattered Plot Observed Trends:

a) Initial Elastic Behavior:

For low drift ratios (0% to approximately 1%), the data points exhibit a linear trend, indicating that the structure is behaving elastically. In this region, spectral acceleration (S_a) increases proportionally with the drift ratio, reflecting the structure's ability to resist seismic forces without significant deformation or damage.

b) Transition to Nonlinear Behavior:

Beyond a drift ratio of approximately 1%, the slope of the curve decreases, showing that the structural response becomes nonlinear. This behavior represents the onset of inelastic deformations, where damage mechanisms like yielding or minor cracking might start to occur.

c) Increased Nonlinearity and Damage:

For higher drift ratios (around 2% to 4%), the spread of data points increases significantly. This indicates variability in response due to the differing characteristics of ground motions. The structure absorbs energy through inelastic mechanisms, such as connection slip and material yielding.

d) Plateau and Limit Behavior:

Beyond a drift ratio of approximately 5%, spectral acceleration reaches a near-plateau, particularly for the higher-intensity ground motions. This trend implies that the structure is nearing or has

reached its performance limits, with significant energy dissipation through damage and limited additional resistance.

e) Scatter in Higher Drift Ratios:

At drift ratios exceeding 6%, the scatter among data points increases substantially, reflecting the diversity in ground motion effects and indicating significant structural degradation. This region may correspond to partial or complete failure mechanisms, where performance objectives are likely exceeded.

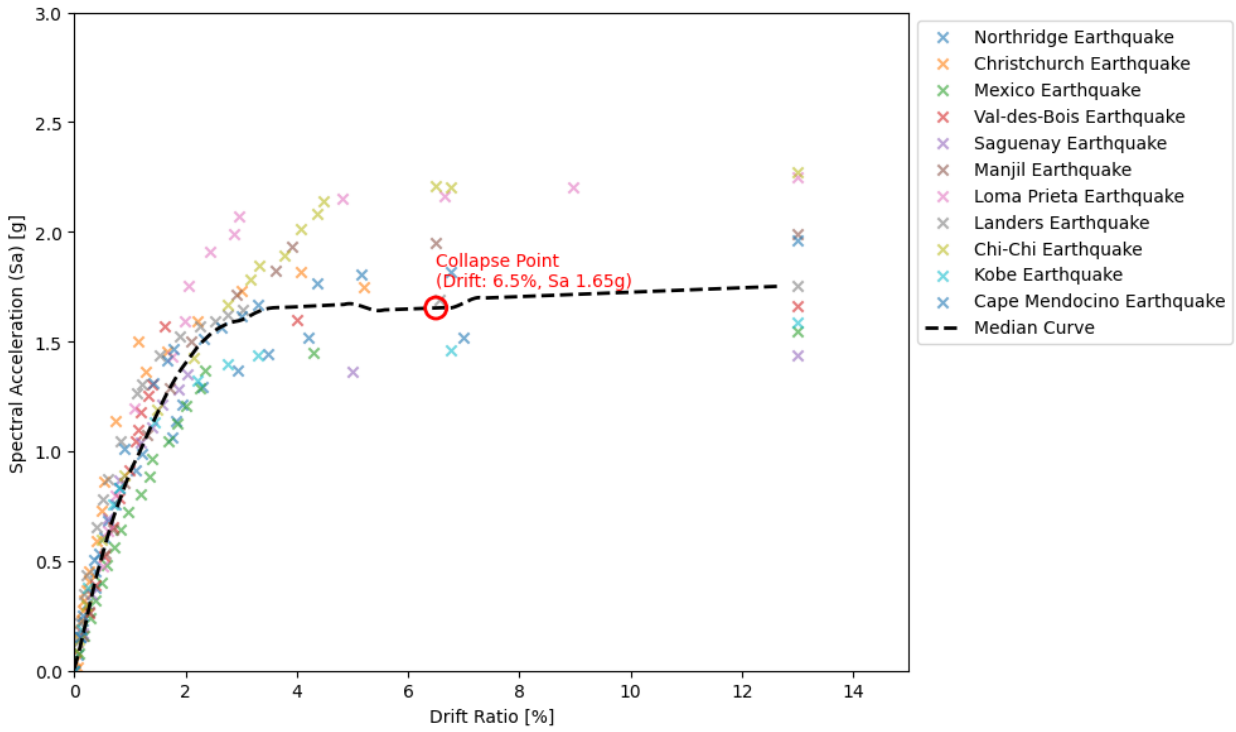

Figure 36. IDA scattered data points for the NEESWood two story light wood frame building Timber 3D model. 11 wide range of ground motion data and 174 corresponding dynamic analysis result is utilized for this plot.s

5.2.2 Median Curve

The median curve as shown in the Figure 37 illustrating the relationship between drift ratio and spectral acceleration was derived from multiple earthquake data sets to represent a central trend across various seismic events. First, drift ratios were standardized on a uniform range (0% to 12%) with 1,000 points to ensure consistency across all datasets, and spectral acceleration values were interpolated linearly. At each drift ratio, the median value was computed to capture the central tendency while reducing the influence of outliers. To enhance readability and ensure smoothness, a Savitzky-Golay filter (Savitzky & Golay, 1964) was applied with a window length of 51 points and a polynomial order of 3, balancing trend preservation with noise reduction. The resulting median curve, displayed as a dashed red line, provides a clear and interpretable trend that highlights the central response of drift ratio and spectral acceleration across all earthquake events, suitable for further analysis and comparison.

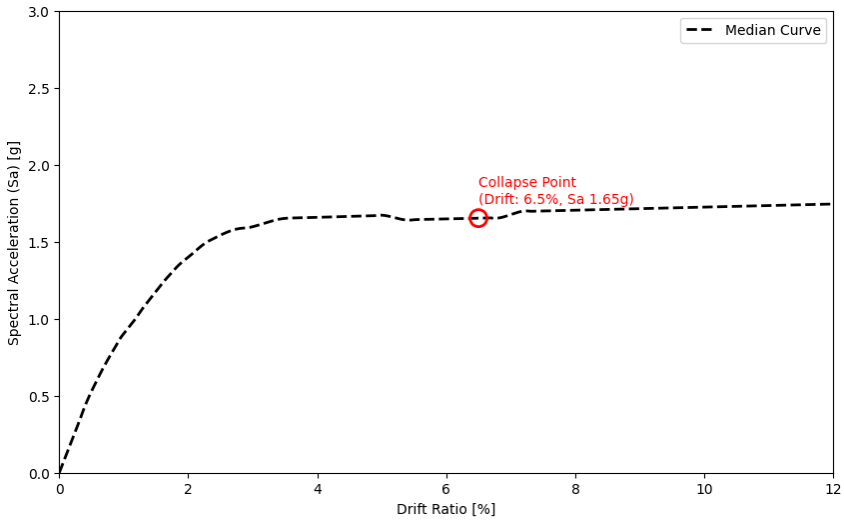

Figure 37. Median incremental dynamic analysis (IDA) curve illustrating the relationship between drift ratio (%) and spectral acceleration (g). The curve represents the median response of the NEESWood two story light wood frame building model based on scattered IDA points from multiple ground motion records. The collapse point is identified at a drift ratio of 6.5% and spectral

acceleration of 1.65g, indicating the intensity level at which the structure reaches its collapse limit state.

This median curve, graphically represents the relationship between drift ratio (%) and spectral acceleration ($\boldsymbol{S_a}$) for the NEESWood two-story light wood frame building model subjected to multiple ground motion records. This curve reflects the aggregate response of the structure to varying earthquake intensities, capturing the trend of increasing drift ratios as spectral acceleration rises. A critical feature of this curve is its distinct transition from an initial steep slope to a plateau region, where drift ratio increases minimally despite rising spectral acceleration. This transition highlights the shift in structural behavior from elastic and nonlinear responses to near-collapse conditions.

The collapse point, marked at a drift ratio of 6.5% and spectral acceleration of 1.65g, is identified where the curve flattens significantly. This flattening signifies that additional increases in seismic demand yield negligible displacement increases, indicating that the structure has reached its performance limit. Justifying the selection of 6.5% drift as the collapse point, it represents the logical and observable threshold at which the structure's deformation capacity is effectively exhausted. While literature (Christovasilis et al., 2009) often suggests a predefined collapse point based on slope change or drift thresholds, such as 7%, the observed behavior of the NEESWood model supports the choice of 6.5%. At this level, the structural response demonstrates a transition into a near-failure state, making it a rational and evidence-based definition of collapse for this analysis.

5.3 Pushover Analysis of NEESWood Two Story Numerical Model

Pushover analysis is a static nonlinear analysis technique widely used to assess the seismic performance of structures by progressively applying lateral forces or displacements to a numerical model. For the calibration of the beta (β) parameter in the Damage Index (DI) framework, pushover analysis plays a critical role in determining global-level parameters, such as the global ultimate displacement (D_{ult}) and equivalent yield force (F_y).

In this study, the pushover analysis is performed on the validated numerical model of the light wood-frame building, where lateral forces are incrementally applied until the structure reaches a predefined displacement or collapse state. The analysis provides insights into the nonlinear behavior of the system, including key parameters like lateral load resistance, stiffness degradation, and post-peak behavior. The resulting pushover curve, as illustrated in Figure 38, represents the relationship between the base shear force (kN) and the average roof displacement (mm).

The parameters D_{ult} (225 mm) and F_y (158 KN) extracted from this curve are essential for calibrating the global beta value. Unlike component-level parameters, which are derived from individual shear walls, these global parameters account for the collective behavior of the entire structure, including interactions between structural and non-structural components. This ensures that the beta calibration reflects the seismic response of the building as a whole, enabling accurate damage assessment for light wood-frame structures under seismic loading.

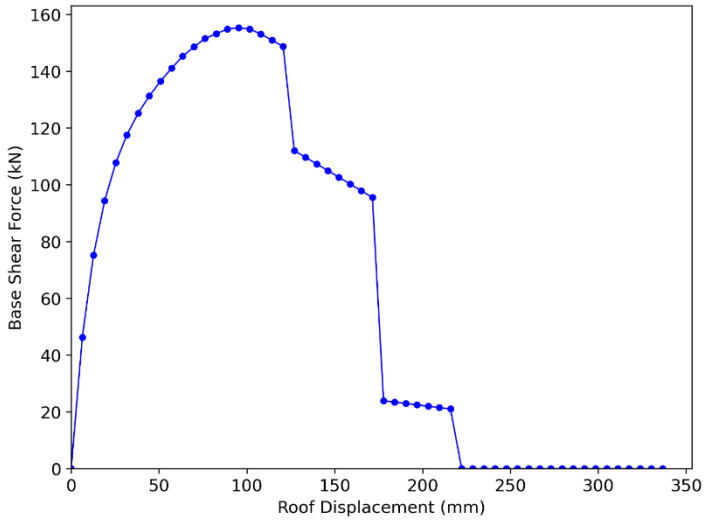

Figure 38. This figure presents the pushover analysis curve, illustrating the relationship between the base shear force and the roof displacement. The force values are expressed in kN, while the displacement is in mm. The curve provides insights into the nonlinear behavior and lateral load resistance of the structure under increasing displacement.

5.4 Global Beta Calibration Calculation for the Benchmark Two-story Light Wood Frame Building

The calibration of the beta (β) parameter is a pivotal step in implementing the Park and Ang Damage Index (DI) framework to assess seismic damage in light wood-frame buildings. This study focuses on calibrating β specifically for the Northridge earthquake ground motion since the Damage Index values are correlated to the observed damage during the benchmark test where Northridge ground motion data was utilized. Given the variability in seismic intensity and characteristics across different earthquakes, the beta parameter must be uniquely calibrated for each event. This ensures that the DI framework accurately reflects the seismic demands imposed by a specific earthquake on the structure.

For the Northridge earthquake, the calibration process involves conducting Incremental Dynamic Analysis (IDA) to extract key global structural response parameters, such as roof displacement and base shear force. These parameters are used to generate a global hysteresis curve, from which the maximum displacement ($D_{\max}$) and hysteretic energy (E) are determined. These values serve as the inputs for calibrating the global β value, ensuring that it represents the collective behavior of the structure under the specific seismic loading conditions of the Northridge event.

5.4.1 Scaled Response Spectrum Northridge Earthquake

Figure 39 presents the response spectrum for the Northridge earthquake ground motion, which was utilized in the NEESWood benchmark test for Phase Five. The response spectrum illustrates the variation of spectral acceleration (S_a) as a function of the structural period (T) for a single-degree-of-freedom (SDOF) system with 5% damping. The spectral acceleration intensity level was scaled to match the collapse intensity observed during the IDA analysis for the NEESWood light wood-frame building (Fundamental period is about 0.30 sec), which was identified at 1.65g.

To achieve the target spectral acceleration of 1.65g, the original Northridge earthquake ground motion data was scaled using a scaling factor of 2.06. Thus, it was made sure that the input motion accurately represent the collapse conditions for the NEESWood structure during the dynamic analysis.

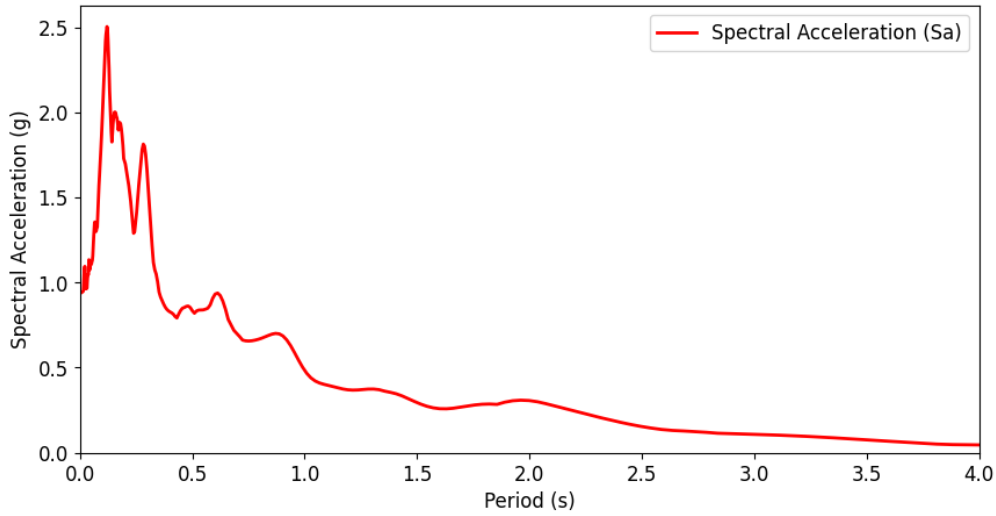

Figure 39. Response spectrum illustrating the variation of spectral acceleration (S_a) with respect to the period (T) for a single-degree-of-freedom (SDOF) system with 5% damping. The ground motion was scaled to match the collapse intensity level of 1.65g at a period 0.30 seconds.

With the scaled Northridge earthquake ground motion data representing the collapse conditions at 1.65g, the next step involves performing dynamic analysis to extract the global structural response necessary for the beta (β) calibration process.

5.4.2 Global Response

Under the global response analysis, the dynamic response for the scaled Northridge earthquake ground motion (calibrated to the collapse intensity of 1.65g) is presented. The response was captured from multiple points on the roof, and the average displacement values were computed to generate a comprehensive system-level hysteresis curve Figure 40. This plot highlights the cyclic

behavior of the structure under seismic loading, showcasing maximum displacement and stiffness degradation.

Additionally, the cumulative energy dissipation over time was calculated and is illustrated in Figure 41. This plot represents the total energy absorbed by the structure during the loading cycle, providing insights into the system's capacity to dissipate seismic energy. These parameters, derived from global system-level responses, form the basis for beta calibration and ensure that the calibrated value accurately reflects the overall seismic performance of the structure.

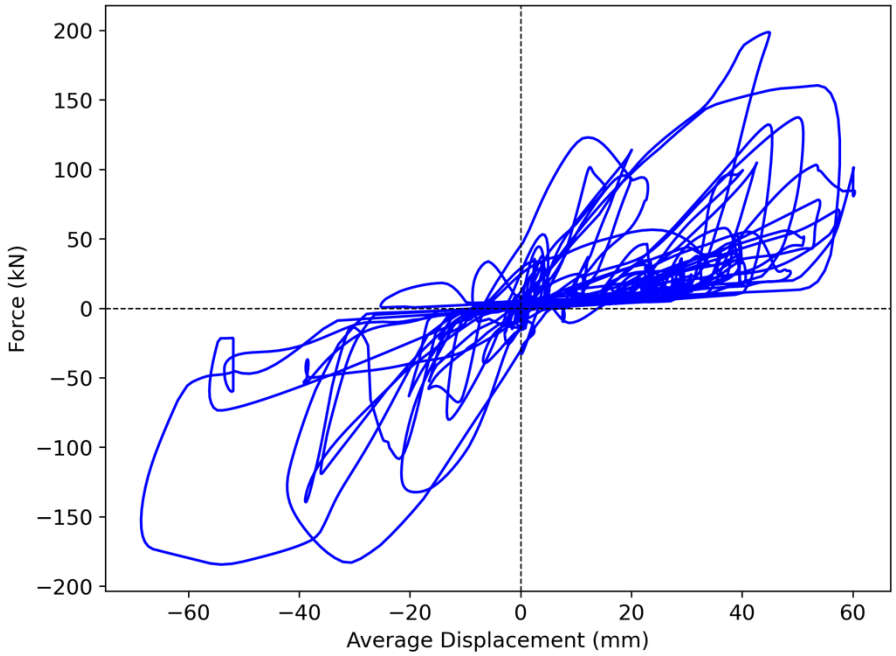

Figure 40. Hysteresis Curve of the System. This figure illustrates the hysteresis response of the global system, showing the relationship between force (kN) and average roof displacement (mm). The curve represents the cyclic behavior of the structure under repeated loading and unloading, capturing its energy dissipation and stiffness degradation over successive cycles.

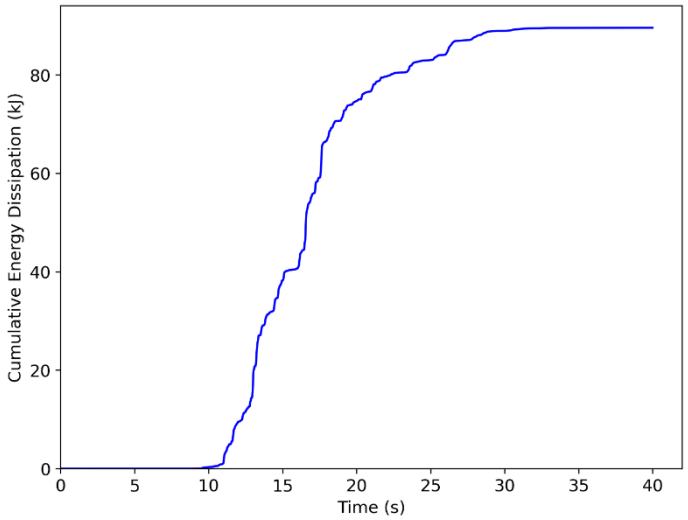

Figure 41. Cumulative Energy Dissipation Over Time. This figure displays the cumulative energy dissipation of the system as a function of time (s). The plot highlights the energy absorbed by the structure during cyclic loading, with energy values calculated in kilojoules (kJ).

5.4.3 Beta Value Sample Calculation

To advance the assessment of seismic performance for the NEESWood light wood-frame building, the next critical step involves the calibration calculation of the beta (β) parameter within the Damage Index (DI) framework. Having identified the collapse intensity through Incremental Dynamic Analysis (IDA) and obtained the corresponding dynamic responses, including maximum displacement and cumulative energy dissipation, we now focus on determining the β value. The following section provides a detailed example of the beta calculation process, showcasing the methodology and step-by-step derivation of the β value based on global system response data maximum displacement of roof $D_{\max}$, energy dissipation (E_i), ultimate displacement (D_{u}), and

yield force (F_y) values, highlighting the methodology employed in calibrating beta for individual walls.

$$DI = \frac{D_{\max}}{D_{\text{ultimate}}} + \beta \cdot \frac{E_i}{F_y \cdot D_{\text{ultimate}}}$$

Where:

DI = 1 (collapse level)

$D_{\max}$ = Maximum displacement during dynamic analysis (from the table) = 60.36 mm

D_{ultimate} = Ultimate displacement = 225 mm (pushover curve)

E_i = Energy dissipation = 89.5 kN-mm

F_y = Equivalent yield force = 158 kN (pushover curve)

β = Calibration parameter to be determined

Step-by-Step Calculation:

a) Reorganize the Equation for Beta:

Solve for β using the given equation:

$$\beta = \frac{DI - \frac{D_{\max}}{D_{\text{ultimate}}}}{\frac{E_i}{F_y \cdot D_{\text{ultimate}}}}$$

b) Calculate $\frac{D_{\max}}{D_{\text{ultimate}}}$:

$$\frac{D_{\max}}{D_{\text{ultimate}}} = \frac{60.36}{225} = 0.27$$

c) Calculate $\frac{E_i}{F_y \cdot D_{\text{ultimate}}}$:

$$F_y \cdot D_{\text{ultimate}} = 158 \cdot 225 = 35{,}550 \text{ kN-mm}$$

$$\frac{E_i}{F_y \cdot D_{\text{ultimate}}} = \frac{89.5 * 1000}{35{,}550} = 2.52$$

d) Substitute Values into the Beta Equation:

$$\beta = \frac{1 - 0.27}{2.52}$$

$$\beta = \frac{0.73}{2.52} = 0.29$$

The global beta calibration has determined a beta (β) value of 0.29, providing a reliable parameter for implementing the Damage Index (DI) framework tailored to NEESWood two story light wood-frame building. This calibrated beta value is now ready for use in component-wise DI calculations, which will ultimately contribute to the calculation of the global-level DI under varying intensity levels of the Northridge earthquake, paving the way for detailed damage assessments and further performance evaluations.

6 Damage Index Calculation and Damage Correlation

The Damage Index (DI) is a vital metric used to quantify the extent of seismic damage in structures, providing insights into both localized and global damage. The process of DI calculation begins at the component level, where individual structural elements, such as walls or frames, are evaluated based on their dynamic response. Component-level DI values are determined by analyzing key parameters, including maximum displacement and cumulative energy dissipation during seismic events. These values capture the unique damage characteristics of each component, enabling a detailed assessment of their performance under seismic loads.

Once the component-level DI values are computed, they are aggregated to determine the Global Damage Index (DI). This involves weighting the contribution of each component based on its energy dissipation relative to the entire structure, thereby offering a holistic view of the building's overall damage state. The DI reflects the cumulative effects of deformation and energy dissipation across all components, providing a comprehensive measure of the structure's seismic vulnerability.

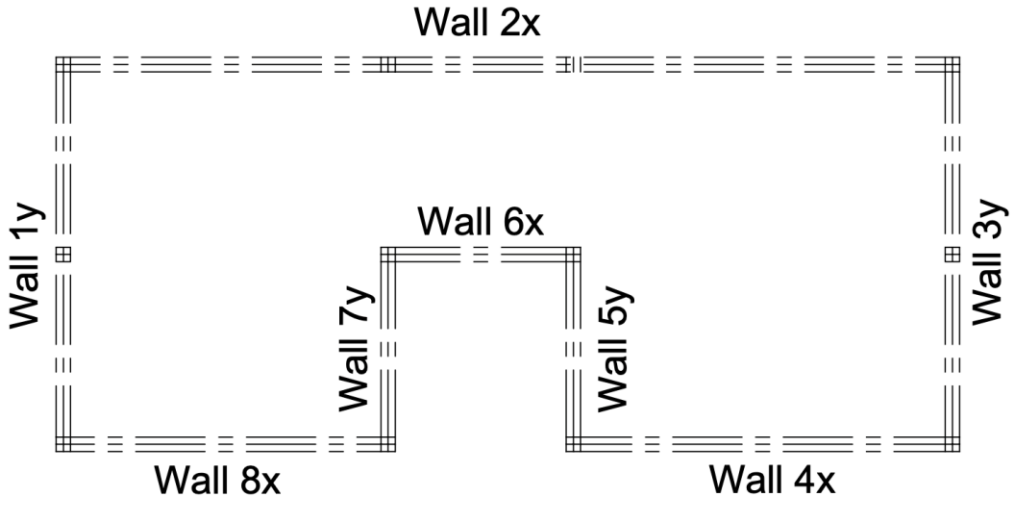

Figure 42. Layout of the wall lines for the NEESWood two story light wood frame building

The NEESWood two-story light wood-frame building, the subject of this study, consists of 16 distinct wall lines—8 on the first floor and 8 on the second floor. Each wall is identified by its orientation (X or Y direction) and contributes uniquely to the structural system's seismic response. Figure 42 illustrates the layout of these walls, which were analyzed individually to calculate their respective DI values. These component-level results were subsequently integrated into the Global Damage Index calculation, facilitating a robust evaluation of the building's performance under varying levels of seismic intensity. This hierarchical approach ensures a thorough understanding of both localized damage mechanisms and the overall structural response.

6.1 Damage Index Calculation for Phase 5, Test 8: Numerical Analysis of Benchmark Response

The purpose of this study is to calibrate the Damage Index (DI) equation to accurately predict the actual damage that a structure might sustain during a given earthquake. By refining the DI equation, the framework aims to bridge the gap between analytical predictions and observed seismic damage, thereby offering a reliable tool for performance-based seismic design and assessment. The Damage Index serves as a critical parameter for quantifying structural performance by combining maximum displacements, cumulative energy dissipation, and calibrated beta values, which represent the hysteretic characteristics of each structural component. Building on the groundwork laid in Chapter 5, where the beta parameter was calibrated for each walls, we are now equipped to proceed with an actual dynamic analysis. This next step involves obtaining the seismic response of individual components of the structure under ground motions and utilizing the calibrated beta values to calculate the Damage Index. This allows for a direct comparison between analytical predictions and physical observations, ensuring that the calibrated equation reflects realistic damage scenarios.

The Northridge earthquake ground motion scaled by a factor of 1.2 was used for the dynamic analysis as a first step. This specific scaling was chosen to replicate the intensity observed during Phase 5 Test 8 of the NEESWood benchmark experiments, where real damage was documented. By aligning the scaled intensity with experimentally observed damage, the calculated DI values can be cross-validated against physical damage patterns, ensuring the accuracy and robustness of the framework.

Table 16. Wall-wise DI values and corresponding energy dissipation

Wall	Floor	D_{max}m)	Energy Dissipation (kN-mm)	DI
Wall 1y	first floor	17.89	6177.58	0.66
Wall 2x	first floor	2.53	6675.46	0.60
Wall 3y	first floor	12.73	5337.27	0.55
Wall 4x	first floor	7.40	10193.20	0.94
Wall 5y	first floor	28.78	9126.95	0.99
Wall 6x	first floor	6.55	10107.47	0.93
Wall 7y	first floor	32.05	9085.07	1.01
Wall 8x	first floor	5.60	10183.98	0.93
Wall 1y	second floor	12.79	5442.14	0.56
Wall 2x	second floor	0.93	2557.48	0.23
Wall 3y	second floor	10.39	5711.34	0.57
Wall 4x	second floor	2.85	4272.81	0.39
Wall 5y	second floor	20.41	8458.68	0.88
Wall 6x	second floor	2.71	4755.21	0.43
Wall 7y	second floor	19.26	8143.07	0.84
Wall 8x	second floor	2.19	4563.74	0.41

The focus on component-level damage allows for a detailed assessment of localized structural behavior, which is critical for understanding how individual walls contribute to the global structural response. Table 17 summarizes the DI calculations for all 16 walls of the two-story NEESWood light wood frame model, separated into first and second floors. These DI values were

computed using the calibrated beta parameters and reflect the maximum displacement and energy dissipation recorded during the dynamic analysis under the scaled Northridge ground motion.

Table 17. Table presenting the calculated Damage Index (DI) for each wall on the first and second floors of the NEESWood two-story light wood frame numerical model. The Northridge earthquake, scaled by a factor of 1.2, was utilized for the dynamic analysis of the Timber 3D model. The DI values are tabulated for the corresponding walls using calibrated Beta values.

6.1.1 Sample DI Calculation for Wall 1Y First Floor

The Global Level Damage Index (Global DI) represents the overall seismic damage of the structure by aggregating the contributions of individual component-level damage indices (DI_i) weighted by their energy dissipation. This section presents the step-by-step calculations to derive the Global DI using the results from Table 17.

The Damage Index (DI_i) for each wall is calculated using the following formula:

$$DI_i = \frac{D_{\max,i}}{D_{\text{alt}}} + \frac{\beta_i \cdot E_i}{F_y \cdot D_{\text{alt}}}$$

Where:

$D_{\max,i}$: Maximum displacement of the i-th component (mm).

D_{alt}: Ultimate displacement capacity of the wall ($D_{\text{alt}} = 149.56$ mm) (ref- Figure 1)

β_i: 0.29

E_i: Energy dissipated by the $i-th$ component from Table 17 =6177.58 KN-mm

F_y: Yield strength of the wall ($F_y =$ 22.12 kN). (ref- Figure 1)

As an example, consider Wall 1y on the first floor:

$$D_{\max,i} = 17.89 \text{ mm}$$

$$\beta_i = 0.29$$

$$E_i = 6177.58\,\text{kN-mm}$$

Substituting the values:

$$DI_{1y,\text{first floor}} = \frac{17.89}{149.56} + \frac{0.29 \cdot 6177.58}{22.12 \cdot 149.56}$$

$$DI_{1y,\text{first floor}} = 0.66$$

6.1.2 Global Damage Index Calculation

The Global Damage Index (DI) serves as a critical parameter for assessing the overall performance and integrity of a structure during seismic events. Unlike component-level DIs, which quantify damage for individual structural elements, the Global DI provides a holistic measure of the cumulative damage sustained by the entire structure. It synthesizes the contributions of all structural components by accounting for their respective energy dissipation capacities and their damage indices.

To compute the Global DI, a weighting factor ($\boldsymbol{\lambda_i}$) is assigned to each component based on the proportion of energy it dissipates relative to the total energy dissipation of all components. The weighting factor ensures that components with higher energy dissipation have a greater influence on the Global DI, reflecting their critical role in the structural response.

This section outlines the detailed calculations performed to derive the Global DI for the NEESWood two-story light wood-frame structure, using the numerical response data from the Northridge earthquake scaled by a factor of 1.2. A sample calculation for the Wall 1Y at the first floor level is demonstrated.

As discussed earlier, the weighting factor (λ_i) represents the proportion of energy dissipated by each wall relative to the total energy dissipated by all walls:

$$\lambda_i = \frac{E_i}{E_{\text{total}}}$$

Where:

$$E_{\text{total}} = \sum_{i=1}^{16} E_i = 110791 \text{ kN-mm}$$

For Wall 1y on the first floor:

$$\lambda_{1y,\text{first floor}} = \frac{6177.58}{110791} = 0.06$$

The Global DI is computed as the weighted sum of the individual DIs:

$$DI_{\text{global}} = \sum_{i=1}^{16} \lambda_i DI_i$$

Table 18. Component-wise Damage Index (DI) calculation for the NEESWood two-story light wood frame structure utilizing numerical response of Northridge earthquake ground motion with scale factor 1.20

Wall	**Floor**	**Component DI_i**	**Lambda λ_i**	$\lambda_i DI_i$
Wall 1y	first floor	0.66	0.06	0.04
Wall 2x	first floor	0.60	0.06	0.04
Wall 3y	first floor	0.55	0.05	0.03
Wall 4x	first floor	0.94	0.09	0.09
Wall 5y	first floor	0.99	0.08	0.08
Wall 6x	first floor	0.93	0.09	0.08
Wall 7y	first floor	1.01	0.08	0.08
Wall 8x	first floor	0.93	0.09	0.09
Wall 1y	second floor	0.56	0.05	0.03
Wall 2x	second floor	0.23	0.02	0.01
Wall 3y	second floor	0.57	0.05	0.03
Wall 4x	second floor	0.39	0.04	0.02
Wall 5y	second floor	0.88	0.08	0.07
Wall 6x	second floor	0.43	0.04	0.02
Wall 7y	second floor	0.84	0.07	0.06
Wall 8x	second floor	0.41	0.04	0.02

Table 18 presents the component-wise Damage Index (DI) calculations for the NEESWood two-story light wood-frame structure. The table summarizes the maximum displacement, energy dissipation, calibrated beta, and computed DI values for each wall on both the first and second floors. Additionally, the weighting factor and its contribution to the Global DI are listed, providing insights into the relative importance of each wall in the overall structural response.

Summing the $\lambda_i DI_i$ values for all walls:

$$DI_{\text{global}} = \sum_{i=1}^{16} \lambda_i DI_i = 0.76$$

6.2 Damage Correlation

The primary purpose of this section is to establish a correlation between the calculated Global Damage Index (DI) from the numerical dynamic analysis and the observed damage from the corresponding benchmark test, specifically Phase 05 Test 08 of the NEESWood two-story light wood-frame building. The calculated Global DI for this test was 0.76, and this value is used as a basis for understanding the severity and extent of damage visible in the benchmark test. By comparing numerical predictions with actual damage, this analysis aims to validate the calibration of the Damage Index equation and assess its reliability for predicting real-world structural performance.

The photographs in Figure 43 illustrate the types of damage sustained during the seismic benchmark test. The observed damage includes both structural and non-structural failures:

Cracking in Gypsum Wallboard:

Figure 43. Observed damages for the NEESWood benchmark test after Phase 05 Test 08

Extensive diagonal, horizontal, and localized cracks were observed near wall intersections and openings, such as doors and windows. These cracks suggest that the gypsum wallboard experienced significant shear and tensile forces due to seismic shaking.

Spalling of Stucco:

The exterior stucco layer exhibited spalling around corners and edges of walls, indicating localized material failure due to high stress concentrations. Spalling is particularly prominent near connections and load-transfer regions.

Buckling and Crushing:

Evidence of buckling in wallboards and crushing of drywall corners demonstrates areas subjected to compressive stresses exceeding material limits. These types of damage often occur in areas of inter-story drift or concentrated force transfer.

Localized Connection Failures:

Cracking and separation were noted along sill plates and wall intersections, highlighting critical points of weakness where forces exceeded connection capacity.

6.3 Correlating Damage Across a Range of Intensity Levels

Following the correlation of observed damage with the calculated Global Damage Index (DI) for Test Phase 5, Test 8, it is equally critical to expand this analysis to a broader range of intensity levels. The benchmark structure used for the NEESWood project was fully furnished and constructed to simulate real-world conditions. This provides a unique opportunity to investigate how the structure responds to varying seismic intensities and how observed damage aligns with calculated DIs across different scenarios.

By analyzing a series of additional tests under Test Phase 5, which were conducted using a wide variety of ground motion intensity levels, we can better understand the progression of structural damage. These tests are essential for:

a) Exploring Intensity-Dependent Damage:

Different earthquake intensity levels elicit varying degrees of structural response, ranging from minor cracking and spalling to extensive deformation and potential collapse. By correlating observed damage with calculated DIs across these tests, we can validate the robustness of the damage index framework.

b) Identifying Damage Trends:

The analysis of damage under varying seismic intensities helps reveal trends, such as the onset of significant cracking or the transition to collapse-level damage. Understanding these trends is vital for assessing building resilience and identifying critical performance thresholds.

As seismic intensity increases, damage typically transitions from localized non-structural damage to widespread structural failures. Investigating these transitions helps refine performance objectives and establish a more comprehensive understanding of structural behavior. The results of these tests will further illuminate how the Global DI captures the cumulative effects of displacement, energy dissipation, and hysteretic behavior under increasing earthquake intensity.

To build upon this analysis, it is essential to correlate the calculated Global Damage Index (DI) values with the seismic intensity parameters used during these benchmark tests. Table 19 provides a summary of the Peak Ground Acceleration (PGA) values in both the X and Y directions, which represent the seismic intensity levels applied to the benchmark structure in the numerical analysis. These PGA values serve as the input for the dynamic simulations, while the corresponding calculated Global DI values offer a quantitative measure of the structural response and damage

under each intensity scenario. By presenting this table, we aim to link the seismic intensity levels with the predicted structural performance, enabling a comprehensive assessment of how well the calculated Global DI reflects the observed damage trends.

Table 19. Peak Ground Acceleration (PGA) in X and Y directions from NEESWood benchmark tests used in numerical analysis and obtained Global DI from numerical response

Test ID	PGA(g) in X Direction	PGA(g) in Y Direction	Global Damage Index
Phase 5, Test 3	0.19	0.22	0.20
Phase 5, Test 6	0.31	0.36	0.52
Phase 5, Test 11	0.47	0.47	0.83

The correlation between the calculated global Damage Index (DI) and the observed damage provides a comprehensive understanding of how the structure responds to varying seismic intensities. The tabulated results in Table 19 present numerical evidence of structural performance and its degradation under increasing ground motion levels. To further validate and contextualize these findings, visual documentation of the damage observed during the corresponding benchmark tests is presented. These figures illustrate the progression of damage at various DI levels, offering a qualitative perspective that complements the numerical analysis. By examining the visual damage and its alignment with the calculated DI, we can critically assess the accuracy and applicability of the DI framework in capturing real-world structural behavior.

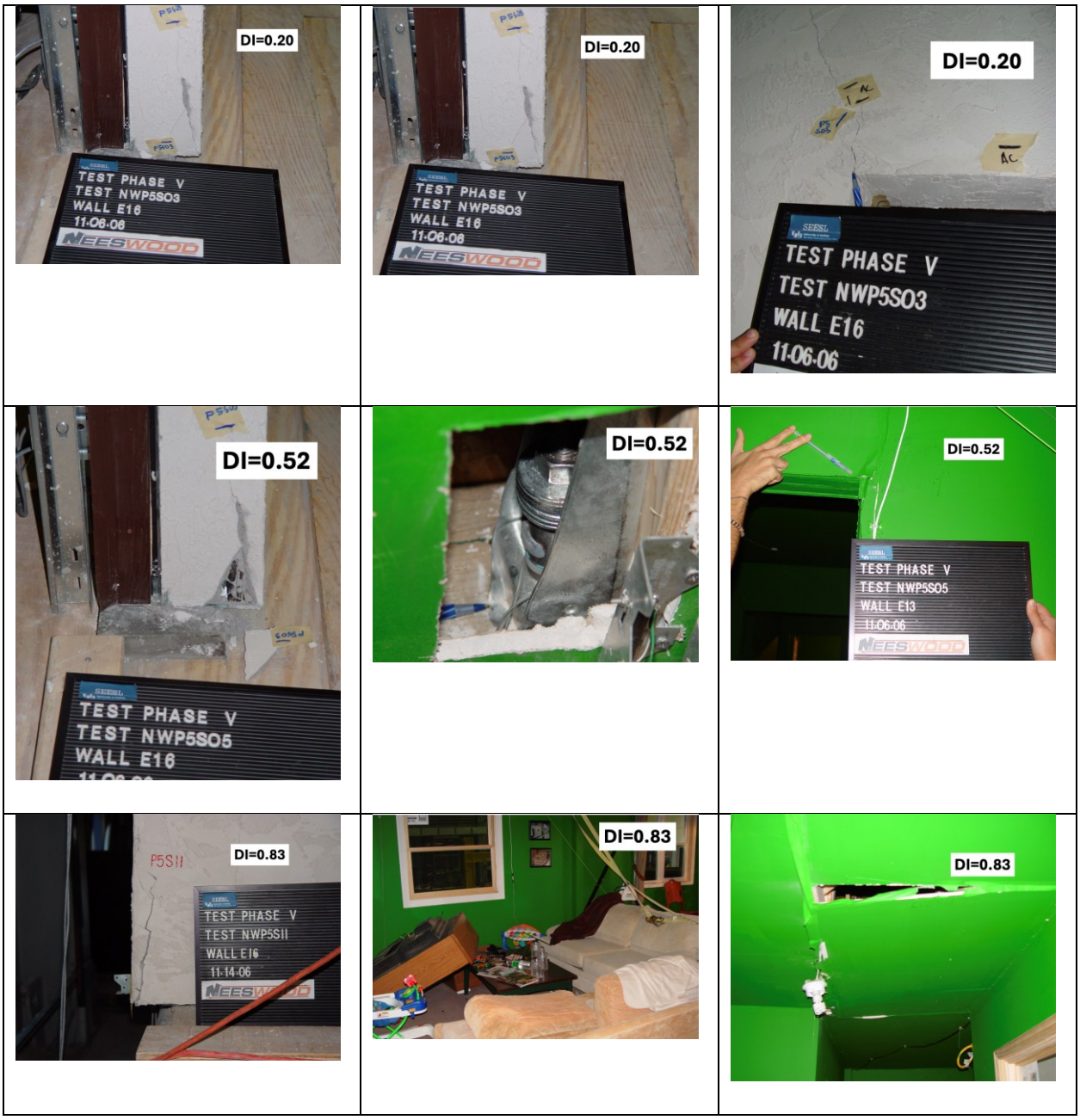

Figure 44. Level of damage observed during different test phases of the NEESWood benchmark test and corresponding global DI value for each of the tests based on numerical dynamic analysis response

The observed damage trends corresponding to the global Damage Index (DI) values reveal a progressive increase in structural damage as the DI increases, providing a clear correlation between the numerical analysis and the physical test results. Here's an analytical breakdown of the trends:

a) DI = 0.20 (Minimal Damage):

   Observed damage is primarily non-structural, with minor cracks evident on wall surfaces and localized areas. This level of damage corresponds to minor seismic excitations, where the structure remains within the elastic range or experiences minimal inelastic behavior. The DI value of 0.20 accurately reflects this early stage of damage, signifying minor energy dissipation and limited displacement.

b) DI = 0.52 (Moderate Damage):

   Damage observations reveal significant spalling of the stucco, diagonal cracking around wall openings, and detachment of non-structural components. The increase in DI indicates that the structure has transitioned to moderate inelastic behavior, with energy dissipation concentrated around joints and weak points. The observed damage aligns with numerical predictions, emphasizing the structural vulnerability at this stage, particularly in areas of high stress concentration.

c) DI = 0.83 (Severe Damage):

   The damage becomes widespread, with visible signs of structural compromise such as large cracks, extensive spalling, and partial failure of wall sections. Internal non-structural components show extensive deformation, and localized collapse in certain regions becomes evident. The high DI value reflects substantial energy dissipation and large displacements, indicative of near-collapse conditions. The numerical predictions provide a

strong correlation to the observed damage, underscoring the validity of the damage index framework.

In addition to calculating the Global Damage Index (DI) from the numerical model response, this study further reinforces the validity of the proposed framework by computing the Global DI directly from the benchmark test response.

The comparison between the Global Damage Index (DI) values derived from the numerical model and those obtained from the experimental benchmark test indicates a generally consistent trend, validating the core assumptions of the proposed framework and beta calibration process. However, some discrepancies—particularly in mid- and high-intensity tests—highlight areas where the validation remains relatively weak and presents opportunities for improvement. The lack of model optimization, while intentional to preserve generality, limited the accuracy of response prediction, especially in replicating nuanced hysteretic behavior. Simplified assumptions regarding material uniformity, connection behavior, and boundary conditions further contributed to deviations from experimental results, which inherently captured more complex energy dissipation mechanisms such as fastener slip and material degradation. Moreover, the experimental setup itself had limitations, including potential noise in sensor data and constrained instrumentation coverage, which may have affected the precision of measured displacements and forces. To strengthen the validation, future work should incorporate targeted calibration, probabilistic modeling of construction variability, and higher-resolution experimental data. These enhancements would improve the predictive fidelity of the numerical model and elevate the reliability of the DI framework in capturing real-world seismic performance of wood-frame structures.

Table 20. Comparison of Global DI values obtained from numerical response and experimental benchmark test response, demonstrating the validity of the beta calibration and the reliability of the developed framework.

	P05T03	**P05T06**	**P05T08**	**P05T11**
Numerical Model	0.20	0.52	0.76	0.83
Benchmark Test	0.13	0.58	0.61	0.79

By applying the same Damage Index frameworks, but utilizing the displacement and energy dissipation observed during the actual shake table test, the experimental Global DI was determined. The calculated values align well with those derived from the numerical model, indicating that the beta calibration performed for the numerical model accurately reflects the real-world behavior of the structure under seismic loading. This additional validation step further confirms that the developed methodology is a reliable tool for assessing seismic damage in light wood-frame buildings.

The results of this study showcase the effectiveness of the developed Damage Index (DI) framework for assessing seismic damage in light wood-frame buildings. The systematic approach, outlined in the flowchart (Figure 45), provides a robust and repeatable methodology for evaluating structural performance under varying seismic intensities.

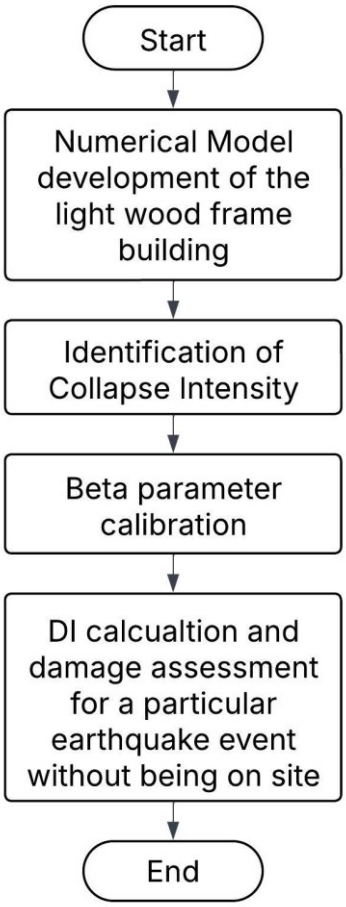

Figure 45. Flowchart outlining the step-by-step framework for seismic damage assessment of light wood-frame buildings using Damage Index (DI).

The framework begins with the development of a validated numerical model of the structure, which captures the unique characteristics of light wood-frame buildings, including their redundancy, load-sharing mechanisms, and material variability. This model forms the foundation for subsequent steps, such as the identification of collapse intensity through Incremental Dynamic Analysis (IDA). The global beta (β) parameter calibration process ensures that the DI equation accurately reflects the cumulative behavior of the structure as a whole.

The results demonstrate a strong correlation between calculated DI values and observed damage patterns during the NEESWood benchmark tests. For example, at a DI of 0.20, minimal damage was observed, primarily consisting of minor cracks in non-structural components. As the DI increased to 0.52, moderate damage, including spalling and cracking around wall openings, became evident. At a DI of 0.83, the damage transitioned to severe, with large cracks, spalling, and partial structural failure observed. These trends validate the capability of the DI framework to accurately capture and predict the progression of structural damage.

In conclusion, the results affirm that the developed framework is a practical and reliable tool for assessing seismic damage in light wood-frame buildings. By integrating numerical and experimental data, it bridges the gap between theoretical predictions and real-world observations. The methodology is not only a step forward in damage assessment but also a critical tool for advancing performance-based seismic design and resilience planning for light wood-frame structures.

7 Conclusion

This thesis presents a comprehensive and validated framework for calculating the Global Damage Index (DI) specifically tailored to light wood-frame buildings, representing a major advancement in seismic performance assessment for this widely used construction type. By addressing the limitations of traditional component-based damage models, the study introduces a global-level methodology that captures the cumulative and system-wide behavior of light-frame structures under seismic loading conditions.

The proposed framework integrates nonlinear numerical modeling, Incremental Dynamic Analysis (IDA), pushover analysis, and experimental validation using data from the NEESWood two-story light-frame wood building shake table test. This multidimensional approach enables accurate prediction of global damage while maintaining sensitivity to both structural and non-structural failure mechanisms.

A key contribution of the study is the calibration of the β parameter in the Park and Ang Damage Index equation, customized for the dynamic characteristics of wood-frame systems. The calibration process utilized critical global response parameters such as roof displacement and base shear force, derived from scaled ground motion simulations of the 1994 Northridge earthquake. The model's predictions were cross-validated against physical observations from full-scale testing, revealing a strong correlation between computed DI values and actual damage patterns.

To enhance interpretability, the study establishes damage classification thresholds based on the computed DI values:

- DI < 0.25 corresponds to minor, non-structural damage, such as superficial cracking or detachment of finishes.

- DI between 0.25 and 0.60 marks the transition to major non-structural damage and initiation of structural damage, typically affecting sill plates, anchorage regions, and local deformation zones.
- DI > 0.60 indicates extensive structural damage, with possible system instability or collapse potential, and reflects significant compromise in lateral load-resisting elements.

These thresholds provide a practical means to interpret DI outputs and connect numerical predictions to real-world consequences. While the thresholds are supported by strong experimental validation, they are preliminary and should be refined further through the development of damage fragility curves and broader datasets encompassing varying ground motions and building typologies.

The framework developed here offers substantial benefits for engineering practice, post-earthquake assessment, and retrofitting strategies. It equips engineers, researchers, and decision-makers with a quantifiable and scalable tool to evaluate seismic vulnerability and prioritize structural interventions. Moreover, by bridging the gap between localized damage measures and holistic building behavior, this approach lays the groundwork for more robust risk models and resilience-based design tools for wood-frame construction.

In conclusion, this study marks a significant step forward in the seismic evaluation of light wood-frame buildings. Future research should aim to extend the framework to multi-story and hybrid systems, incorporate long-duration and near-fault ground motions, and enhance calibration through a statistical, multi-building dataset to support region-wide seismic resilience efforts.

7.1 Future Work

While this thesis establishes a robust and validated framework for the calculation of the Damage Index (DI) tailored to light wood-frame buildings, there remains considerable scope for refining

and expanding the methodology. The work presented represents a critical foundation, but future research is essential to enhance its applicability and precision.

A key area for advancement lies in the development of damage fragility curves specifically for light wood-frame construction. Unlike steel and concrete buildings, where well-defined fragility functions and limit-state criteria have been developed, light wood-frame structures lack systematic studies that connect DI values with observed physical damage. The threshold classifications proposed in this study—ranging from minor non-structural to severe structural damage—serve as initial estimates but require further calibration through large-scale experimental campaigns and analytical studies. Future work should incorporate a wide range of seismic inputs, including various ground motion types (e.g., crustal and subduction earthquakes) and intensity levels, as well as diverse building geometries and configurations.

Additionally, the global-level beta calibration process introduced in this thesis must be validated across more complex structural systems, such as multi-story light-frame buildings. This will involve additional experimental testing and refined numerical modeling to ensure that the interaction between structural and non-structural components is accurately captured under different loading conditions. Incorporating advanced material models, such as nonlinear hysteretic behavior and degradation effects, along with soil-structure interaction, could provide a more comprehensive understanding of seismic performance.

Further research should also aim to establish quantitative limit-state criteria based on DI values. By correlating specific DI thresholds with defined damage states—such as reparable non-structural damage, localized structural yielding, or near-collapse—engineers can adopt this framework in practical seismic design, retrofitting, and post-earthquake assessment strategies. Doing so will help

align light wood-frame assessment methods with those already available for reinforced concrete and steel structures.

In conclusion, while this thesis lays the groundwork for DI-based seismic assessment in light wood-frame buildings, continued research toward the development of fragility curves, DI-based limit states, and enhanced modeling approaches will be instrumental in advancing this methodology into a widely accepted and applicable engineering tool for seismic risk mitigation.

8 References

Bahmani, P., Van De Lindt, J. W., Mochizuki, G., & Pryor, S. (2014). Four-Story Full-Scale Soft-Story Light wood frame Building Shake Table Test at NEES@UCSD.

Christovasilis, I. P., Filiatrault, A., & Wanitkorkul, A. (n.d.). Seismic Testing of a Full-Scale Two-Story Light-Frame Wood Building: NEESWood Benchmark Test.

Christovasilis, I. P., Filiatrault, A., Constantinou, M. C., & Wanitkorkul, A. (2009). Incremental dynamic analysis of woodframe buildings. Earthquake Engineering & Structural Dynamics, 38(4), 477–496. https://doi.org/10.1002/eqe.864

Christovasilis, I. P., Filiatrault, A., & Wanitkorkul, A. (2007). Seismic Testing of a Full-Scale Two-Story Light-Frame Wood Building: NEESWood Benchmark Test. University at Buffalo.

Dolsek, M. (2009). Incremental dynamic analysis with consideration of modeling uncertainties. Earthquake Engineering & Structural Dynamics, 38(6), 805–825.

Estrella, X., Guindos, P., Almazán, J. L., & Malek, S. (2020). Efficient nonlinear modeling of strong wood frame shear walls for mid-rise buildings. Engineering Structures, 215, 110670. https://doi.org/10.1016/j.engstruct.2020.110670

FEMA P58 (2012). Seismic Performance Assessment of Buildings. Federal Emergency Management Agency.

FEMA P695 (2009). Quantification of Building Seismic Performance Factors. Federal Emergency Management Agency.

Folz, B., & Filiatrault, A. (2001). Cyclic Analysis of Wood Shear Walls. Journal of Structural Engineering, 127(4), 433–441. https://doi.org/10.1061/(ASCE)0733-9445(2001)127:4(433)

He, M., Magnusson, H., Lam, F., & Prion, H. G. L. (1999). Cyclic Performance of Perforated Wood Shear Walls with Oversize OSB Panels. Journal of Structural Engineering, 125(1), 10–18. https://doi.org/10.1061/(ASCE)0733-9445(1999)125:1(10)

Ioannou, I., Douglas, J., & Rossetto, T. (2015). Assessing the impact of ground-motion variability and uncertainty on empirical fragility curves. Soil Dynamics and Earthquake Engineering, 69, 83–92.

Kasal, B., Leichti, R. J., & Itani, R. Y. (1994). Nonlinear Finite-Element Model of Complete Light-Frame Wood Structures. Journal of Structural Engineering, 120(1), 100–119. https://doi.org/10.1061/(ASCE)0733-9445(1994)120:1(100)

Lallemant, D., Kiremidjian, A., & Burton, H. (2015). Statistical procedures for developing earthquake damage fragility curves. Earthquake Engineering & Structural Dynamics, 44(9), 1373-1389.

Liang, H. (2007). Reliability evaluation and damage reduction of woodframe buildings under seismic loads. University of Illinois at Urbana-Champaign.

Liang, H., Wen, Y.-K., & Foliente, G. C. (2011). Damage Modeling and Damage Limit State Criterion for Wood-Frame Buildings Subjected to Seismic Loads. Journal of Structural Engineering, 137(1), 41–48. https://doi.org/10.1061/(ASCE)ST.1943-541X.0000272

Lozano, J. M., Tien, I., Nichols, E., & Frost, J. D. (2024). Impact of ground motion uncertainty evolution from post-earthquake data on building damage assessment. Earthquake Spectra, 40(4), 2430-2455.

Pacific Earthquake Engineering Research Center. (2013). NGA West2 ground motion database [Dataset]. https://ngawest2.berkeley.edu/

Pan, Y., Ventura, C. E., & Liam Finn, W. D. (2018). Effects of Ground Motion Duration on the Seismic Performance and Collapse Rate of Light-Frame Wood Houses. Journal of Structural Engineering, 144(8), 04018112. https://doi.org/10.1061/(ASCE)ST.1943-541X.0002104

Pan, Y., Ventura, C. E., & Tannert, T. (2020a). Damage index fragility assessment of low-rise light-frame wood buildings under long duration subduction earthquakes. Structural Safety, 84, 101940. https://doi.org/10.1016/j.strusafe.2020.101940

Pan, Y., Ventura, C. E., & Tannert, T. (2020b). Damage index fragility assessment of low-rise light-frame wood buildings under long duration subduction earthquakes. Structural Safety, 84, 101940. https://doi.org/10.1016/j.strusafe.2020.101940

Pang, W. C., & Rosowsky, D. V. (2010). Beam–spring model for timber diaphragm and shear walls. Proceedings of the Institution of Civil Engineers - Structures and Buildings, 163(4), 227–244. https://doi.org/10.1680/stbu.2010.163.4.227

Pang, W. C., Rosowsky, D. V., Pei, S., & Van De Lindt, J. W. (2007). Evolutionary Parameter Hysteretic Model for Wood Shear Walls. Journal of Structural Engineering, 133(8), 1118–1129. https://doi.org/10.1061/(ASCE)0733-9445(2007)133:8(1118)

Park, Y., & Ang, A. H. -S. (1985). Mechanistic Seismic Damage Model for Reinforced Concrete. Journal of Structural Engineering, 111(4), 722–739. https://doi.org/10.1061/(ASCE)0733-9445(1985)111:4(722)

Park, Y.-J., Ang, A. H. -S., & Wen, Y. K. (1987). Damage Limiting Aseismic Design of Buildings. SAGE Publication.

Pei, S., & Van De Lindt, J. W. (2009). Coupled shear-bending formulation for seismic analysis of stacked wood shear wall systems. Earthquake Engineering & Structural Dynamics, 38(14), 1631–1647. https://doi.org/10.1002/eqe.926

Pei, S., Van De Lindt, J. W., Wehbe, N., & Liu, H. (2013). Experimental Study of Collapse Limits for Wood Frame Shear Walls. Journal of Structural Engineering, 139(9), 1489–1497. https://doi.org/10.1061/(ASCE)ST.1943-541X.0000730

Savitzky, A., & Golay, M. J. E. (1964). Smoothing and Differentiation of Data by Simplified Least Squares Procedures. Analytical Chemistry, 36(8), 1627–1639. https://doi.org/10.1021/ac60214a047

Stewart, W. G. (1987). ‘‘The seismic design of plywood sheathed shear walls.’’ PhD thesis, University of Canterbury, Christchurch, New Zealand.

Update Seismic Rehabilitation Guidance Program Definition and Guidance Development: Part - 1: Workshop Proceeding (2008). FEMA (Appendix C).

Van De Lindt, J. W. (2004). Evolution of Wood Shear Wall Testing, Modeling, and Reliability Analysis: Bibliography. Practice Periodical on Structural Design and Construction, 9(1), 44–53. https://doi.org/10.1061/(ASCE)1084-0680(2004)9:1(44)

Van De Lindt, J. W. (2005). Damage-Based Seismic Reliability Concept for Woodframe Structures. Journal of Structural Engineering, 131(4), 668–675. https://doi.org/10.1061/(ASCE)0733-9445(2005)131:4(668)

Van De Lindt, J. W. (2009). Development of a Performance-Based Seismic Design Philosophy for Mid-Rise Woodframe Construction (Capstone test) [Dataset]. DesignSafe-CI. https://www.designsafe-ci.org/data/browser/public/nees.public/NEES-2010-0895

Vamvatsikos, D., & Cornell, C. A. (2002). Incremental dynamic analysis. Earthquake Engineering & Structural Dynamics, 31(3), 491–514. https://doi.org/10.1002/eqe.141

Ventura, C. E., Pan, Y., Bebamzadeh, A., & Motamedi, M. (2021). Numerical analysis of wood frame structure subjected to long duration subduction ground motion.

Véliz, F., Chacón, M. F., Lagos, J., Berwart, S., López, N., & Guindos, P. (2024). Structural performance of strong timber diaphragms: High-capacity light-timber frames and cross-laminated timber. Structures, 63, 106335. https://doi.org/10.1016/j.istruc.2024.106335

Véliz, F., Estrella, X., Lagos, J., & Guindos, P. (2023). Testing and nonlinear modelling of industrialized light-frame wooden diaphragms including optimized nailing and nonstructural sheathing. Engineering Structures, 297, 117017. https://doi.org/10.1016/j.engstruct.2023.117017

Zhou, L. (n.d.). Structural response of mid-rise hybrid building system consisting of a light wood frame structure and stiff core.